BEHAVIOUR OF WELDED TUBULAR STRUCTURES IN FIRE

A Thesis submitted to the University of Manchester for the degree of

Doctor of Philosophy

in the Faculty of Engineering and Physical Sciences

2015

EMRE OZYURT

School of Mechanical, Aerospace and Civil Engineering

TABLE OF CONTENTS

Total word count: 36,174

LIST OF FIGURES

LIST OF TABLES

NOTATION

CHS	Circular hollow sections
RHS	Rectangular hollow sections
SHS	Square hollow sections
FE	Finite element
A_{chord}	Cross section area of chord member
A_v	Chord effective shear area
B	Overall in-of-plane depth of chord member
B_e	Effective chord length
b	Overall in-of-plane depth of brace member
b_e	Effective width of element
$c_{0,1}$	Coefficients in the joint capacity equations based on geometric parameters
D	Diameter of chord
D_e	Effective diameter of fire
d	Diameter of brace
E	Elastic (Young's) modulus
$F_{assumed}$	Compression brace force from truss analysis for the assumed maximum truss deflection of span/30
$F_{cric,i}$	The increase in the tension force of the critical member when the i^{th} adjacent member is heated
$F_{elevated}$	Elevated temperature force in a truss member at failure
$F_{max, Abaqus}$	Force in a truss member at elevated temperature
F_{max}	Compression brace forces calculated using the proposed analytical method for the actual maximum truss deflection at failure
$F_{max, proposed}$	Total compressive force in the brace member in fire (calculated using proposed analytical method)
$F_{other\ brace\ member}$	Total compressive force in the brace member away from the centre of a truss at elevated temperatures
$F_{other\ brace\ member}$	Total compressive force in the brace member away from the centre of a truss at ambient temperature
$F_{maximum\ chord\ compression}$	Maximum chord compression force

$F_{max,\ L/30}$	Force in a truss member for the assumed maximum truss deflection of span/30
$F_{truss\ centre}$	Total compressive force in the brace member at the truss centre in fire
$F_{truss\ centre,0}$	Total compressive force in the brace member at the truss centre at ambient temperature
$F_{20°C}$	Initial force in a truss member at ambient temperature
F_{β}	Function for the axial restraint stiffness
F_{ρ}	Function for the initial axial load level
F_{λ}	Function for the column slenderness
f_a	Allowable punching shear stress
f_b	Buckling stress
f_u	Ultimate strength
$f_{u,b}$	Ultimate strength of brace member
$f_{u,c}$	Ultimate strength of chord member
f_y	Yield strength
f_{y0}	Yield stress of chord member
$f_{y,brace}$	Yield stress of brace member
$f_{y,c}$	Yield strength of chord member
$f_{y,b}$	Yield strength of brace member
g	Gap length between weld toes of braces
H	Overall out-of-plane width of chord member
H_f	Height of the ceiling in fire compartment
h	Overall out-of-plane width of brace member
I	Second moment of area
K_c	Axial stiffness of a column at elevated temperatures
K_s	Axial stiffness of the restraint
k_b	Axial stiffness of a brace member
k_1	Axial stiffness of the restraint at the top of the column
k_2	Axial stiffness of the restraint at the bottom of the column
$k_{c,0}$	Axial stiffness of the column at ambient temperature
$k_{E,\theta}$	Reduction factors for modulus of elasticity at temperature θ
k_f	Modification factor for axial restraint ratio
k_l	Axial stiffness of the axial restraint

k_{spring}	Axial restrained stiffness
k_{total}	Total axial restrained stiffness
$k_{y,\theta}$	Reduction factor for yield strength at temperatures θ
L	Length of span in a truss
L_c	Length of chord
L_f	Length of flame
l	Length of a column
l_b	Length of brace
M_A	Bending moment in the ring model approach
N_A	Axial force in the ring model approach
N_{chord}	Axial force applied to chord member
N_i	Joint resistance
N_{pl}	Axial load capacity of the chord
$N_{pl,chord}$	Axial yield capacity of chord member
Q_f	Chord stress function
Q_u	Function for the effect of geometric parameters
P	Externally applied load
$P_{chord\ pre\text{-}load}$	Tubular joint under chord pre-load
$P_{no\ chord\ pre\text{-}load}$	Tubular joint without chord pre-load
P_{max}	Buckling capacity of the member at elevated temperature
$P_{initial}$	Axially applied load in the member
P_{ult}	Ultimate capacity of the joint
$P_{20°C}$	Ultimate joint capacity at ambient temperatures
P_θ	Ultimate joint capacity at elevated temperatures
T	Wall thickness of chord
$T_{buckling}$	Buckling temperature of a restrained column
T_f	Failure temperature of a column
$T_{failure}$	Failure temperature of a restrained column
T_{max}	The highest temperature in the critical truss member
T_0	Limiting temperature of the unrestrained column
$T_{20°C}$	Failure temperature from individual member analysis without axial restraint
T_θ	Failure temperature from individual member analysis with axial restraint

t	Wall thickness of brace
V_{eD}	Shear force in the gap of a K-joint
V_p	Punching shear strength
$V_{pl,Rd}$	Shear yield capacity of the chord
x	Distance from the fire source to a point in horizontal plane

GREEK SYMBOLS

β	Diameter ratio (=d/D)
β_1	Axial restraint stiffness ratio
γ	Width to thickness ratio of the chord (=D/2T)
τ	Wall thickness ratio (=t/T)
θ	Brace-to-chord intersection angle
α	Chord length parameter (=$2L_c$/D)
α_{th}	Coefficient of thermal elongation of steel
ψ	Angle which refers to the position of yield hinge in the ring model approach
δ_{max}	Maximum vertical deflection in a truss
δ_1	Relative displacement of the axial displacement of the brace relative to the central chord
ε	Engineering strain
ε_T	True strain
σ	Engineering stress
σ_T	True stress
$\Delta\varepsilon_{th}$	Free thermal strain of the column
$\Delta\varepsilon_{mec}$	Increase in the column mechanical strain due to reduction in the steel stiffness
ΔP	Additional compression force in the member
ΔF_{max}	Additional force in the compression brace member at failure
$\Delta F_{assumed}$	Additional force in the compression brace member at the assumed maximum truss deflection of L/30
$\Delta F_{multiple\ members}$	The increase in the compression force of the critical member when the adjacent members are heated
$\Delta F_{single\ \ member}$	The increase in the compression force of the critical member when one member is heated

$\Delta F_{truss\ centre}$	The maximum increase in compression force in the brace member at the centre of the truss
$\Delta F_{other\ brace\ member}$	The maximum increase in compression force in the brace member away from the centre of the truss
ΔT_{ABAQUS}	Reduction in the member failure temperature due to restrained thermal expansion, from the ABAQUS simulation model
ΔT_f	Reduction in column failure temperature
ΔT_{max}	Temperature increase in the critical member
ΔT_{Wang} *et al.*	The reduction in the member failure temperature based on the regression equations of Wang et al. (2010)
ρ_N	Load ratio in the member
λ	Member slenderness

ABSTRACT

This thesis presents the results of a research project to develop methods to carry out fire safety design of welded steel tubular trusses at elevated temperatures due to fire exposure. It deals with three subjects: resistance of welded tubular joints at elevated temperatures, effects of large truss deflection in fire on member design and effects of localised heating.

The objectives of the project are achieved through numerical finite element modelling at elevated temperatures using the commercial Finite Element software ABAQUS v6.10-1 (2011). Validation of the simulation model for joints is based on comparison against the test results of Nguyen et al. (2010) and Kurobane et al. (1986). Validation of the simulation model for trusses is through checking against the test results of Edwards (2004) and Liu et al. (2010).

For welded tubular joints, extensive numerical simulations have been conducted on T-, Y-, X-, N- and non-overlapped K-joints subjected to brace axial compression or tension, considering a wide range of geometrical parameters. Uniform temperature distribution was assumed for both the chord and brace members. Results of the numerical simulations indicate for gap K- and N-joints (two brace members, one in tension and the other in compression) and for T-, Y- and X-joints with the brace member under axial tensile load (one brace member only, in tension), it is suitable to use the same ambient temperature calculation equation as in the CIDECT (Wardenier et al., 2010a) or EN 1993-1-8 (CEN, 2005b) design guides and simply replace the ambient temperature strength of steel with the elevated temperature value. However, for T-, Y- and X-joints under brace compression load (one brace member only, in compression), the effect of large chord deformation should be considered. Large chord deformation changes the chord geometry and invalidates the assumed yield line mechanism at ambient temperature. For approximation, the results of this research indicate that it is acceptable to modify the ambient temperature joint strength by a reduction factor for the elastic modulus of steel at elevated temperatures.

In the current fire safety design method for steel truss, a member based approach is used. In this approach, the truss member forces are calculated at ambient temperature based on linear elastic analysis. These forces are then used to calculate the truss member limiting temperatures. An extensive parametric study has been carried out to investigate whether this method is appropriate. The parametric study encompasses different design parameters over a wide range of values, including truss type, joint type, truss span-to-depth ratio, critical member slenderness, applied load ratio, number of brace members, initial imperfection and thermal elongation. The results of this research show that due to a truss undergoing large displacements at elevated temperatures, some truss members (compression brace members near the truss centre) experience large increases in member forces. Therefore, using the ambient temperature member force, as in the current truss fire safety design method, may overestimate the truss member critical temperature by 100 °C. A method has been proposed to analytically calculate the increase in brace compressive force due to large truss deformation. In this method, the maximum truss displacement is assumed to be span/30. A comparison of the results calculated using the proposed method against the truss parametric study results has shown good agreement with the two sets of results, with the calculation results generally being slightly on the safe side.

When different members of a truss are heated to different temperatures due to localised fire exposure, the brace members in compression experience increased compression due to restrained thermal expansion. To calculate the critical temperature of a brace member in a localised heated truss, it is necessary to consider this effect of restrained thermal expansion. It is also necessary to consider the beneficial effects of the adjacent members being heated, which tends to reduce the increase in compressive force in the critical member under consideration. Again, an extensive set of parametric studies have been conducted, for different load ratio, slenderness and axial restraint ratio. The results of this parametric study suggest that to calculate the critical temperature of a brace member, it is not necessary to consider the effects of the third or further adjacent members being heated. For the remainder of the heated members, this thesis has proposed a linear elastic, static analysis method at ambient temperature to calculate the additional compressive force (some negative, indicating tension) in the critical member caused by the heated members (including the critical member itself and the adjacent members). The additional compressive force is then used to calculate the limiting temperature of the critical member. For this purpose, the approximate analytical equation of Wang et al. (2010) has been demonstrated to be suitable.

DECLARATION

No portion of the work referred to in the thesis has been submitted in support of an application for another degree or qualification of this or any other university or other institute of learning.

COPYRIGHT

ACKNOWLEDGEMENTS

First and foremost, I would like to express my sincere gratitude to my supervisor, Prof. Yong C. Wang for his constant encouragement, valuable guidance and support in completing this thesis. Prof. Wang's technical contributions to this work are deep and inextricable.

I wish to express my gratitude to the academic staffs of the School of M.A.C.E. Particularly, I would like to thank Dr. Tianjian Ji and Dr. Adrian Bell for their very useful advice in my yearly transfer reports.

Many thanks to the IT Services team of the School of M.A.C.E. for providing the software and hardware I needed. I would also like to thank the library and postgraduate admission staff of the school.

I gratefully acknowledge my colleagues in the research group, especially to Ashkan Shahbazian, B. Kaan Cirpici, Mostafa Jafarian, Chen Lu and Yuchuan He for their support and help.

The financial support from the Turkish Educational Government was essential for my research and living costs.

Finally, I would like to thank my parents, sister, brother-in-law, niece and nephew for their support and encouragement.

Emre Ozyurt

June 2015

LIST OF PUBLICATIONS

- Ozyurt, E. & Wang, Y. C. (2015) Effects of Truss Behaviour on Critical Temperatures of Welded Steel Tubular Truss Members Exposed to Uniform Fire, Engineering Structures, 88, 225-240.
- Ozyurt, E. & Wang, Y. C. (2015) Effects of Truss Behaviour on Critical Temperatures of Welded Steel Tubular Truss Members Exposed to Fire, Tubular Structures XV, Rio, Brazil (Oral presentation).
- Ozyurt, E. & Wang, Y. C. (2014) Elevated temperature resistance of welded tubular joints under axial load in the brace member, Engineering Structures, 59, 574-586.
- Ozyurt, E. & Wang, Y. C. (2013) Resistance of T- and K-Joints to Tubular Members at Elevated Temperatures, the Application of Structural Fire Engineering (ASFE), April 2013, Prague, Czech Republic (Oral presentation).

CHAPTER 1 INTRODUCTION

1.1 Background

The popularity of hollow structural sections of all types has increased in recent decades owing to their attractive appearance, light weight and structural advantages. They have been widely used in onshore and offshore structures, e.g. large span roof trusses (Figure 1.1), bridges, towers, space-trusses, lattice girders, space-frame roof systems, offshore platforms, and so on. For these structures, fire presents one of the most severe design conditions, because the mechanical properties of the steel degrade as the temperature increases. It is important that the behaviour of the tubular structures at high temperatures is thoroughly understood and reliable methods are available to calculate their strengths.

This thesis deals with welded steel tubular trusses. To ensure their safety in fire, both the tubular members and joints should be checked. Currently, there is no design method to calculate the ultimate load carrying capacity of welded tubular joints at elevated temperatures. Although it may be possible to use the equations for ambient temperature design in design codes such as EN 1993-1-8 (CEN, 2005b) or design guides such as CIDECT guide No.1 (Wardenier et al., 2010a), by replacing the yield stress of steel at ambient temperature by those at elevated temperatures, this approach may not always be appropriate because these design equations have been derived based on small deflections in the chord face. At elevated temperatures, as observed by Nguyen at al. (2010), the chord face may undergo large distortions and their effects should be considered.

For truss members, their design at ambient temperature is relatively easy, involving mainly design checks for tension and compression resistance after performing static analysis to obtain the member forces. At present, under fire conditions, the current method for truss member design involves calculating the member force using static analysis at ambient temperature and then finding the critical temperature of the member using the ambient temperature member force. The member force – critical temperature relationship can be evaluated using design methods such as those in BS 5950 Part 8 (BSI, 2003) and EN 1993-1-2 (CEN, 2005a). However, the member force obtained from static analysis at ambient temperature may not be correct at

elevated temperatures due to either large deformations of the truss or axial restraint to the heated members from the cooler structural members in a localised fire. These two different fire scenarios may result in additional forces in the critical truss members. They should be considered in tubular truss design in fire.

In summary, it can be stated that the basis for the design of both welded tubular joints and welded tubular truss members at elevated temperatures is not robust. It is important to thoroughly understand the different aspects of these behaviours so as to develop a simple and safe design method.

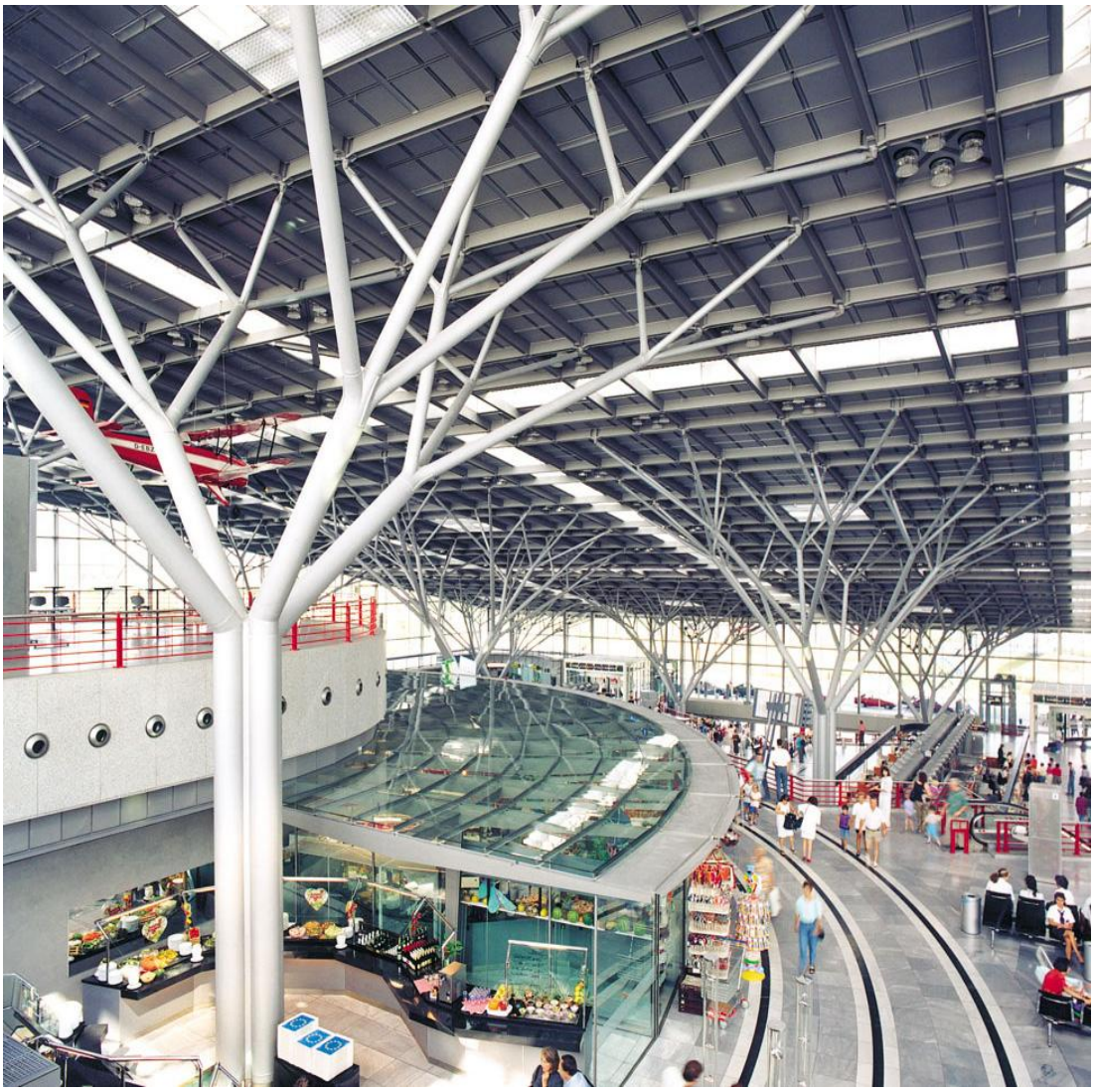

Figure 1.1 Airport departure hall in Stuttgart, Germany (Wardenier et al., 2010a)

1.2 Research Significance and Objectives

The main objectives of the research reported in this thesis are:

- ✓ To validate the numerical models for steel tubular truss joints and trusses developed using ABAQUS v6.10-1 (2010).

- ✓ To use the validated truss joint numerical simulation model to perform extensive numerical simulations to obtain the ultimate capacities of different types of welded steel tubular joints at elevated temperatures to develop a thorough understanding of the structural behaviour and to generate a database for the development of an analytical method.

- ✓ To use the validated truss numerical simulation model to extensively investigate the behaviour of welded tubular trusses under different heating conditions, including both uniform fire exposure or localised fire exposure to the trusses, so as to assess whether the current member-based fire resistance design approach is safe, and if not, to generate a database of numerical results for the development of improved design methods.

- ✓ To develop and validate improved analytical methods to take into consideration the additional compression forces in truss members due to changes in truss geometries at high temperatures and restrained thermal expansion.

1.3 Thesis Outline

This thesis is divided into seven chapters:

Chapter 1 gives a general introduction to the research background and the research objectives.

Chapter 2 presents a comprehensive review of the behaviour of welded tubular trusses and truss joints at ambient and elevated temperatures, focusing on the additional effects of high temperatures so as to identify the specific issues that will require further research.

Chapter 3 presents the numerical simulation models, established using ABAQUS, for welded tubular trusses and joints, and compares the simulation results against available experimental results for validation of the simulation models. The experimental results include those of Tan et al. (2012) on welded tubular T-joints at elevated temperatures, the test results of Kurobane et al. (1986) on K-joints at ambient temperature, the fire test results of Edwards (2004) on SHS lattice girders and the fire test results of Liu et al. (2010) on steel planar tubular trusses.

Chapter 4 examines the strengths of welded steel tubular joints at elevated temperatures, based on the numerical simulation results for different types of CHS or SHS tubular joints with axially loaded brace members at different levels of elevated temperatures. An analytical method will be developed and checked against the numerical simulation results.

Chapter 5 provides the results of an extensive parametric study of different types of steel tubular trusses with uniform heating of the truss members. The key output of this parametric study is to propose and validate an analytical method and a second-order truss analysis method that take into consideration the additional compression forces in truss members due to large truss displacement at high temperatures.

Chapter 6 investigates the effects of restrained thermal behaviour when trusses are subject to localised fire. The main issue under investigation is how to account for the effects of different number of members being heated to different temperatures on the development of the compression force of the most critical member. An analytical method will be developed.

Chapter 7 summarises the research of this thesis and discusses possible future relevant research studies.

CHAPTER 2 LITERATURE REVIEW

2.1 Introduction

The aim of this research project is to develop methods to evaluate the resistance of welded tubular structures at elevated temperatures. This will include the two groups of components of welded truss: joints and members. Furthermore, in large trusses, the fire exposure may be localised, which would result in non-uniform temperature distribution in the trusses. Non-uniform distribution of temperatures in different members of a truss gives rise to non-uniform thermal expansion, resulting in thermal forces. It is important that these issues are thoroughly understood so as to develop appropriate methods for design use. Based on this short introduction, the literature review will be conducted to establish the current state of the art in the following three parts:

- Behaviour and analysis of welded truss joints at ambient and elevated temperatures;
- Behaviour of welded tubular trusses with uniform elevated temperatures;
- Behaviour of welded tubular trusses with non-uniform temperature distributions in members.

2.2 Behaviour and Analysis of Tubular Joints at Ambient Temperatures

There have been a large number of research studies, including experiments, numerical simulations and theoretical analyses, of welded tubular joints at ambient temperature. Therefore, it will not be possible for this literature review to thoroughly cover all aspects of tubular joint behaviour at ambient temperature. The main purpose of this section is to explain the behaviour of welded joints, to identify their failure modes and the most influential design parameters. To conclude this section, an assessment will be made to discuss whether the current joint resistance calculation methods at ambient temperature can be extended to elevated temperatures by replacing the ambient temperature mechanical properties by the corresponding ones at elevated temperatures.

2.2.1 Configuration of tubular joints

Tubular joints may be uni-planar, where all the members of the joint are located in the same plane, or spatial. This research is concerned only with planar trusses, and by extension, uni-planar joints. The main uni-planar types are T-, X-, Y- and K-joints, as shown in Figure 2.1.

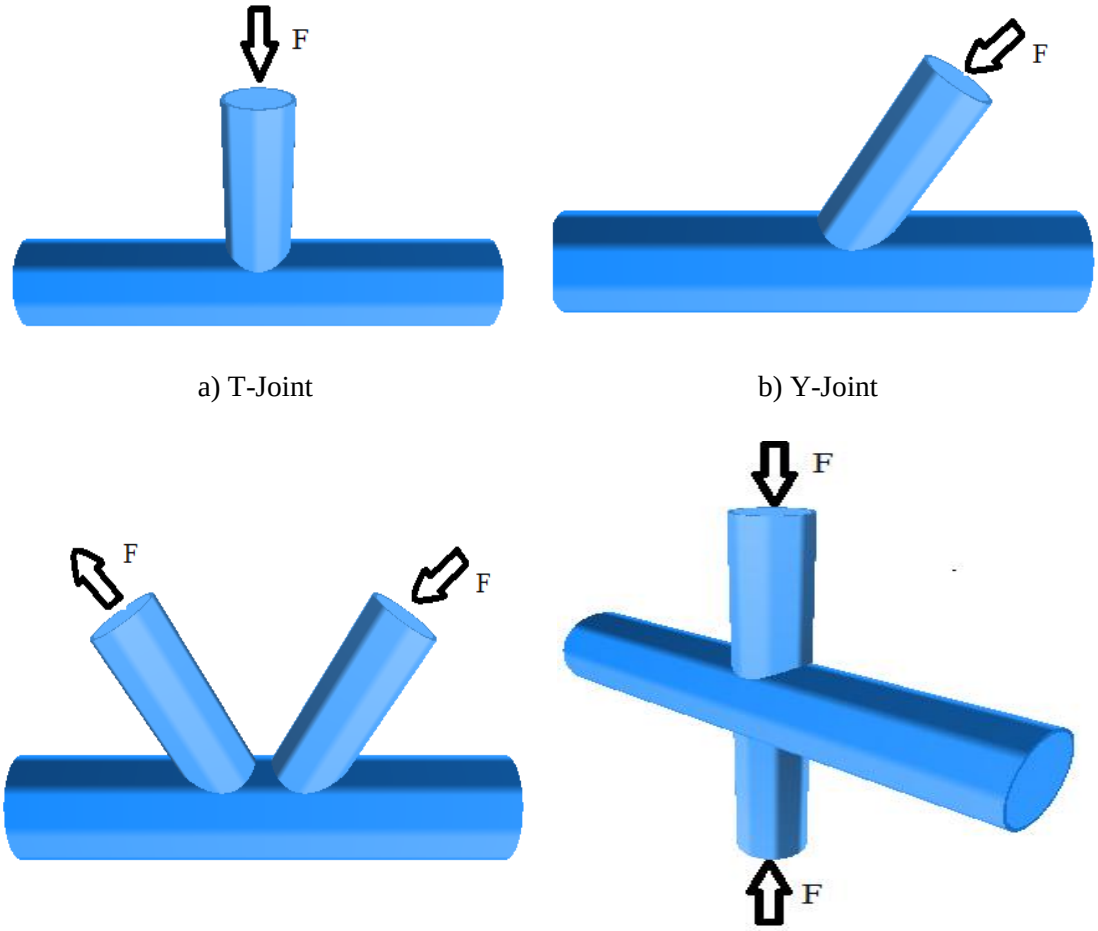

a) T-Joint b) Y-Joint

c) K-Joint d) X-Joint

Figure 2.1 Classification of planar tubular joints

Figure 2.2 shows the geometric configuration of a typical CHS K-joint. Based on numerous research studies (Wardenier et al., 2010a; Van der Vegte et al., 2008a; 2008b), the geometrical factors that are most influential on the behaviour of welded joints are:

Diameter ratio $\beta = \frac{d}{D}$

Width to thickness ratio of the chord $\gamma = \frac{D}{2T}$

Wall thickness ratio $\tau = \frac{t}{T}$

Chord length parameter $\alpha = \frac{2L_c}{D}$

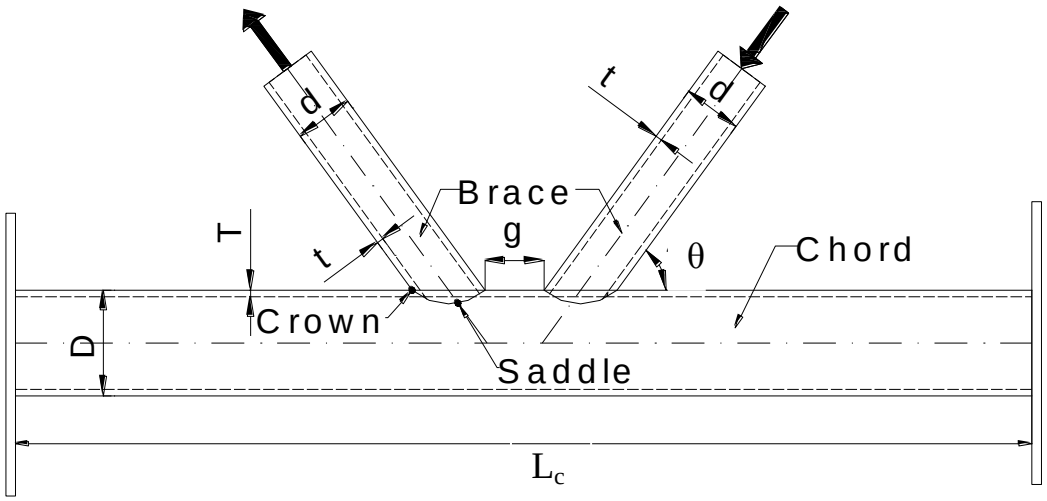

Figure 2.2 Configuration of a typical CHS K-joint

If a rectangular brace or chord member is used, the brace/chord diameter is replaced by the corresponding dimensions of the rectangular member.

To demonstrate the extensiveness of existing research studies on welded tubular joints at ambient temperature, Table 2.1 shows a selection of the more influential studies and their main findings.

Table 2.1 indicates that all welded tubular truss geometrical and loading conditions have been investigated at ambient temperature and the existing EN 1993-1-8 (CEN, 2005b) and CIDECT design guide provide comprehensive design recommendations. Indeed, Professor Jeffrey Packer, an eminent researcher on welded tubular joints, used his prestigious Kurobane lecture at the International Symposium on Tubular Structures (ISTS) in 2003 to emphasise that there was a large volume of ambient temperature research on welded tubular connections with mature worldwide implementation of design for tubular joints into national and international design guides (Packer, 2003).

Table 2.1 Summary of a selection of the main research on tubular joints at ambient temperature

Joint Type	Loading Conditions	References	Failure Modes	Main Findings
T & Y JOINTS	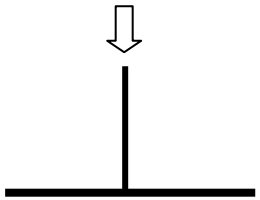	Togo (1967), Marshall et al. (1974), Lu et al. (1994), Wardenier (1982), Makino et al. (1996)	Chord plastification	▪ The current design guide equations in EN 1993-1-8 (CEN, 2005b) and CIDECT (Wardenier et al., 2010a) for chord plastification are based on the ring model proposed by Togo (1967). ▪ The ultimate strength of tubular joints is limited by checking the ultimate deformation limit of 0.03D (Lu et al., 1994). ▪ Makino et al. (1996) collated all published test results worldwide at the time. This database was used by van der Vegte et al. (2008a; 2008b) to develop the new strength formulae.
			Punching shear	▪ The punching shear approach of Marshall et al. is the basis for EN 1993-1-8 (CEN, 2005b) and CIDECT (Wardenier et al., 2010a).

T & Y JOINTS				▪ Wardenier noted that punching shear can be a critical failure mode for joints with small β.
	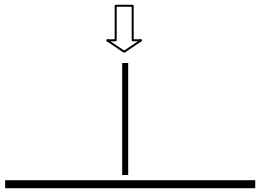		Local failure	▪ Local buckling may occur in thin-walled tubular joints with wall thickness less than 4 mm. (Wardenier, 1982). ▪ Wardenier (1982) proposed to predict the joint capacity by cheking only for both chord plastification and punching shear failure resistances if geometiric limitations are imposed.
	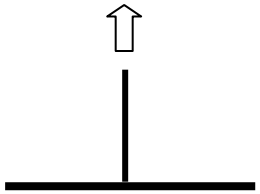	Wardenier (1982), Kurobane et al. (1984)	Tearing	▪ Tearing along the weld toes may occur in T-, Y-, and X-joints under tension. ▪ Tearing can be overcome by using appropriate welding (Wardenier, 1982).
	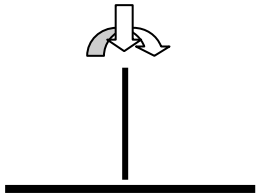	Van der Vegte et al. (2008a; 2008b), Qian et al. (2008)	Chord plastification Punching shear	▪ Brace member under combined axial compression and bending moment. ▪ A maximum rotation of 0.1 radian of brace member is specified in the current design guides based on Lu's deformation limit.

T & Y JOINTS	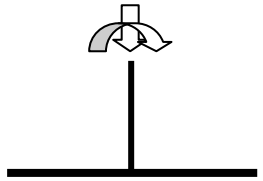			▪ The resistances of in-plane bending moments for T-, Y- and X- joints are based on the modified punching shear resistance of Gibstein (1976). ▪ A new design equation, based on a statistical analysis proposed by van der Vegte et al. (2008b) and adapted in EN 1993-1-8 (CEN, 2005b) and CIDECT (Wardenier et al., 2010a).
	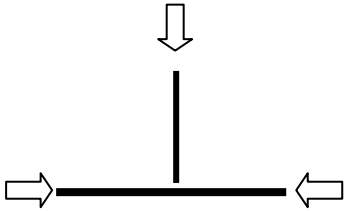	Kurobane et al. (1984), van der Vegte et al. (2000; 2001c; 2003), Liu et al. (2002) and Wardenier et al. (2007)	Chord plastification	▪ Effects of chord compression: compressive chord pre-load reduces the ultimate capacity of T-, Y- and X-joints. ▪ Basis of EN 1993-1-8 (CEN, 2005b) and CIDECT (Wardenier et al., 2010a) design equations.
	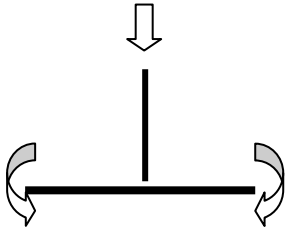	Van der Vegte et al.(2006)	Chord plastification Chord in-plane bending	▪ Effects of chord bending moment and length ▪ Chord length parameter, α, has no effect on the joint capacity. ▪ A chord length of 10*D* is sufficient to avoid the influence of the boundary conditions.

K AND N JOINTS	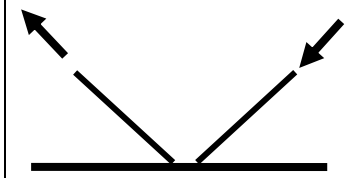	Dexter et al. (1999a; 1999b), Qian (2005; 2007), van der Vegte et al. (2007b) and Wardenier (2007)	Chord plastification, Chord punching shear, Local failure, Chord shear failure	▪ Failure mechanisms of K-joints are different for gap and overlapped joints. ▪ Shear failure may take place in gap K- and N-joints. ▪ Critical parameters: β and θ. ▪ Basis of EN 1993-1-8 (CEN, 2005b) and CIDECT (Wardenier et al., 2010a) design equations.
	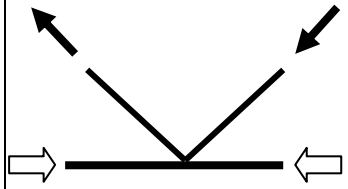	Van der Vegte et al. (2002; 2003; 2008a; 2008b) and Liu et al. (2006)	Chord plastification, Local failure	▪ Effects of chord compression: reducing joint capacity. ▪ The modification factor is independent of geometric parameters. ▪ Basis of EN 1993-1-8 (CEN, 2005b) and CIDECT (Wardenier et al., 2010a) design equations.

X JOINTS	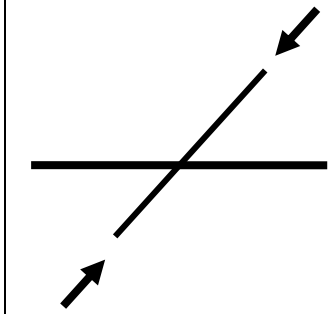	Choo et al. (2003b; 2003a), Qian (2005)	Chord plastification and Chord punching shear	▪ Exact ring model of van der Vegte (1995) is a better representation for thick-walled X-joints with wall thickness greater than 50 mm. ▪ Chord shear failure can happen when $\cos\theta > \beta$. ▪ Basis of EN 1993-1-8 (CEN, 2005b) and CIDECT (Wardenier et al., 2010a) design equations.
	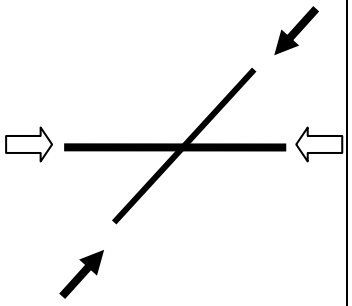	Togo (1967), van der Vegte et al. (2001a; 2007a), Liu et al. (2002) and Wardenier et al. (2007)	Chord plastification	▪ Effects of chord axial force: compression force has detrimental effect on joint capacity; tension force has limited effect. ▪ Basis of the EN 1993-1-8 (CEN, 2005b) and CIDECT (Wardenier et al., 2010a) design guides.

2.2.2 Failure modes of welded tubular joints

Based on the existing research investigations as demonstrated in Table 2.1, the following modes of failure of welded tubular joints have been identified:

a) chord plastification (chord face failure), (see Figure 2.3a)
b) chord side wall failure (chord web failure), (see Figure 2.3b)
c) chord shear failure (see in Figure 2.3c)
d) chord punching shear failure (see Figure 2.3d)
e) brace failure (buckling, yielding), (see Figure 2.3e)
f) local buckling (see Figure 2.3f)

These failure modes are shown in Figure 2.3.

Mode	Between CHS joints	Between RHS joints
a	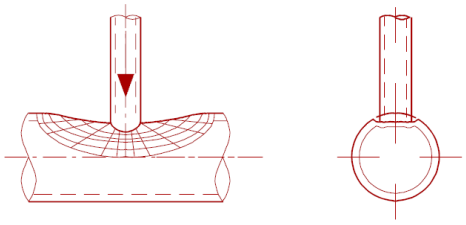	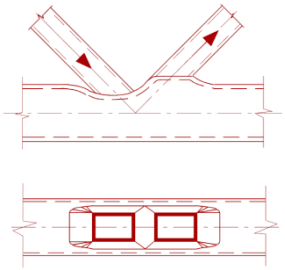
b	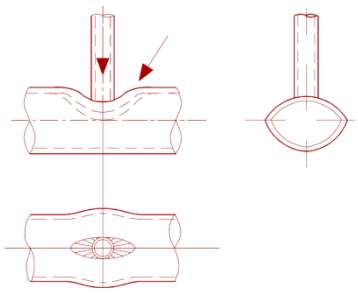	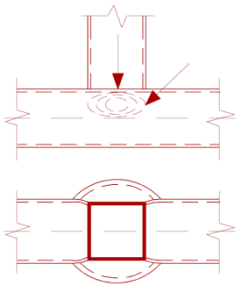
c	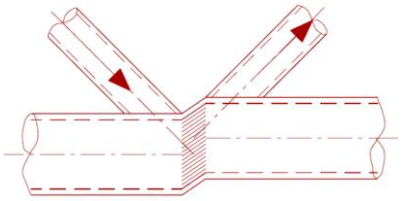	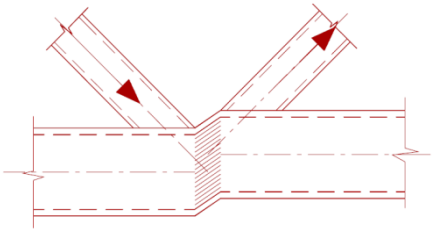
d	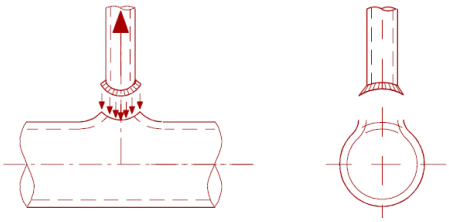	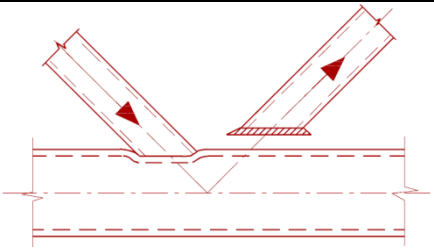

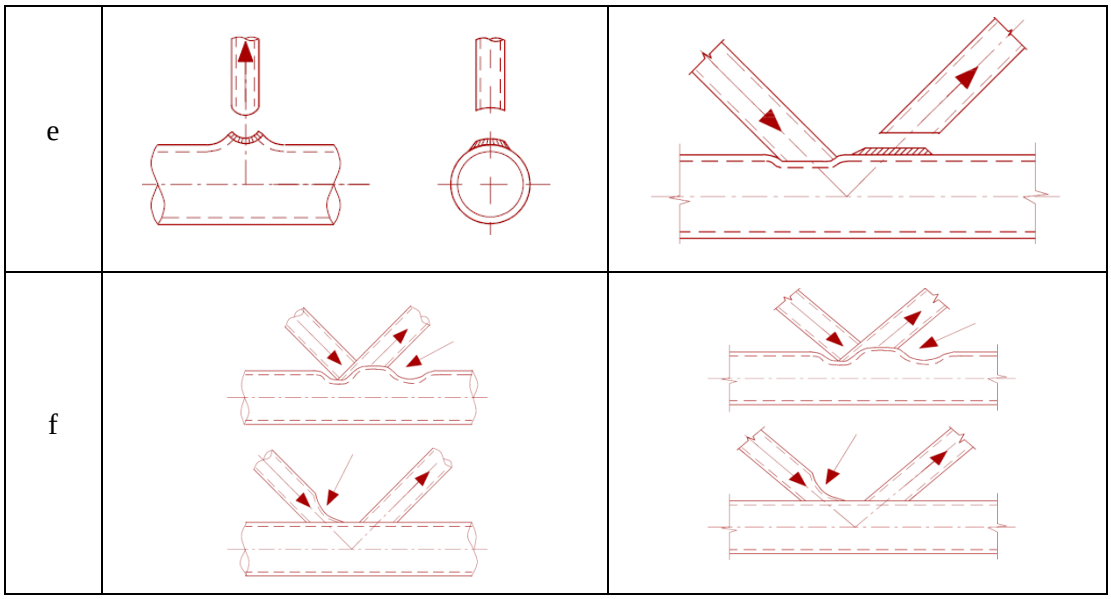

Figure 2.3 Welded tubular joint failure modes under brace axial load (CEN, 2005b)

For these failure modes, design equations are recommended in EN 1993-1-8 (CEN, 2005b) and CIDECT (Wardenier et al., 2010a). It can be noted that the EN 1993-1-8 and CIDECT equations are very similar as can be seen in Table 2.2. In fact, the EN 1993-1-8 equations were adapted from the CIDECT equations, with some minor modifications.

Table 2.2 Design axial resistances of welded joints between CHS and RHS members

Failure Mode	Joint Type	EN 1993-1-8 (CEN, 2005b)	CIDECT guide No.1 and No. 3 (Wardenier et al., 2010a)
Chord Face Failure	T, Y, X, K and N joints	$N_i = Q_u Q_f \frac{f_{y0} T^2}{\sin\theta}$	$N_i = Q_u Q_f \frac{f_{y0} T^2}{\sin\theta}$
	T and Y joints	$Q_u = (2.8 + 14.2\,\beta^2)\gamma^{0.2} \;\; for\ CHS$ $Q_u = \frac{1}{(1-\beta)}\left(\frac{2\beta}{\sin\theta} + 4\sqrt{1-\beta}\right) \;\; for\ RHS$	$Q_u = 2.6(1 + 6.8\,\beta^2)\gamma^{0.2} \;\; for\ CHS$ $Q_{u,RHS} = \frac{2(h/B)}{(1-\beta)\sin\theta} + \frac{4}{\sqrt{1-\beta}} \;\; for\ RHS$
	X joints	$Q_u = \left(\frac{5.2}{1 - 0.81\beta}\right) \;\; for\ CHS$ $Q_u\ is\ the\ same\ as\ for\ RHS\ T\ and\ Y\ joints$	$Q_u = 2.6(\frac{1+\beta}{1-0.7\beta})\gamma^{0.15}$ $Q_u\ is\ the\ same\ as\ for\ RHS\ T\ and\ Y\ joints$
	K and N joints	$Q_u = \left(1 + \frac{0.024\gamma^{1.2}}{1 + \exp\left(0.5\frac{g}{T} - 1.33\right)}\right)\left(1.8 + 10.2\frac{d}{D}\right)\gamma^{0.2}$ $Q_u = 8.9\gamma^{0.5}\left(\frac{b_1 + b_2}{2B}\right) \;\; for\ RHS$	$Q_u = \left[1 + \frac{1}{1.2 + \left(\frac{g}{T}\right)^{0.8}}\right] 1.65(1 + 8\beta^{1.6})\gamma^{0.3} \;\; for\ CHS$ $Q_u = 14\beta\gamma^{0.3} \;\; for\ RHS$

Chord punching shear failure	T, Y, X, K and N joints	$N_i = 0.58 f_{y0} \pi d T \frac{1+\sin\theta}{2\sin^2\theta}$ $for\ CHS$ $N_i = \frac{0.58 f_{y0} T}{\sin\theta}\left(\frac{2h}{\sin\theta}+\frac{20b}{B/T}\right)$ $for\ RHS$	$N_i = 0.58 f_{y0} \pi d T \frac{1+\sin\theta}{2\sin^2\theta}$ $for\ CHS$ $N_i = \frac{0.58 f_{y0} T}{\sin\theta}\left(\frac{2h}{\sin\theta}+\frac{20b}{B/T}\right)$ $for\ RHS$
Chord side wall failure	T. Y and X joints	$N_i = \frac{f_b T Q_f}{\sin\theta}\left[\frac{2h}{\sin\theta}+10T\right]$ $for\ RHS\ if\ \beta = 1.0.$	
Local buckling failure of brace	T. Y and X joints	$N_i = f_{y0} t \frac{\pi}{4}(2d-4t+2b_e)$ $but\ b_e \le d\ for\ CHS$ $N_i = f_{y0} t(2d-4t+2b_e)$ $where\ b_e = \frac{10}{D/T}\frac{f_{y,0} T}{f_{y,brace} t} d$ $but\ b_e \le d\ for\ RHS$	
Chord shear failure	K and N joints	$N_i = \frac{\pi}{4}\left[(A_{chord}-2DT)f_{y0}+2DTf_{y0}\sqrt{1-\left(\frac{V_{Ed}}{V_{pl,Rd}}\right)^2}\right]$ $for\ CHS$ $N_i = \left[(A_{chord}-A_v)f_{y0}+A_v f_{y0}\sqrt{1-\left(\frac{V_{Ed}}{V_{pl,Rd}}\right)^2}\right]$ $for\ RHS$	
Brace failure	K and N joints	$N_i = f_{y0} t(3d-4t+b_e)\frac{\pi}{4}$ $for\ CHS$ $N_i = f_{y0} t(2h-4t+b+b_e)\frac{\pi}{4}, where\ b_e = \frac{10}{D/T}\frac{f_{y,0} T}{f_{y,brace} t} d$ $but\ b_e \le d\ for\ RHS$	

The objective of this research is to find a method to calculate the resistance of welded tubular joints at elevated temperatures. The first option would be to assess whether it would be possible to replace the ambient temperature yield stress of steel by those at elevated temperatures. For this, it is best to examine the different failure modes.

2.2.2.1 Chord plastification

For chord plastification, Togo (1967) developed the ring mode. In this mode, the effects of normal and shear forces on the plastic moment capacity of the chord were excluded and the 3D joint configuration was converted into a 2D model, in which a ring shape represented the chord cross section as illustrated in Figure 2.4. In the ring model, it is assumed that most of the loading is transferred at the saddles of the brace, since the chord behaves most stiffly around the connection perimeter. Consequently, for the case of an axially loaded T joint in the brace, the load in the brace P is divided into two equal parts of 0.5P. The brace forces are assumed as line loads on a certain length of the chord. Plastic hinges are assumed to occur in the following order: at the cross section from point 1 ($\psi_1 = arcsin\beta$), point 2 ($\psi_2 = \psi = 1.2 + 0.8\beta^2$) and point 3 ($\psi_3 = \pi$) as marked in Figure 2.4. Using the principle of virtual work, Togo (1967) derived Equation 2.1 to calculate the strength equation of the chord member (N_i). The coefficients c_0 and c_1 in the current EN 1993-1-8 (CEN, 2005b) and CIDECT (Wardenier et al., 2010a) design equations were calibrated against experimental results.

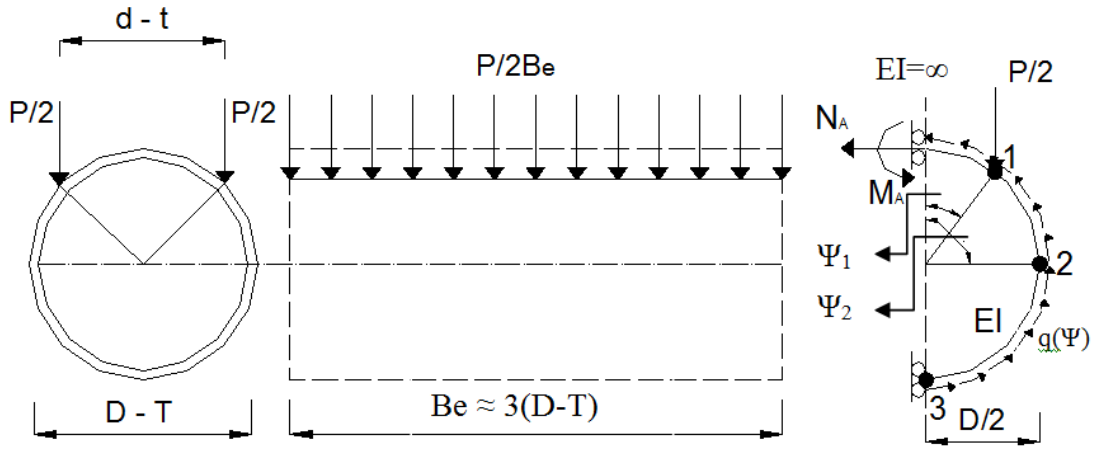

Figure 2.4 Ring model of a T-joint (Togo, 1967)

$$N_i = \frac{c_0}{(1 - c_1\beta)} \frac{T^2 f_{y0}}{\sin\theta} Q_f \qquad 2.1$$

In some cases, the plastic hinge mechanism occurs after large deformation of the chord face. Such large deformations may affect the serviceability performance of the truss. Because there is no explicit method of calculating chord face deformation to check the serviceability performance, a practical method is to limit the chord face deformation at the ultimate limit state. Such a deformation limit has been introduced by Lu et al. (1994), being 0.03D where D is the width (or diameter) of the chord. The design strength (P_{ult}) of a tubular joint is that of the load developing the plastic hinge mechanism or the load at a deformation of 0.03D, as shown in Figure 2.5a and Figure 2.5b respectively, whichever is lower.

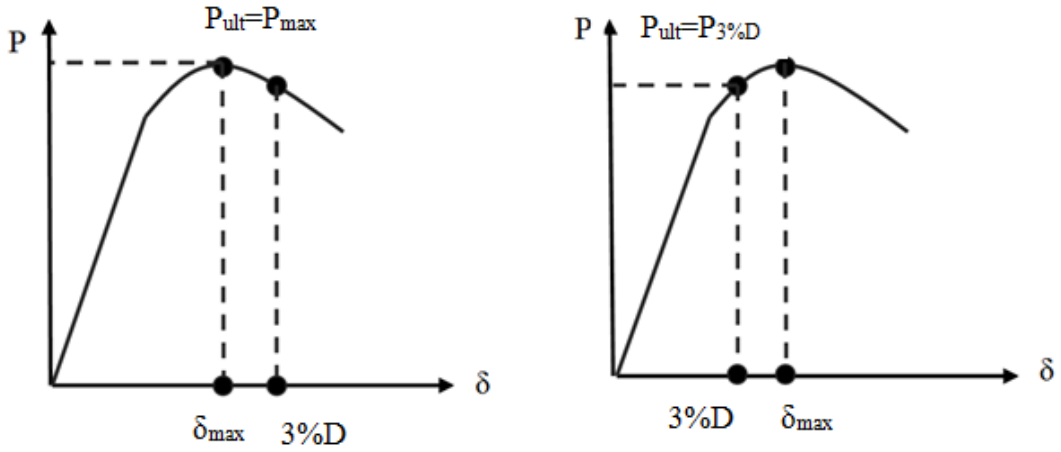

a) $\delta_{max} < 3\%$ D b) $\delta_{max} > 3\%$ D

Figure 2.5 Definition of joint strength under chord plastification

For application at elevated temperatures, one question that needs to be asked is whether the current design equations can be applied to high temperatures by merely multiplying the reduction factor of the steel yield strength at the corresponding elevated temperatures. In the simple ring model at ambient temperature, the chord face is undeformed. At high temperatures, as demonstrated by the tests of Nguyen et al. (2010; 2012) and Tan et al. (2012), ovalisation of the chord face may happen, as shown in Figure 2.6. Furthermore, the ring model is based on simplification of a three dimensional joint to a two dimensional ring, which excludes the effects in the longitudinal direction of the chord. It is clearly necessary to investigate the effects of

chord face deformation at elevated temperatures. Chapter 4 of this thesis will report details of the author's investigation.

a) 200 mm away from centre

b) Centre

Figure 2.6 Deformed cross sections of T-joints at different temperatures (Tan et al., 2012)

2.2.2.2 Punching shear model

The punching shear strength, V_p, was established by Marshall and Toprac (1974). It is calculated (Equation 2.2) by multiplying the punching shear area and the allowable punching shear stress in the chord, which is assumed to be uniform around the intersection between the brace and the chord, as shown in Figure 2.7.

$$V_p = 0.58 f_{y0} \pi d T \frac{1 + \sin\theta}{2 \sin^2\theta} \quad 2.2$$

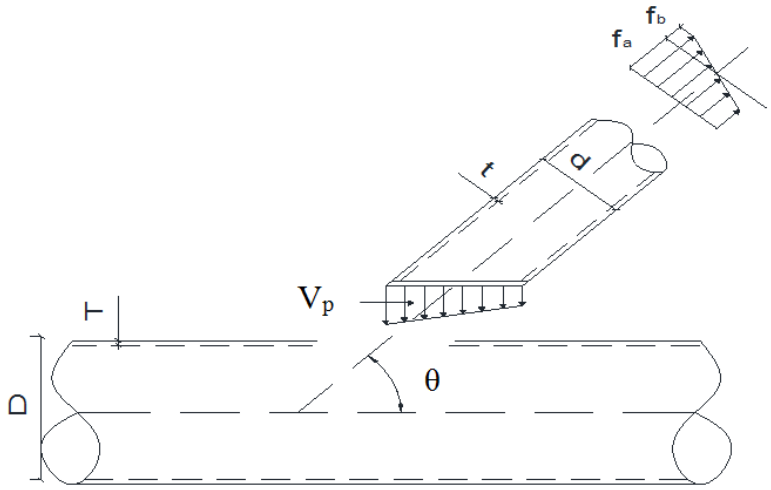

Figure 2.7 Punching shear stress model

Punching shear failure is more common in tension loaded joints with small β ratios. Because deformation of the chord face involved in the punching shear failure mode is small, at elevated temperatures, it is expected that the current model is applicable to elevated temperatures provided the reduced yield strength of steel is used.

2.2.2.3 Chord shear failure

The chord shear failure mode is critical only for gap K- or N-joints with a large diameter ratio. The chord shear capacity, V_{pl} is given by:

$$V_{pl} = \frac{2}{\pi} A_{chord}\left(0.58\, f_{y0}\right) \qquad 2.3$$

The axial load capacity of the chord, N_{pl} is given by:

$$N_{pl} = \pi\,(D - T)\,T\,f_{y0} \qquad 2.4$$

At elevated temperatures, because the chord shear failure mechanism would be the same as at ambient temperature, the above method is considered applicable to elevated temperatures provided the reduced steel yield strength is used.

2.2.2.4 Summary of analytical models

In the current design recommendations, the brace thickness to diameter ratio, d/t, is limited to preclude local buckling. Tearing failure can also be eliminated by using appropriate welding. Furthermore, as long as a joint is checked for chord plastification, the chord shear failure can be overcome. Indeed, within the limits of

applicability imposed in EN 1993-1-8 (CEN, 2005b) and CIDECT (Wardenier et al., 2010a), the failure modes are reduced to chord plastification and chord punching shear. For elevated temperature applications, the chord punching shear model at ambient temperature is expected to be applicable without modifications, provided the reduced steel yield strength is used. For chord plasitification, further research will be conducted to investigate the effects of chord ovalisation.

2.3 Behaviour and Design of Welded Steel Tubular Trusses in Fire

2.3.1 Trusses with uniformly heated members in fire

For truss design, both the members and the joints should be checked. At ambient temperature, checking truss members is relatively easy, involving mainly design checks for a tension or a compression resistance check after performing static analysis to obtain the member forces. Under fire conditions, the existing method for truss member design involves calculating the member forces using static analysis at ambient temperature and then finding the critical temperature, defined as the maximum temperature at which the member can resist the applied load, using the ambient temperature member force. The member force – critical temperature relationship can be calculated using design methods such as those in BS 5950 Part 8 (BSI, 2003) and EN 1993-1-2 (CEN, 2005a). However, the member forces obtained from truss static analysis at ambient temperature may not be correct at elevated temperatures due to large deformations of the truss. Therefore, further research is necessary. This section reviews the available investigations on steel and composite trusses under fire conditions where the entire truss is exposed to fire resulting in uniform heating of all the truss members.

Choi (2004) performed 2D finite element analyses to investigate the behaviour of typical long-span composite floor trusses at elevated temperatures, to mimic the floor trusses in the World Trade Center Buildings 1 and 2 during the September 11, 2001 fire (McAllister et al., 2002). It was found that failure of the truss was caused by progressive buckling of the diagonal members. He compared the failure temperatures of the critical members with the limiting temperatures based on BS5950 Part 8 (BSI, 2003). It was found that the BS 5950 limiting temperatures overestimate those of pin-ended compression members but underestimate those of tension members. However, he did not investigate the design forces in the truss members at elevated temperatures.

Edwards (2004) tested two protected SHS lattice girders and compared their behaviour with a member-based fire design method using BS 5950 Part 8 (BSI, 2003). Edwards reported that the design method may underestimate the truss member critical temperatures. This study gave limited analysis of the test results, but provided valuable experimental data to validate the numerical simulation model of the author, which will be presented in Chapter 3.

Chang et al. (2005) used the specialist finite element program, SAFIR (Franssen, 2011), to simulate the behaviour of open-web steel trusses with or without fire protection under different fire scenarios. They compared the axial forces in the truss members at ambient temperature with those at elevated temperature. However, their study was concerned with trusses with external restraints in the longitudinal direction to simulate the surrounding columns. This study excluded buckling of truss members, so it is not a realistic representation of structural behaviour under fire conditions.

Flint et al. (2006) carried out a similar study to Choi et al. (2003) and examined the effect of thermal expansion on the behaviour of long span composite trusses in fire. They observed buckling of the web members, as in Choi et al. (2003). However, their trusses did not suffer sudden failure after initial buckling of the web members. A possible explanation is the rigid boundary conditions provided by the concrete slab generating an alternative load path.

Burns et al. (2009) performed finite element simulations on the behaviour of long-span composite trusses using the specialist fire engineering program VULCAN (1996). The trusses were assumed to be simply supported and pin-jointed. Their results show that the axial forces in the web members within the high-shear zone increased up to 35% of the ambient temperature values as a result of thermal expansion. After initial buckling of the web member, redistribution of the load was insufficient to prevent the truss from global failure.

Meng et al. (2010) and Liu et al. (2010) have presented a limited amount of experimental and parametric data of the structural behaviour of steel planar tubular trusses subjected to fire. It was noted that the truss failure was triggered by buckling in the brace member. The trusses used in these tests are not representative of realistic dimensions due to the very small number of truss elements. Nevertheless, these tests

provide useful experimental results to verify the author's finite element model, which will be presented in Chapter 3.

Kotsovinos (2013) attempted to recreate the failure mechanism of the WTC towers and reached similar conclusions as others (e.g. Usmani (2003), FEMA report (2002) and NIST report (2005)). This study noted that additional forces were generated in the truss members as a result of thermal expansion. He also compared the effects of vertically travelling fires on tall buildings with simultaneous fire exposure. It was suggested that the simultaneous fire exposure should be used in the design of tall buildings, because the vertically travelling fires had positive effects on the structural response.

As a summary, the review in this section shows that recent research studies on steel trusses have focused on the truss collapse mechanism, as a response to the collapse of the World Trade Center buildings on September 11, 2001. The main emphasis is whether or not initial failure of a truss member (usually a web member) would lead to total collapse of the truss. There is a lack of detailed assessment of the initiating condition, and in particular, how the truss member forces change at elevated temperatures. Force redistribution in trusses may occur due to geometrical changes of the trusses at large deformations. This thesis will investigate truss member behaviour in detail (Chapter 5).

2.3.2 Trusses with non-uniformly heated members exposed to localised fire

Welded steel tubular trusses are frequently used to cover very large spaces, such as airports, exhibition halls, shopping malls and sport halls. For these large structures, the fire exposure can be assumed to be localised because of the small size of the fire compared to the dimensions of the truss. Under localised fire, the different members of a truss will experience different temperatures. Therefore, in addition to the issues identified in uniformly heated trusses, non-uniformly heated trusses also have to consider differential heating of different members causing additional forces due to restrained thermal expansion.

2.3.2.1 Localised fire and temperature distributions in non-uniformly heated trusses

EN-1991-1-2 (CEN, 2002) gives a method to calculate the size of a localised fire, giving information on the height of the flame, the rate of heat release and fire temperature as a function of the distance to the fire source. The localised fire model is based on the research of Hasemi et al. (1984).

Figure 2.8 shows a definition of the variable parameters involved in quantifying localised fire. Because the focus of this research is the structural behaviour of trusses with non-uniform temperature distribution in the truss members, the truss member temperatures will be assumed, not calculated using the localised fire behaviour and heat transfer analysis.

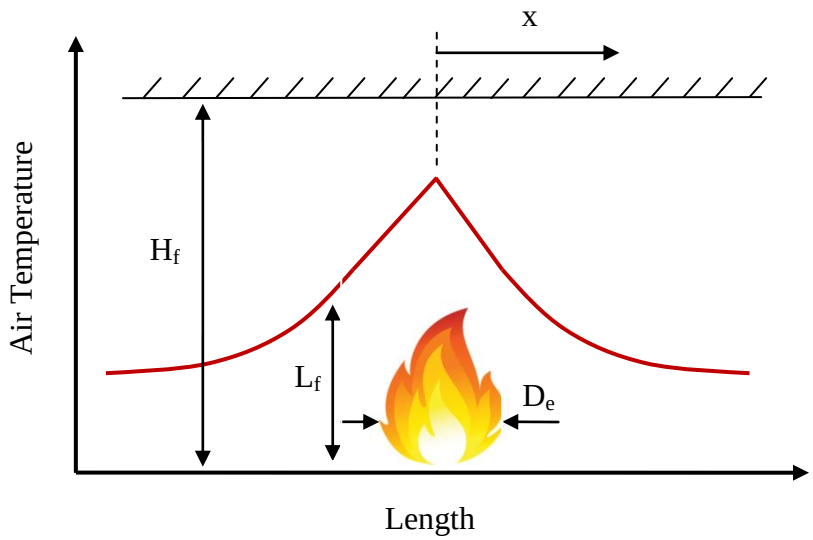

Figure 2.8 Localised fire parameters (CEN, 2002)

Chen et al. (2012) tested and numerically modelled a steel roof truss without fire-proof coating under localised pool fire conditions to obtain information on the truss temperature distributions and displacements. Figure 2.9 presents typical temperature distribution in the truss. The members directly above the fire experienced the highest temperature. Away from the fire, the truss members experienced reduced temperatures, the reduced temperatures in the adjacent members ranging from 50% to 80% of those in the most heated member.

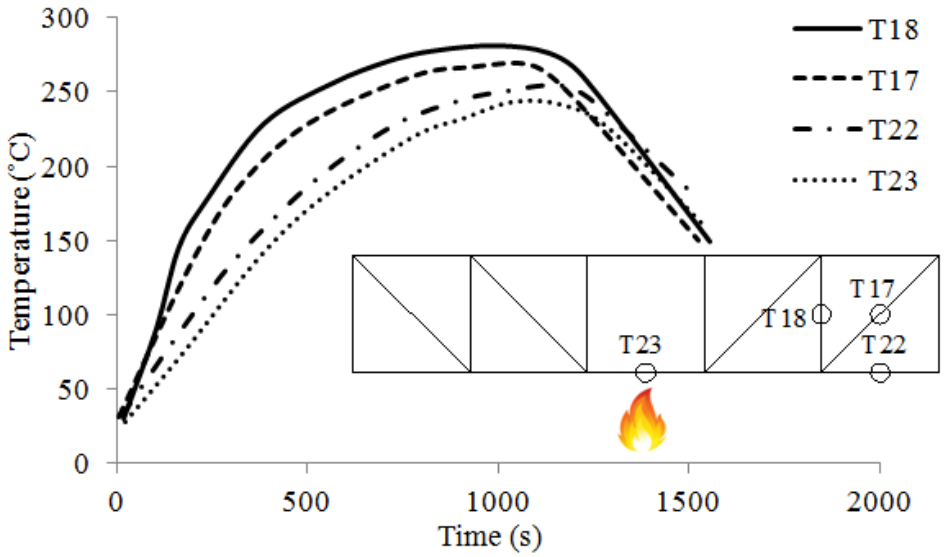

Figure 2.9 Temperature distribution in the truss (Chen et al., 2012)

Lin et al. (2014) carried out numerical simulations to investigate the effects of loading ratio, temperature distribution, fire location and size on the fire resistance of steel roof trusses under local fire exposure. Non-uniform temperature distribution along the truss was calculated by using equations of Du et al. (2012). Figure 2.10 shows typical temperature distribution along a truss, indicating temperatures away from the most heated truss member ranging from 65% to 75% of the highest temperature.

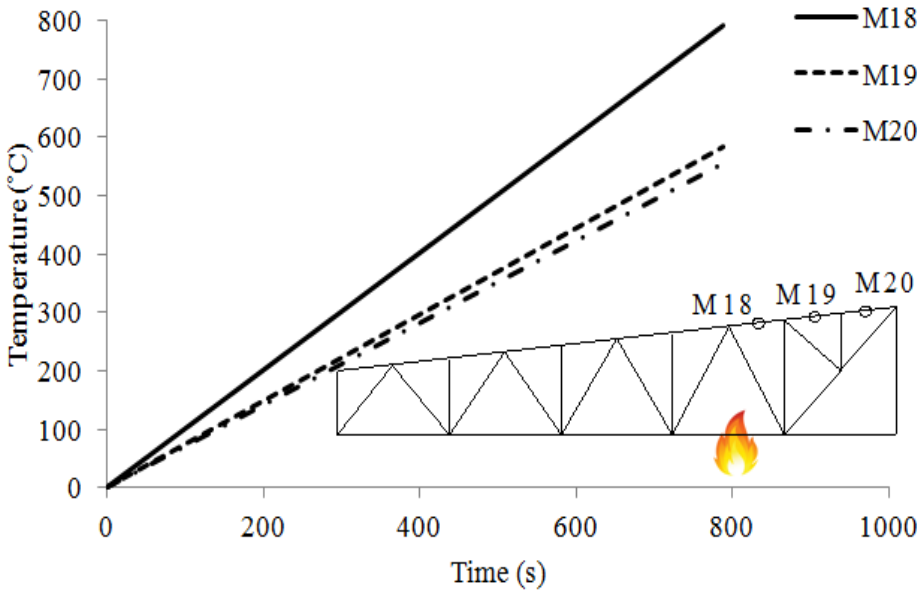

Figure 2.10 Temperature distributions in the chord members (Lin et al., 2014)

Yu et al. (2014) simulated the behaviour of steel space framed structures under localised travelling fires. The trusses were assumed to be pin-jointed at each end with a span of 32 m. A simplified fire spread model was used along the longitudinal direction of the structure as shown in Figure 2.11. Half of the span of the truss was divided into 4 zones and uniform temperature distribution was assumed in each zone. The maximum temperature was roughly 800 °C in the fire zone and the temperatures in other zones were approximately 600 °C, 400 °C and 250 °C depending on the distance from the fire zone. They found that the forces in all the heated compression members significantly increased due to the thermal elongation being restrained.

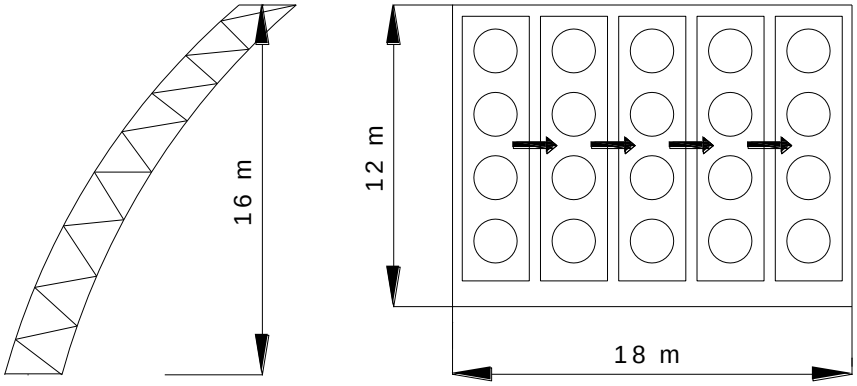

Figure 2.11 Fire spread direction (Yu et al., 2014)

Based on the review of this section, it is clear that there are large temperature variations in the different members of a truss when the truss is subjected to a localised fire. In order to gain an insight into the general behaviour of such trusses, temperature distributions in different members of the truss will be assumed, to cover different representative situations, in the author's research (Chapter 6).

2.3.2.2 Behaviour of restrained steel columns

When the different members of a truss experience different temperatures in a localised fire, restraint to the most heated truss member, which is usually the critical member, would induce additional compression force in the member. This section will review relevant research studies on restrained compression members.

An early study was presented in Wang and Moore (1994a); (1994b), who developed a methodology to evaluate the additional compression force in steel columns due to restrained thermal expansion. Referring to Figure 2.12, which shows a steel column

with axial restraint, the additional compression force in the member may be calculated using the following equation:

$$\Delta P = \frac{K_s K_c}{K_s + K_c}(\Delta\varepsilon_{th} - \Delta\varepsilon_{mec})\, l \qquad 2.5$$

where

K_s is axial stiffness of the restraint

K_c is axial stiffness of the column at elevated temperatures

$\Delta\varepsilon_{th}$ is free thermal strain of the column

$\Delta\varepsilon_{mec}$ is increase in the column mechanical strain due to reduction in the steel stiffness

The above equation was demonstrated to give an accurate prediction of the additional compression force in the column. The effect of $\Delta\varepsilon_{mec}$ becomes significant at high temperatures and high column loads.

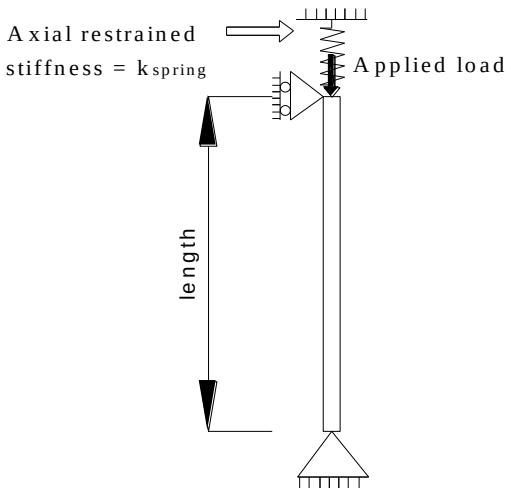

Figure 2.12 Definition of axially restrained steel column (Wang et al., 1994a)

Ali et al. (1998) tested 37 axially restrained steel columns in fire to investigate the influences of the column slenderness ratio, axial restraint ratio and column load ratio on the failure temperatures of the columns. The experimental results confirmed the general trend of decreasing column limiting temperature due to restrained thermal expansion.

Franssen (2000) used SAFIR to numerically investigate the behaviour and failure of axially restrained columns at elevated temperatures. Franssen noted that the increased column compression due to restrained thermal expansion would reduce the initial failure temperature of the column. However, if column failure is defined as the inability of the column to sustain the initially applied load in the column, the column failure temperature may be much higher than the initial column failure temperature under the increased load due to restrained thermal expansion. Franssen suggested that when dealing with restrained heated columns, the restraint may be considered to have infinite stiffness. However, this may not be correct because the post-buckling behaviour of a restrained column depends on the restraint stiffness. Under some conditions (moderate restraint stiffness), the column initial failure temperature is the same as the column final failure temperature, as found by Wang (2004) below.

Wang (2004) examined the post-buckling behaviour of axially restrained columns, considering the effects of the level of axial stiffness of the restraint. An analytical method was derived to trace the entire column load-temperature relationship, including increasing axial compression due to restrained thermal expansion, initial buckling and post-buckling behaviour, as shown in Figure 2.13. At low and moderate restraint stiffness (about 10% of the column axial stiffness), the axial force in the column decreases to below the initially applied load in the column, quickly after initial buckling. This means that the column failure temperature (as defined by Franssen to be the temperature at which the column load drops to below the initially applied load) is the same as the column initial buckling temperature. At high restraint stiffness, the post-buckling behaviour is more gradual and the column failure temperature is much higher than the column initial buckling temperature.

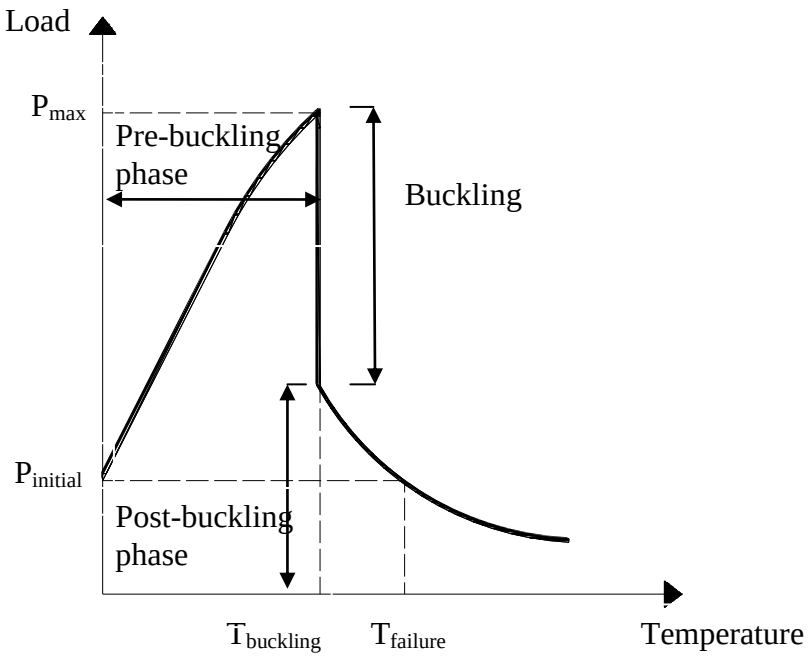

Figure 2.13 Load – temperature behaviour of restrained steel column in fire (Wang, 2004)

The previous research studies have identified the important factors that affect the behaviour and failure temperatures of axially restrained steel columns. However, they do not provide analytical solutions to calculating the column failure temperatures. To rectify these shortcomings, Wang et al. (2010) carried out a regression analysis of their extensive numerical simulations and derived a set of analytical equations to calculate the restrained column buckling and failure temperatures at elevated temperatures. Both axially loaded columns and columns with combined axial load and bending moment were considered. Referring to Figure 2.14 for the restrained column dimensions and properties, the following equations have been proposed:

$$T_f = T_0 - \Delta T_f \tag{2.6}$$

where T_0 is the limiting temperature of the unrestrained column; ΔT_f is the reduction in column failure temperature due to restrained thermal expansion.

$$\Delta T_f = F_\beta F_\rho F_\lambda \tag{2.7}$$

$$F_{\beta_l} = 12.432 - 12.796e^{-\beta_l/0.081} \tag{2.8}$$

$$F_\rho = 0.042 + 0.849\rho_N - 0.689{\rho_N}^2 + 0.204{\rho_N}^3 \tag{2.9}$$

$$F_\lambda = 28.624 + 1.053\lambda - 0.004\lambda^2 \quad (2.10)$$

F_β, F_ρ and F_λ refer to influences of the axial restraint stiffness, the initial axial load level and the column slenderness respectively on ΔT_f.

in which

$$\beta_l = \frac{k_l}{k_{c.0}} \quad (2.11)$$

where

β_l is axial restraint stiffness ratio

ρ_N is load ratio in the member

λ is member slenderness

k_l is axial stiffness of the axial restraint

$k_{c.0}$ is axial stiffness of the column at ambient temperature ($k_{c.0} = \frac{EA}{l}$)

The ranges of application are: $\beta_l < 0.10$; $\rho_N < 0.70$; $\lambda < 80$.

These analytical equations were derived based on numerical simulations of I-sections. They will be assessed for application to restrained tubular truss members in this research (Chapter 6).

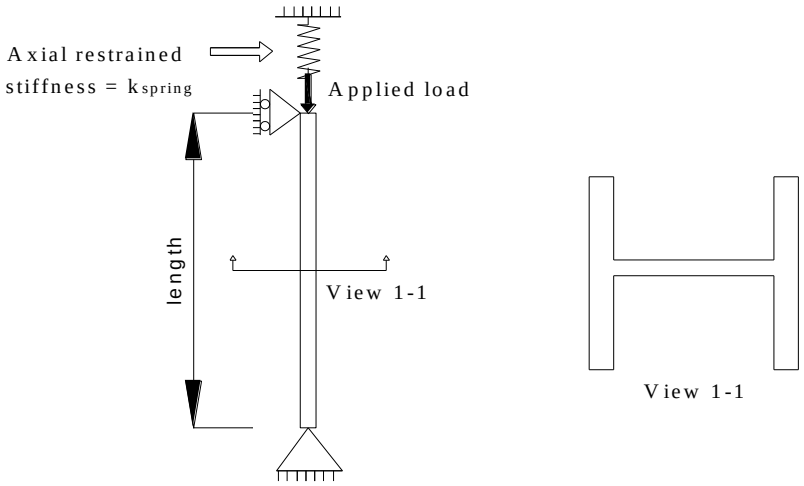

Figure 2.14 Finite element model of Wang et al. for axially restrained column (2010)

It is clear from the above literature review on restrained steel members that the additional compressive forces are considerable when the column is heated and the rest of the structural members are cool. The research studies reviewed in this section were conducted on single members. It is anticipated that the observations and conclusions of these research studies would be applicable to restrained truss members. However, to facilitate the design of steel trusses under localised fire, it is important to consider the effects of heating different numbers of members in the truss. This will be investigated in Chapter 6 of this thesis.

2.4 Originality and Objectives of This Research

Fire resistance design of a welded steel tubular truss requires calculation of the truss member forces and resistances of all the truss members and joints. Both will be addressed in this thesis, with chapter 4 being devoted to joints and chapters dealing with truss members.

From the above review of literature, it is clear that there have been many studies on the ultimate strength of welded tubular joints at ambient temperature and extensive design equations are available. Detailed assessments of different joint failure modes have concluded that the ambient temperature joint strength calculation equations can be applied to elevated temperatures after replacing the ambient temperature yield strength of steel with the elevated temperature values. The exception is the effect of large chord deformation on the chord plastification failure mode.

With regard to welded truss members, the literature review has revealed a lack of detailed investigation of how the truss member forces change at high temperatures, due to large deformation of the truss and different temperatures if the thermal expansions of some truss members are restrained by others. To facilitate design of welded steel tubular trusses exposed to fire attack, analytical methods should be developed. Together, they justify detailed research investigations. Specifically, the main objectives of this research are as follows:

(1) To develop a method to calculate the strength of welded steel tubular joints under the failure mode of chord plastification;
(2) To investigate how truss member forces change at elevated temperatures due to large truss deformations;

(3) To understand how, in trusses with different members heated to different temperatures as under the condition of localised heating, the failure temperature of the most heated member would change when different numbers of adjacent members are heated to different temperatures.

It should be pointed out that this thesis focuses on the mechanical response of welded trusses and their joints at elevated temperatures, in particular, methods to calculate their limiting temperatures. Although fire is not explicitly considered, the findings of this research can be readily applied to evaluate the fire resistance of such structures under different types of fire exposure such as those shown in Figure 2.15, by comparison of the structural temperatures attained under fire exposure to the limiting temperatures of the structure.

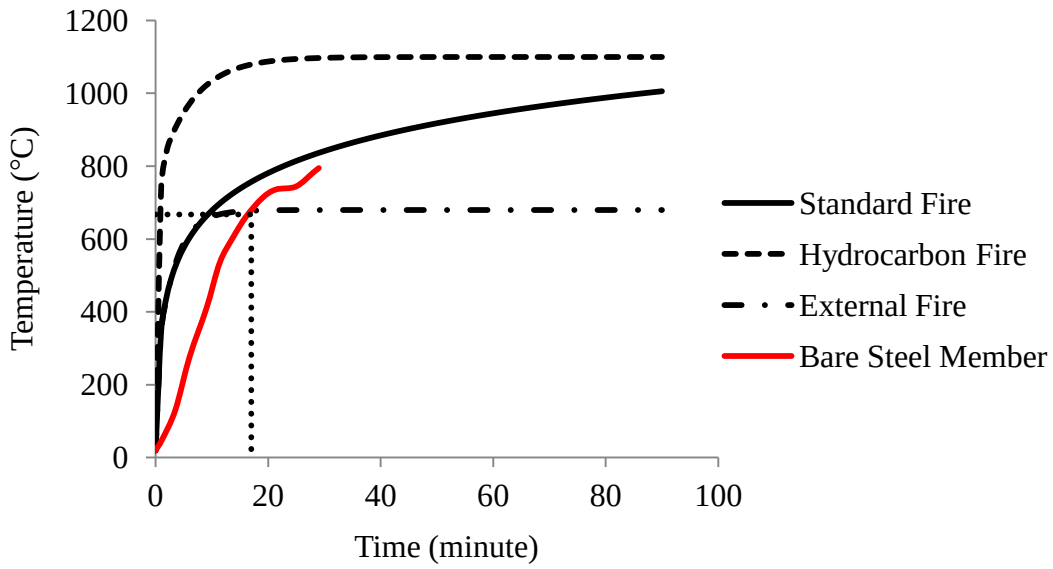

Figure 2.15 Standard time – temperature curves (CEN, 2002)

2.5 Conclusions

This chapter has presented a thorough review of welded steel tubular truss behaviour and design at ambient and elevated temperatures. The review is divided into two parts: focusing on the joints and on the members.

Welded steel tubular joints have been extensively researched at ambient temperature. These research studies have addressed all different failure modes and design equations are available in design codes and design guides such as EN 1993-1-8 (CEN, 2005b) and CIDECT (Wardenier et al., 2010a). These design equations can be

extended to elevated temperatures. However, for chord plastification, further research is necessary because large chord deformation may change the chord plastification mechanism.

The review on truss member behaviour has revealed a lack of detailed investigation on how the truss member forces change at elevated temperatures from those at ambient temperature. There are two sources of such change: due to change of truss geometry when the truss deflections are large, and due to restrained thermal expansion when different truss members are heated to different temperatures, as in the case of a localised fire attack.

The main work of this thesis will address these three topics.

CHAPTER 3 VALIDATIONS OF NUMERICAL SIMULATION MODEL

3.1 Introduction

The research of this thesis will be based on numerical simulations of steel tubular trusses and joints. It is important that the numerical simulation models are valid. The numerical models will be developed using the general finite element package ABAQUS/Standard v6.10-1 (2010). This chapter will present the numerical simulation models and compare the simulation results against available experimental results of steel tubular trusses and joints at elevated temperatures and in fire.

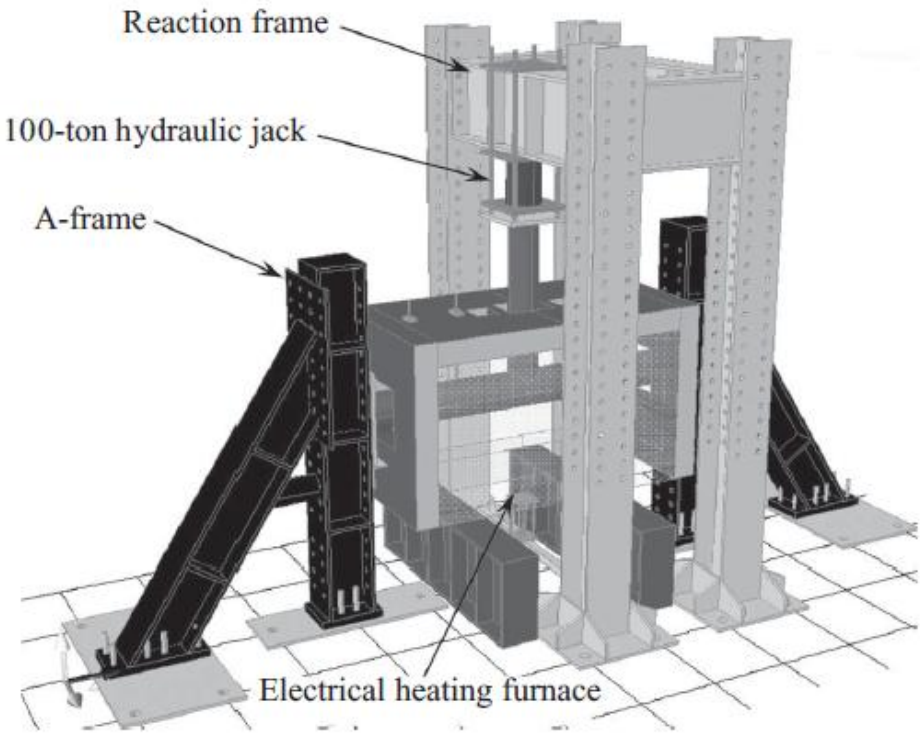

Figure 3.1 Overall setup of the T-joints tests at elevated temperatures (Nguyen et al., 2012)

3.2 Validation of Finite Element Model for Tubular Joints

The numerical model for welded steel tubular joints will be checked against the elevated temperature tests of Nguyen et al. (2010)and the ambient temperature tests of Kurobane et al. (1986). Nguyen et al. (2010) tested tubular T-joints (Figure 3.2(a)) at 20 °C, 550 °C and 700 °C, which appear to be the only elevated temperature tests on joints. The comparison against the test results of Kurobane et al. (1986) at ambient temperature, on K-joints, is to ensure that the numerical model can simulate different types of joints. Figure 3.2(b) shows Kurobane et al.'s test arrangement. Owing to symmetry in loading and geometry, to reduce the computational time, only a quarter of the T-joints and half of the K-joints will be modelled, with the boundary conditions for symmetry being applied to the nodes in the various planes of symmetry.

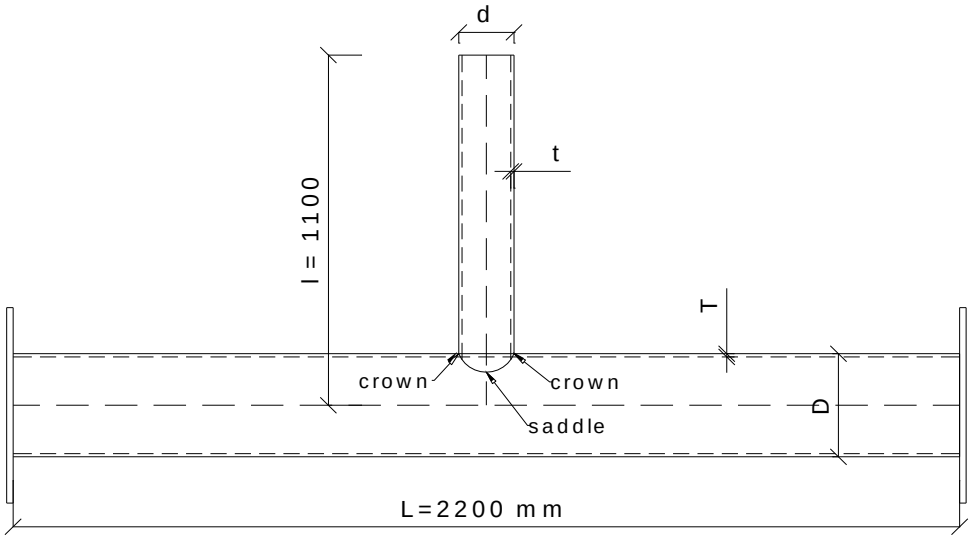

a) PT3-joint (Nguyen et al., 2012)

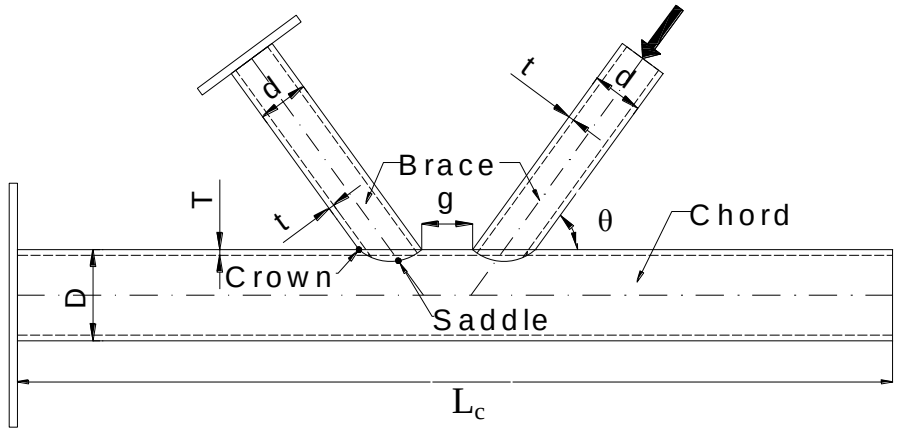

b) G2C- joint (Kurobane et al., 1986)

Figure 3.2 Typical test arrangements and geometries

Table 3.1 lists the dimensions of the test joints used in the validation, where the following symbols are used to define the joint dimensions.

- Chord outside diameter, D
- Brace outside diameter, d
- Chord thickness, T
- Brace thickness, t
- Chord length, L_c
- Gap between braces, g

The dimensionless parameter, β, is the ratio of the brace diameter to the chord diameter (=d/D). θ is the angle between the brace and chord members.

The elevated temperature tests of Nguyen et al. (2010) were carried out under the steady state condition in which the temperature of the structure was raised to the required level and the mechanical load was then applied. Because of this, the Riks method will be chosen to simulate the large deformation behaviour.

Table 3.1 Dimensions of the joint test specimens used for validation

Joint Name	D (mm)	d (mm)	T (mm)	t (mm)	g (mm)	β (d/D)	θ (^{0})
PT3 (Nguyen et al., 2012)	244.5 (L_c=2200)	168.3 (l_b=1100)	6.3	6.3	-	0.69	90
G2C (Kurobane et al., 1986)	216.4 (L_c=1560)	165.0 (l_b=800)	7.82	5.28	29.5	0.76	60

Figure 3.3 shows the boundary conditions used in the tests and also in the numerical simulation model.

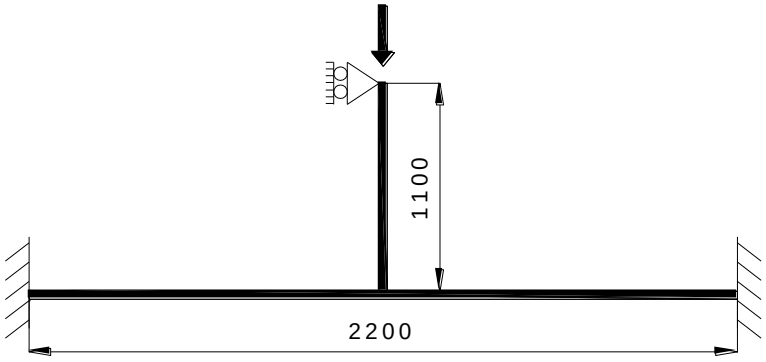

a) Nguyen et al., 2010

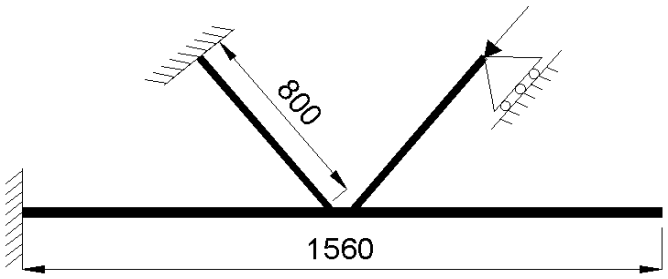

b) Kurobane et al., 1986

Figure 3.3 Boundary conditions of the tested joints (dimensions in mm)

3.2.1 Material properties

For the tubular T-joints tested by Nguyen et al. (2010), the steel grade was S355 with a nominal yield strength f_y= 380 N/mm^2 and an ultimate strength f_u= 519 N/mm^2

from the coupon tests at ambient temperature. The elastic modulus of steel was assumed to be 210 GPa. The elevated temperature stress- strain curves will be based on EN-1993-1-2 (CEN, 2005a). In the ABAQUS simulation model, the engineering stress-strain curve is converted into a true stress and logarithmic strain curve to consider the nonlinear effects of large displacements by using the following equations (Boresi et al., 2003).

$$\varepsilon_T = \ln(1 + \varepsilon) \quad 3.1$$

$$\sigma_T = \sigma.(1 + \varepsilon) \quad 3.2$$

where ε_T , is the true strain

ε , is the engineering strain

σ_T , is the true stress

σ , is the engineering stress

For the K-joint tests performed by Kurobane et al. (1986), the nominal yield strengths were $f_{y,c}$= 480 N/mm^2, $f_{y,b}$= 363 N/mm^2 and the ultimate strengths were $f_{u,c}$= 532 N/mm^2, $f_{u,b}$= 436 N/mm^2 for the chord and brace members respectively.

3.2.2 Interactions and load application

In the case of welded joint models, both the brace and chord members are tied with weld elements using the ABAQUS "tie" function. The discretisation method is defined as the surface to surface contact. The brace and chord members at the connection region are chosen as the master surface, while the weld element is the slave surface. In the models not including weld, the brace and chord members are tied together instead of using the weld elements.

There are two methods to apply the mechanical loads in ABAQUS: Static and Riks methods. In order to examine the effects of large deformations in the joints after reaching the maximum load, the Riks method will be chosen. The applied loads are applied in small increments of the total to capture the non-linear structural behaviour.

3.2.3 Mesh convergence

A mesh convergence study has been carried out to determine the suitable simulation model. The same mesh size will then be applied to simulation models for all other joints. The ABAQUS element type S8R is used. Test PT3 of Nguyen et al. (2010) is selected for this case, and Figure 3.4 shows the mesh layout. Figure 3.5(a) and Figure

3.5(b) present the mesh sensitivity study results for the tubular sections and for the weld in the joint zone near the welds. Mesh sizes of 10 mm and 5mm can be seen to be suitable for the members and the weld. Outside the joint zone, a coarse mesh (20 mm) can be used.

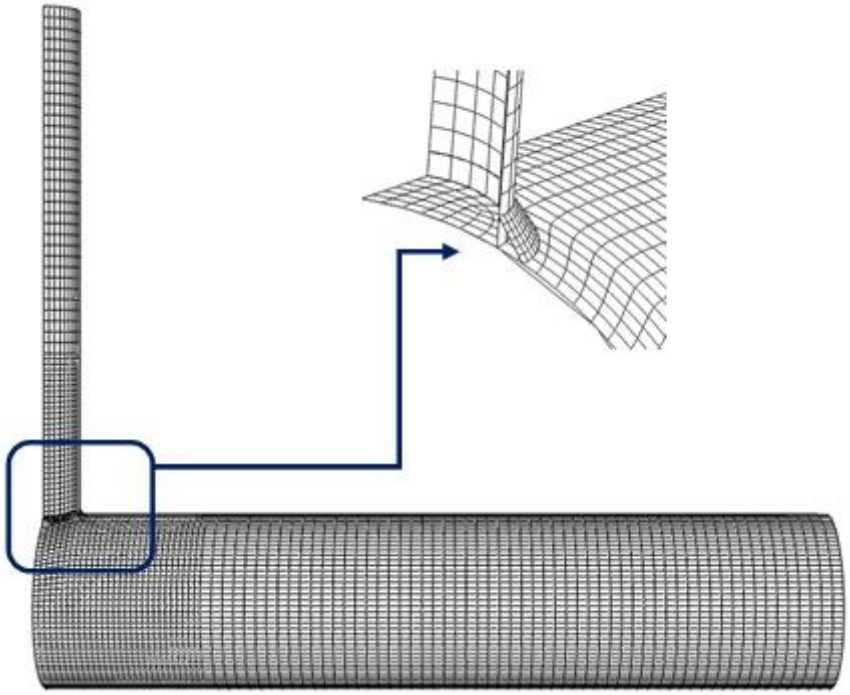

Figure 3.4 Mesh layout

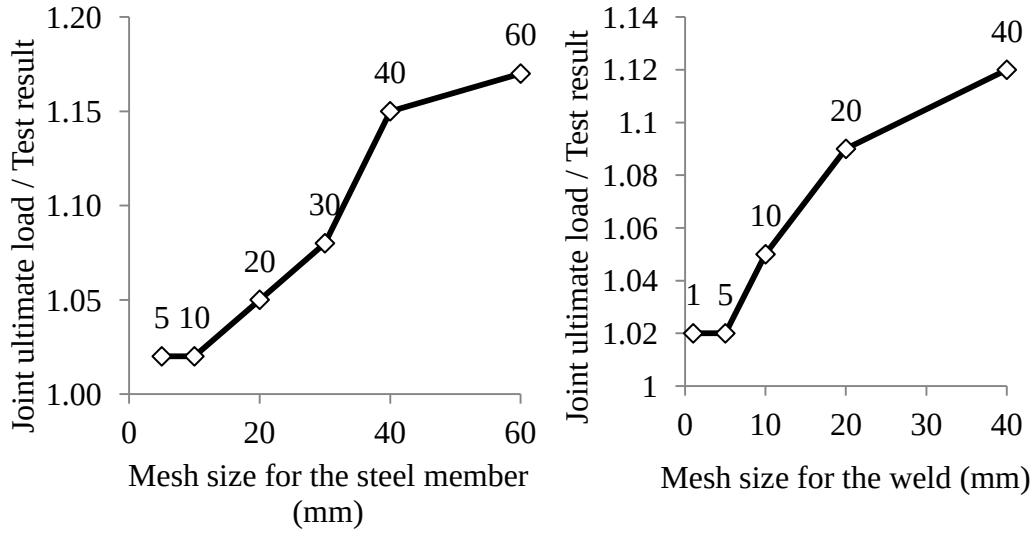

a) Steel members b) Weld

Figure 3.5 Mesh size sensitivity study results

3.2.4 Finite element type

For the chord and brace members, ABAQUS element types C3D20R (20-noded solid element, Figure 3.6(d)), S8R (8-noded quadrilateral shell element, Figure 3.6(b)) or S4R (4-noded shell element, Figure 3.6(a)) may be used. For weld modelling, quadratic wedge, a solid element (C3D15, Figure 3.6(c)), 8-noded quadrilateral shell element (S8R) or 4-noded shell element (S4R) may be used.

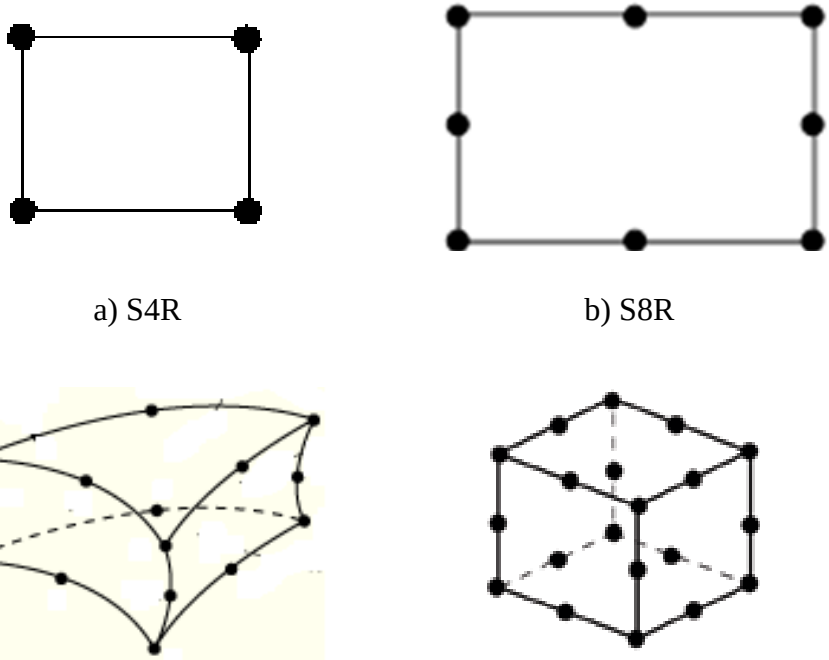

a) S4R b) S8R

c) C3D15 d) C3D20

Figure 3.6 Element types used in the simulations (ABAQUS/Standard, 2010)

Figure 3.7 shows the 3D mesh with weld details by using shell or solid elements.

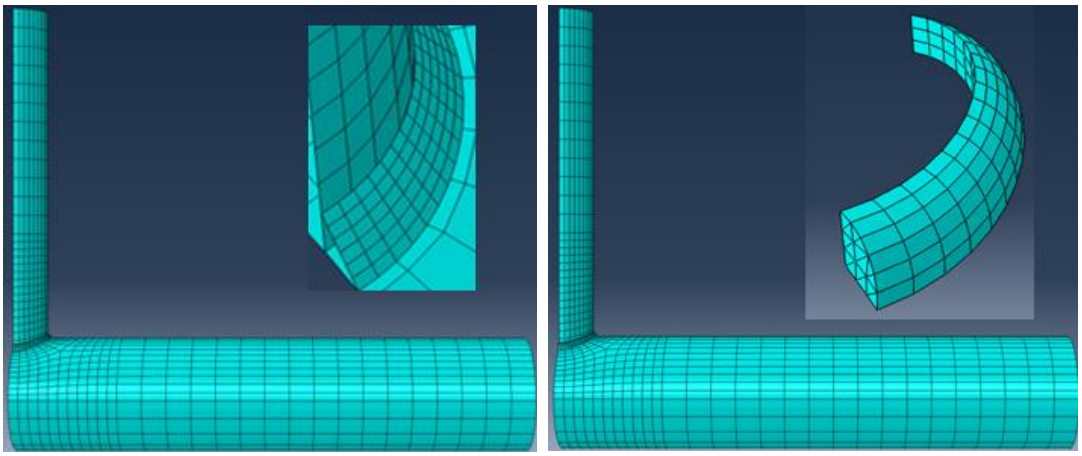

a) Shell Element b) Solid Element

Figure 3.7 Mesh and weld detail for test joint PT3 by using different types of element

Figure 3.8 compares the simulation and test load-deflection curves of test PT3 of Nguyen et al. (2010) at ambient temperature. Also shown in Figure 3.8 is the 3% deflection limit (0.03*D*), according to Lu et al. (1994) which is used to determine the ultimate load carrying capacity of the joints. From the comparisons, it can be seen that the 8-noded shell elements and solid elements give a close examination to the test result of Nguyen et al., but using the 4-noded thick shell elements overestimates the ultimate capacity of the PT3 joint. There is some difference between the predicted plastic behaviour and the test result before the specimen reached the maximum load. This may be caused by initial plastic deformation of the joint due to faulty operation of the hydraulic jack at the loading step as noted by Nguyen during the test. However, this did not affect the ultimate strength and post-peak behaviour, which are closely simulated by the numerical model.

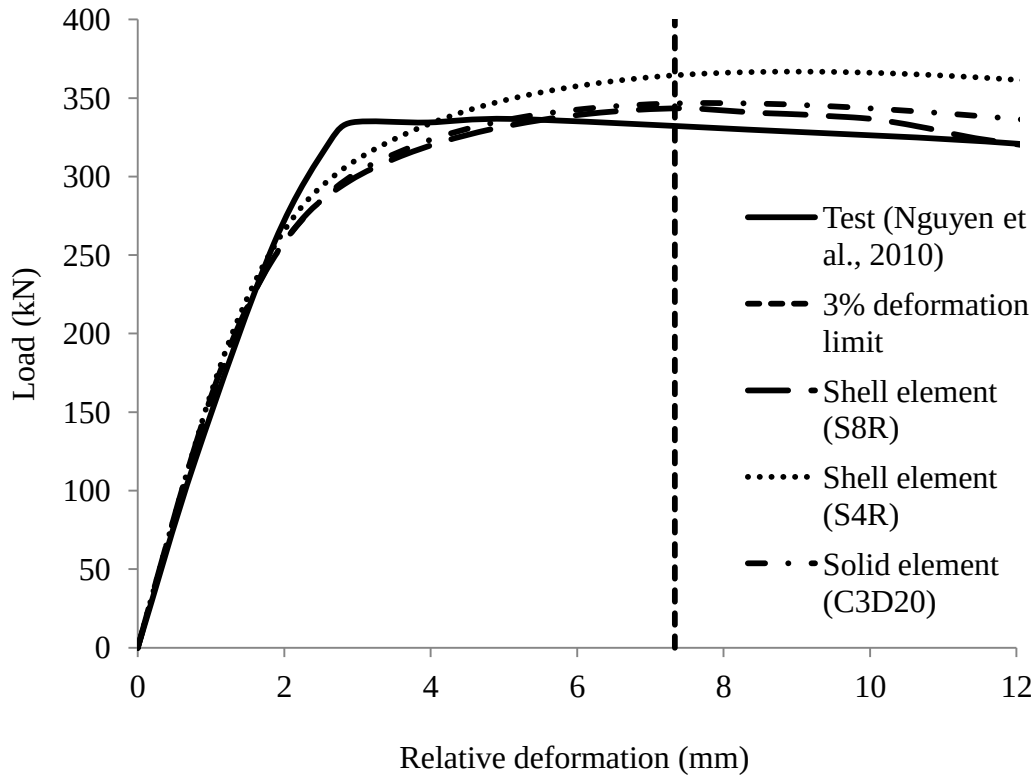

Figure 3.8 Comparisons between using different types of finite elements at ambient temperature, test PT3 (Nguyen et al., 2012)

Table 3.2 summarises the simulation results using the different types of element. As already mentioned, using the 4-noded shell elements (S4R) overestimated the joint load carrying capacity. Although both the 8-noded thick shell and solid elements gave good results, modelling the joint using solid elements required considerably more computational time than using shell elements. In particular, when using solid elements, ABAQUS requires at least two layers of elements so as not to overestimate the real behaviour.

Table 3.2 Sensitivity of numerical results for test PT3 of Nguyen et al. (2010) at ambient temperature

	Number of elements	Relative CPU-time	Ultimate load (kN)	Strength Ratio
Test result of Nguyen et al.	-	-	338.8	1.00
Solid elements (C3D15)	9699	11.9	346.5	1.02
Shell elements (S8R)	3555	1.00	343.4	1.01
Shell elements (S4R)	3555	0.24	366.8	1.08

As a recommendation, 8-noded thick shell elements (S8R) with 5 integration points through the element thickness are suitable to model the brace and chord members. The same method was used by van der Vegte et al. (1995; 2005). For modelling the weld, quadratic wedge solid elements (C3D15) can be used for accurate meshing of the weld geometry (Cofer et al., 1992).

3.2.5 The effect of modelling weld geometry on strength of tubular joints

The most complex region in the tubular joint is that surrounding the weld, even in the simplest connection. ABAQUS provides a number of methods for modelling the weld geometry by using shell or solid elements. This section compares the simulation results using the following three methods of modelling the weld:

- Including the weld using solid elements,
- Including the weld using shell elements,
- Excluding the weld.

Table 3.3 compares the simulation results. Provided the weld is included, using either shell or solid elements gives satisfactory results. If the weld is not included, the predicted ultimate capacity of the joint is 11% lower than the test result. These results agree with the findings of van der Vegte et al. (1995), who found that

excluding the weld may give a predicted joint capacity more than 20% lower than the test results.

Table 3.3 Comparison of numerical results for test PT3 of Nguyen et al. (2010) with or without modelling the weld

	Ultimate load (kN)	Strength Ratio
Test result of Nguyen et al. (2010)	338.8	1.00
Including the using solid elements (C3D15)	343.4	1.01
Including the weld using shell elements (S8R)	345.2	1.02
Excluding the weld	301.3	0.89

Modelling the weld using 3D solid elements is more realistic than using shell elements because it allows varying thicknesses of weld to be modelled. Solid elements will be used in all future numerical simulation models.

3.3 Validations against Available Test Results for Tubular Joints

Figure 3.9 (a) compares the simulation load-deflection curves with the test results of Nguyen et al. (2010) for joint PT3 at three different temperatures and Figure 3.9 (b) for joint G2C of Kurobane et al. (1986). The relative displacement refers to the difference of the axial displacement of the brace (δ_1) relative to the central chord. In all cases, the agreement is excellent for T-joints. For the K-joint, the results in Figure 3.9 (b) also indicate very good agreement. Figure 3.10 further compares the simulated and observed deformed shapes of the PT3 joint at 20 °C and 700 °C. Failure was due to chord plastification at both ambient and elevated temperatures. The positions of the plastic hinges were close to the brace member at high temperatures as observed in the test and simulation model. The numerical model clearly gave a faithful representation of the test.

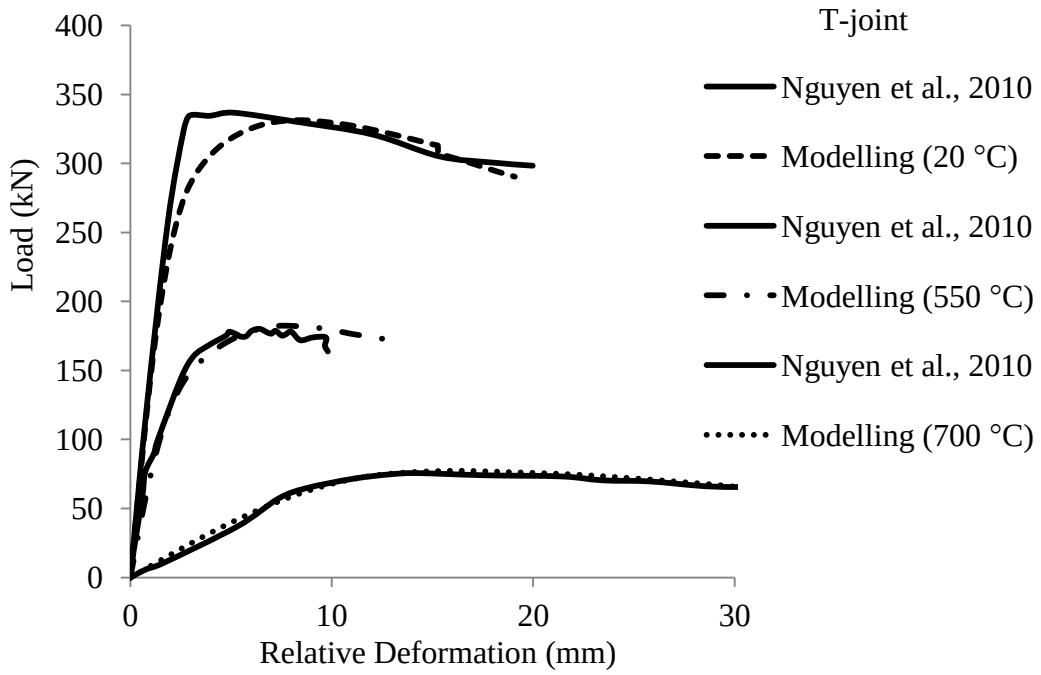

a) PT3-joint (Nguyen et al., 2012)

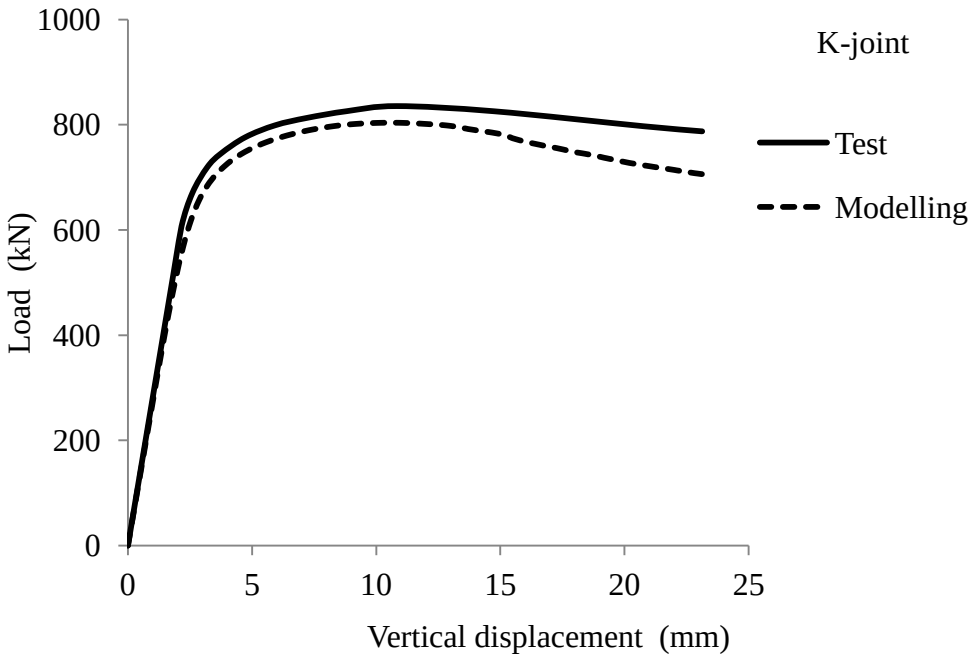

b) G2C- joint (Kurobane et al., 1986)

Figure 3.9 Comparison for load-displacement curves for T- and K-joints

From these comparisons, it can be concluded that the numerical simulation model is suitable for simulation of the behaviour of T- and K- welded tubular joints. These models will be used to conduct the parametric study in the next chapter to obtain the ultimate load carrying capacities of welded tubular joints at different temperatures.

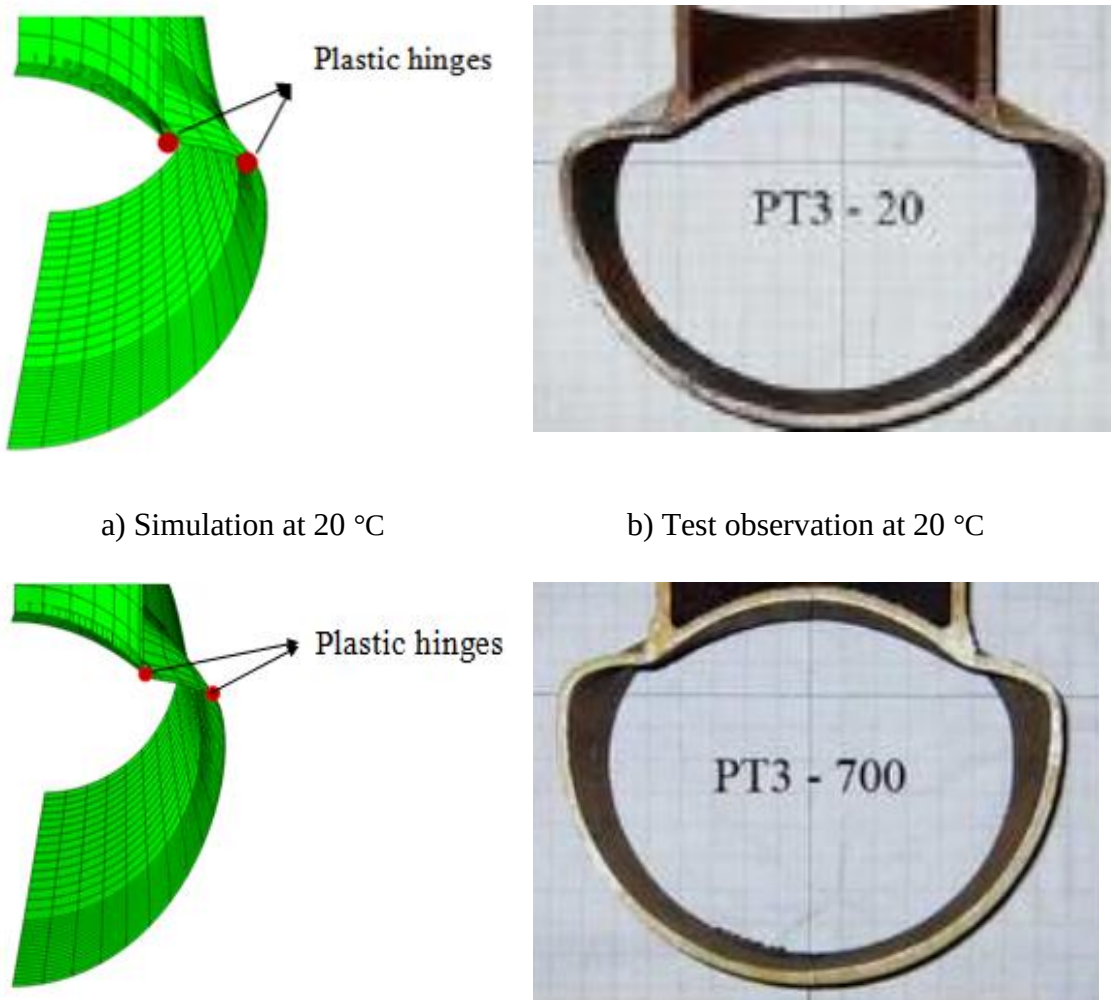

a) Simulation at 20 °C

b) Test observation at 20 °C

c) Simulation at 700 °C

d) Test observation at 700 °C

Figure 3.10 Comparison of deformed shapes of joint PT3 between FE modelling and test observations (Nguyen et al., 2012)

3.3.1 Comparison of failure loads between numerical and test results and design guide predictions

Having established the numerical simulation model at ambient temperature, this section compares the modelling results with those at elevated temperatures. Table 3.4 summarises the comparison between the modelling results, the test results of Nguyen et al. (2010) and the steel yield strength reduction factors of EN 1993-1-2 (CEN, 2005a). All the results are normalised to those at ambient temperature.

Table 3.4 Comparison between modelling and test results and EN 1993-1-2 yield strength reduction factors

Test temperature	20 °C	200 °C	400 °C	526 °C	680 °C
Test results of Nguyen et al. (2010)	1.00	-	-	0.53	0.22
Simulation results	1.00	0.91	0.85	0.55	0.23
Steel yield strength reduction factor from EN-1993-1-2 (CEN, 2005a)	1.00	1.00	1.00	0.70	0.28

It can be seen that the numerical simulation results and test results are in good agreement at different levels of the test temperature. However, the steel yield strength reduction factors at elevated temperatures are generally higher than the numerical simulation and test strength ratios. This will be further examined in the next chapter.

3.4 Validation of Trusses at Elevated Temperatures

To validate the simulation model for welded steel tubular trusses, the simulation results will be compared against the fire tests of Edwards (2004) and the elevated temperature tests of Liu et al. (2010). Figure 3.11 and Figure 3.12 show the different test arrangements. Table 3.5 summarises the applied loads in the test girders of Edwards (2004).

Table 3.5 Applied loads at the top chord of the girders of Edwards (2004)

Girder	1/4 point	Centre
A	96 kN	210 kN
B	78 kN	216 kN

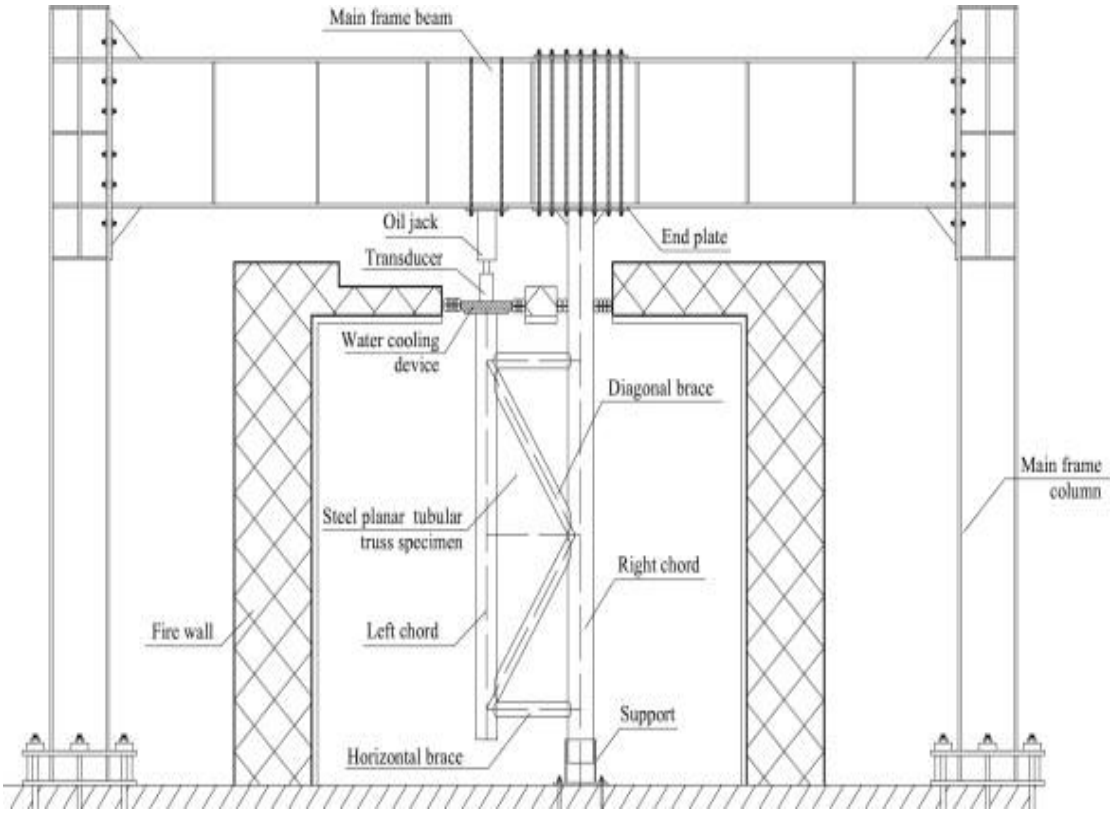

a) Test setup of the truss at elevated temperatures

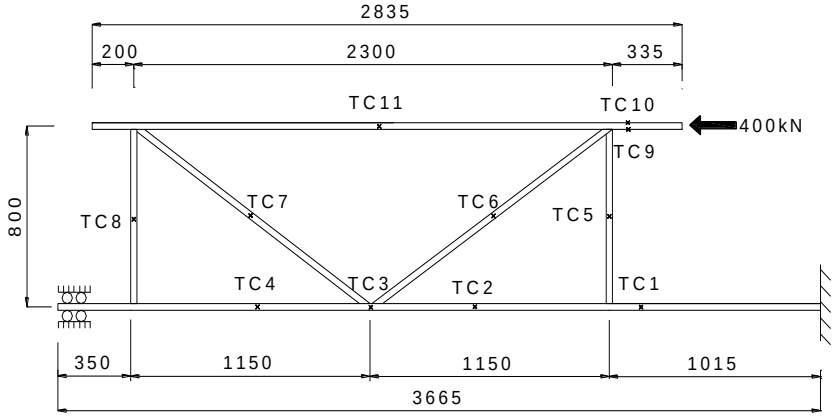

b) Test specimen SP1 (dimensions in mm)

Figure 3.11 Details of test specimen of Liu et al. (2010)

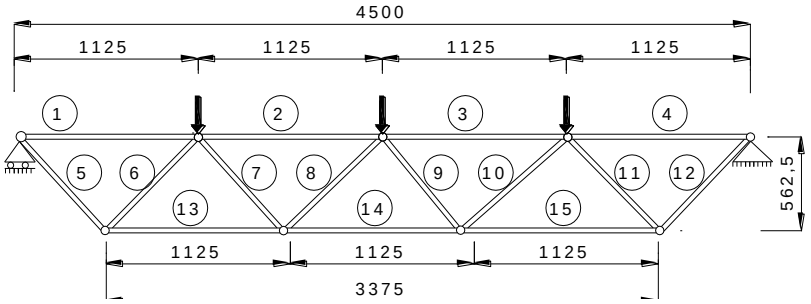

Figure 3.12 Fire test girders of Edwards (2004) (dimensions in mm)

3.4.1 Material properties

Table 3.6 summarises the member sizes and material grades for the tests of Edwards (2004) and Liu et al. (2010). For both tests, the ambient temperature mechanical properties are based on their coupon results. In the fire tests of Edwards (2004), extensive temperature measurements of the truss members were made in both tests and the recorded temperatures will be used in the author's numerical simulation.

Table 3.6 Dimensions and ambient temperature mechanical properties of the test trusses

Member Type	Dimensions (mm)	Steel Grade	Young's modulus (GPa)	Yield stress (MPa)	Tensile Stress (MPa)
Test A & B (Edwards, 2004)		SHS			
Inner bracings (Members 7, 8, 9 and 10)	50 x 50 x 5.0 for Test A 60 x 60 x 4.0 for Test B	43C (S275)	190	280	440
Outer bracings (Members 5,6, 11 and 12)	60 x 60 x 8.0 for Test A 60 x 60 x 8.0 for Test B	43C (S275)	190	280	440
Top chord (Members 1, 2, 3 and 4)	100 x 100 x 10.0 for Test A & B	50C (S355)	210	400	575
Bottom chord (Members 13, 14 and 15)	100 x 100 x 10.0 for Test A & B	50C (S355)	210	400	575
SP1 (Liu et al., 2010)		CHS			
Brace	102x5	Q345B	202	376	559
Top chord	180x8	Q345B	193	368	553
Bottom chord	219x8	Q345B	196	381	565

The elevated temperature engineering stress-strain curves are shown in Figure 3.13, based on EN-1993-1-2 (CEN, 2005a).

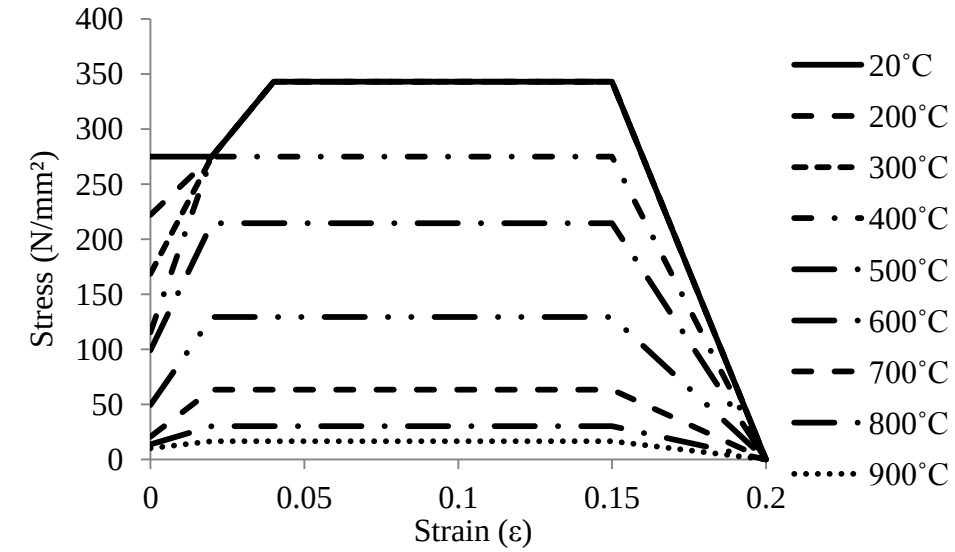

a) f_y = 275 N/mm^2

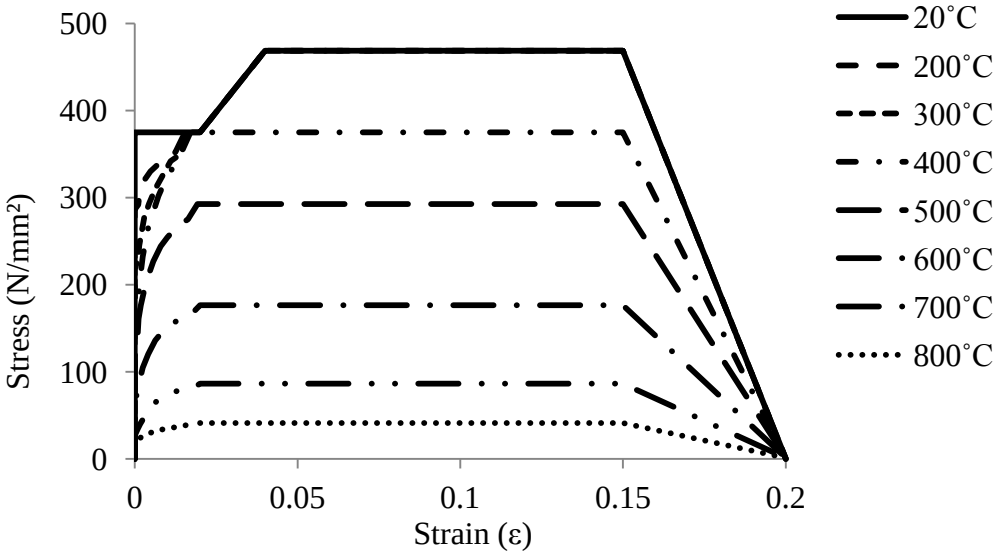

b) f_y = 375 N/mm^2

Figure 3.13 Engineering stress-strain relationships of steel at elevated temperatures (according to EN 1993-1-2 (CEN, 2005a))

3.4.2 Finite element type and initial

For the chord and brace members, ABAQUS element types S4R (4-noded shell element) or B21 (2-noded line element) may be used. In the case of modelling using shell elements, quadratic wedge solid elements (C3D15) instead of shell elements are used for the weld to allow accurate meshing of the weld geometry (Cofer et al., 1992). At the weld-tubular section interface, the brace and chord members are tied with the weld elements using the ABAQUS "tie" function with surface to surface

contact. The brace and chord members are chosen as the master surface and the weld elements as the slave surface. Owing to symmetry in loading and geometry, to reduce computational time, only half of the truss is modelled when using shell elements, with the boundary conditions for symmetry being applied to the nodes in the various planes of symmetry as shown in Figure 3.14. The attached plate on top of the chord at detail A is to enable application of the mechanical load without local stress concentration.

Eigenvalue buckling analysis was performed on the numerical models in order to define the possible buckling modes for compressed members in the trusses. The initial imperfections were based on the lowest buckling mode from the eigenvalue analysis. The maximum initial imperfection was according to EN 1993-1-1 (CEN, 2005c), being the member length / 250.

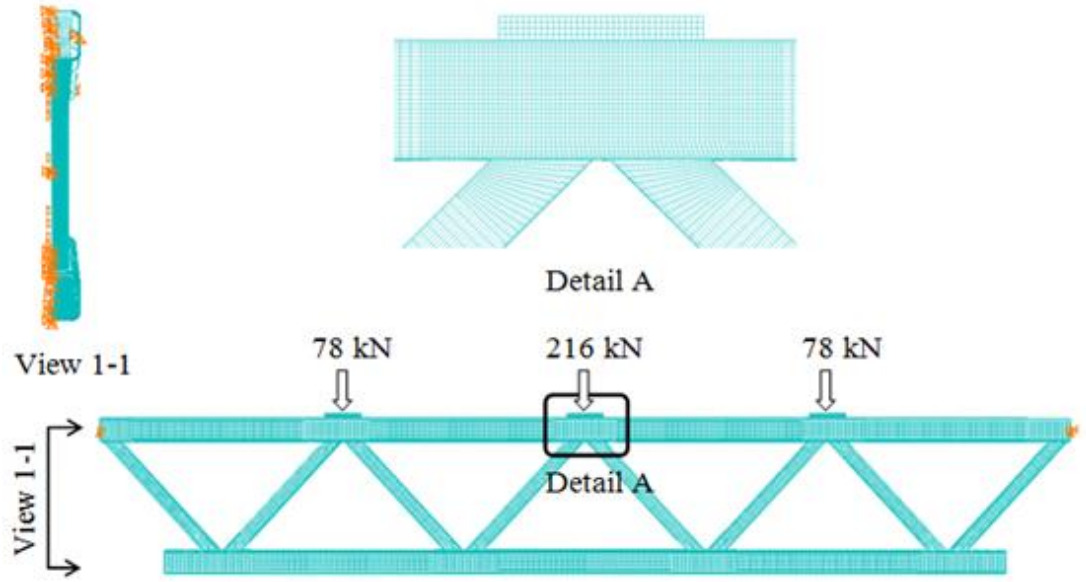

(a) Girder (test) B (Edwards, 2004)

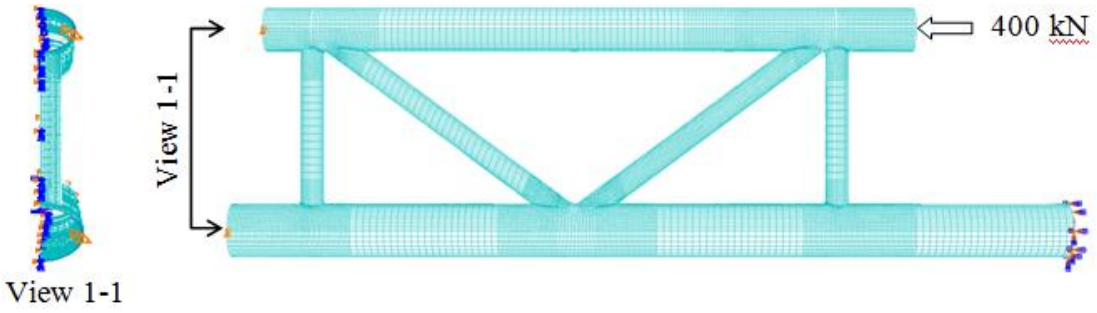

(b) SP1 (Liu et al., 2010)

Figure 3.14 Truss simulation models of the test trusses for validation study

3.4.3 Comparison of results for test SP1 of Liu et al. (2010)

Figure 3.15 shows the recorded test temperatures (see Figure 3.11 for locations of the thermocouples). These temperature curves were used in the numerical simulation.

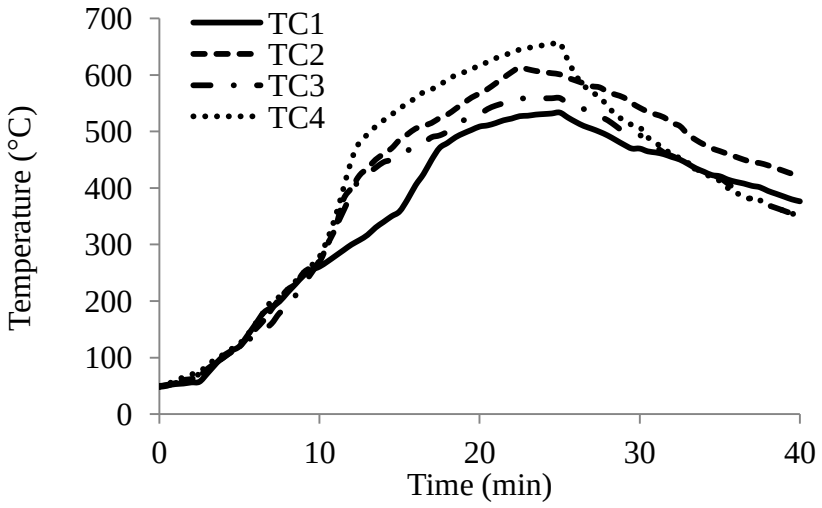

a) TC1 - TC4

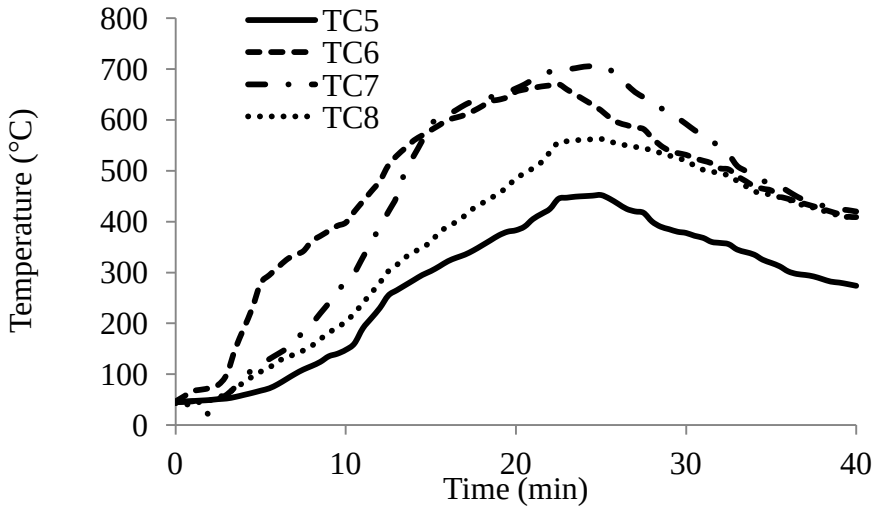

b) TC5 – TC8

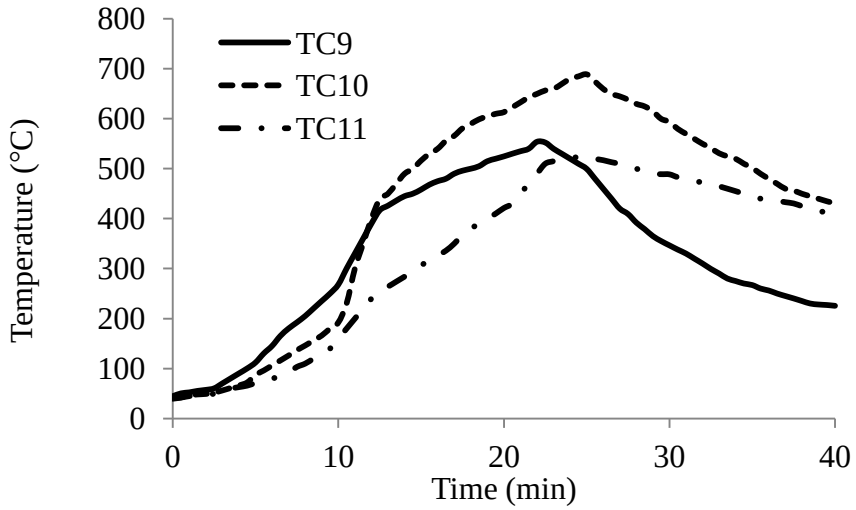

c) TC9 – TC11

Figure 3.15 Recorded temperature-time curves of thermocouples TC1 – TC11 for test SP1 (Liu et al., 2010)

The test truss failed due to buckling of the diagonal brace member in compression. Figure 3.16 compares the observed failure mode of the truss and the simulated deformed shapes using both shell elements and line elements for the brace and chord members. The agreement between the test and simulation results is excellent. This indicates that using line elements is acceptable if failure of the truss is due to member, not joint, failure. Figure 3.17 compares the detailed simulation displacement-temperature curves with the test results of Liu et al. (2010). From the comparison, it can be seen that both the 4-noded shell elements and line elements give a close approximation of the test results. Form the test, the maximum temperatures, at which the truss is no longer able to support the applied loads, from the simulations using shell elements and using line elements are 678 °C, 642 °C and 636 °C respectively. This agreement is acceptable.

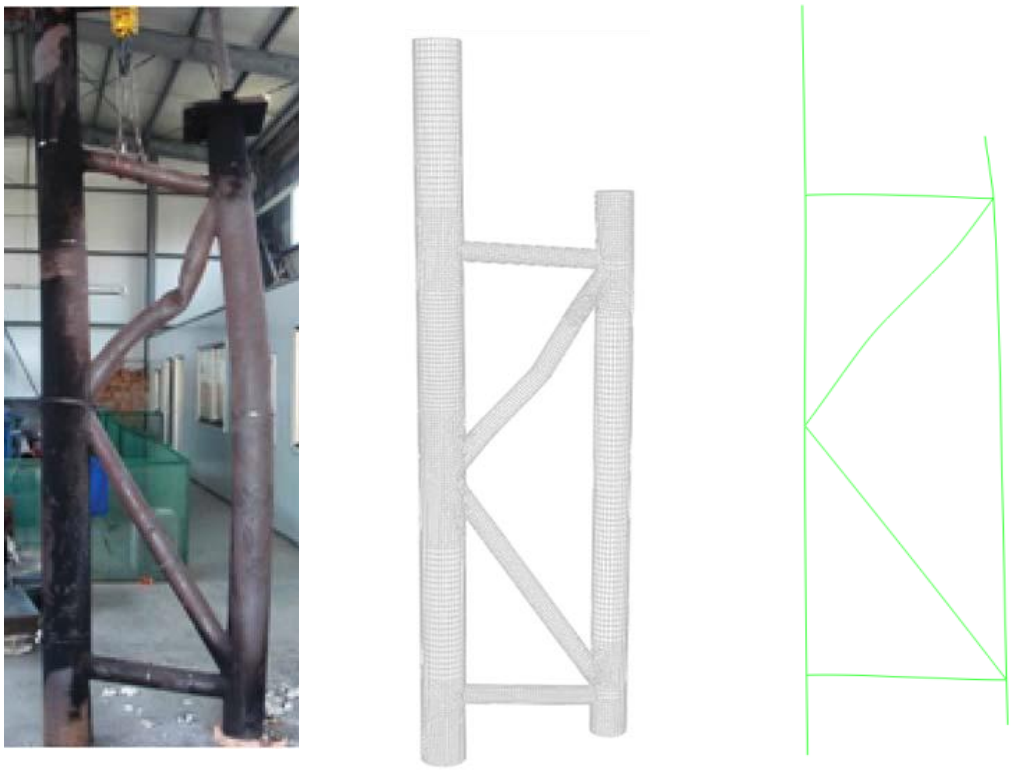

a) Test observation (Liu et al., 2010)

b) Using shell elements

c) Using beam elements

Figure 3.16 Comparison of failure modes

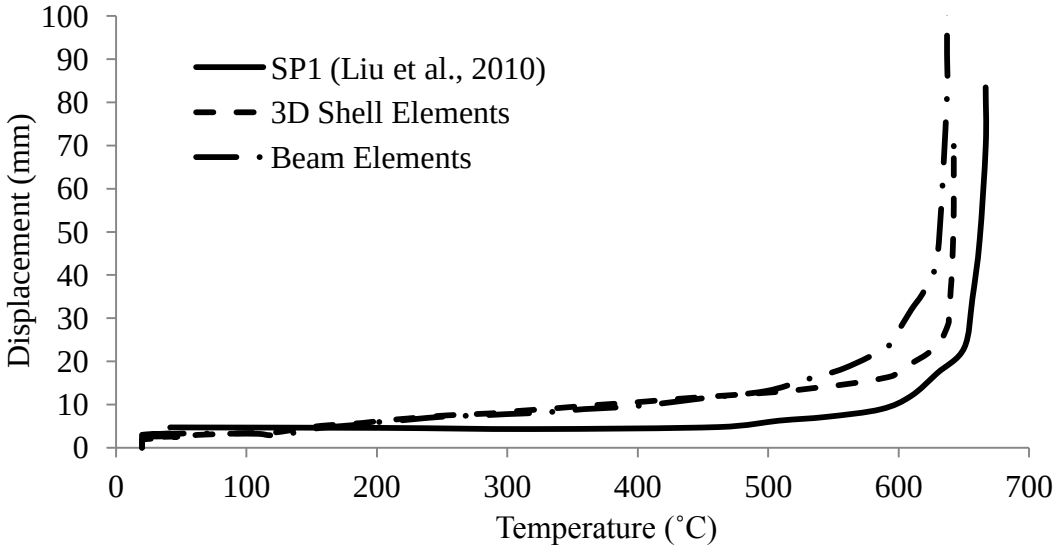

Figure 3.17 Comparison for displacement-temperature curves of SP1

3.4.4 Comparison of results for Girder (Test) of Edwards (2004)

Figure 3.18 shows the recorded temperatures in the different truss members.

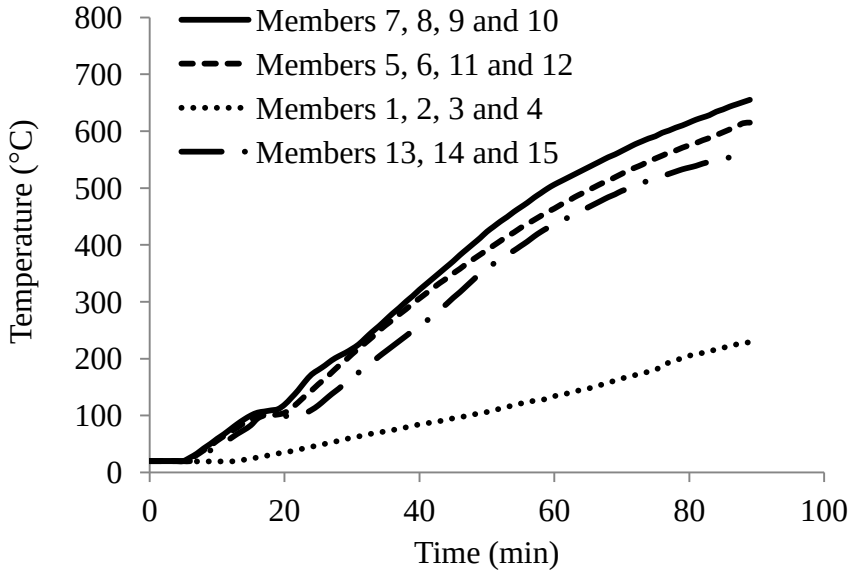

a) Girder A

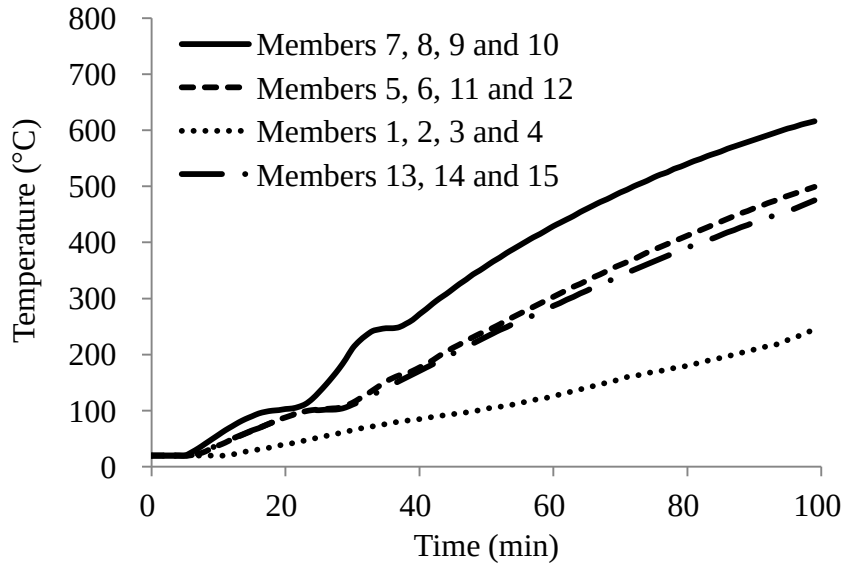

a) Girder B

Figure 3.18 Temperature-time curves of test girders (Edwards, 2004)

Figure 3.19 compares the displacement-temperature curves at the centre point of the top chord member. The agreement with the test result is excellent using both the line and shell elements.

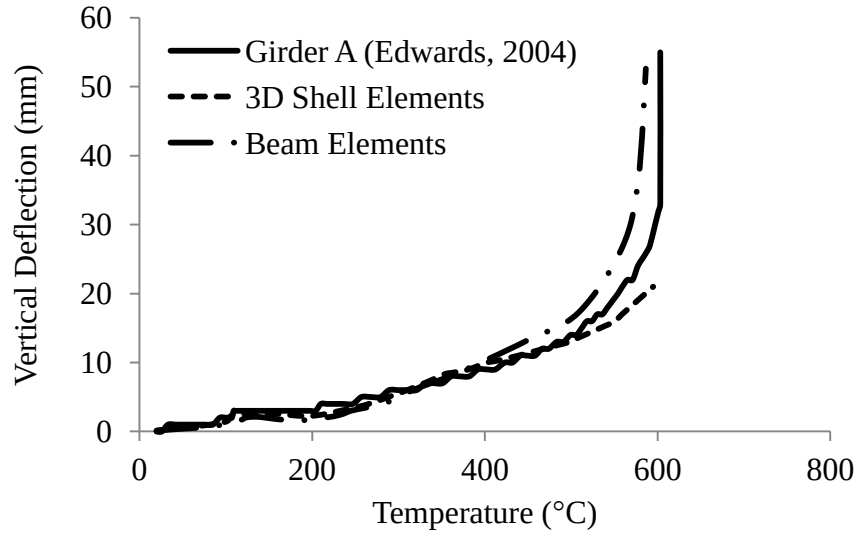

a) Girder A

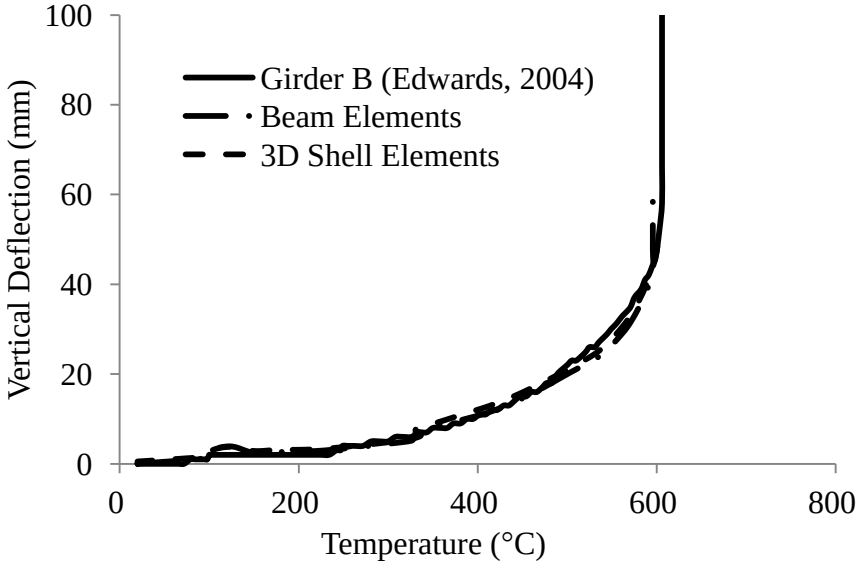

b) Girder B

Figure 3.19 Comparison for displacement-temperature curves of Girders of Edwards (2004)

Figure 3.20 and Figure 3.21 compare the simulated and observed failure modes of the girders. The failure mode of Girder B obtained from the test, from the simulations using shell elements and using line elements, was due to buckling of the middle diagonal compressive brace members (members 8 and 9 in Figure 3.12) at 606 °C, 602 °C and 595 °C respectively. For Girder A, the failure was due to buckling in the outer compression brace members (members 6 and 11 in Figure 3.12) at 603 °C from the test, 595 °C from the simulations using 3D shell elements and 586 °C from the numerical study using 2D line elements. It is clear that the numerical

simulation model, either using 2D line elements or 3D shell elements, is suitable for simulating the overall behaviour of welded tubular trusses in fire. However, from a computational point of view, using line elements is preferable because the simulation was very fast. The line element model will be used to conduct the parametric study in Chapter 5.

a) Test observation (Edwards, 2004)

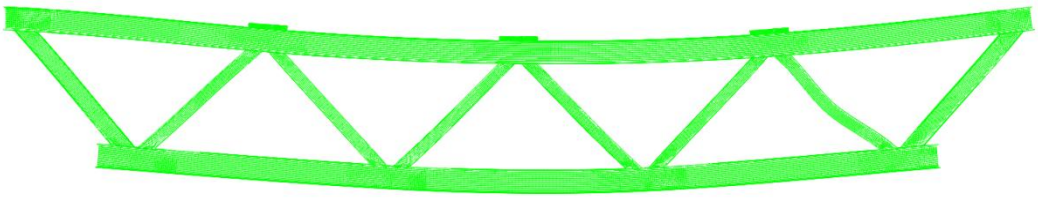

b) Failure Mode using shell elements

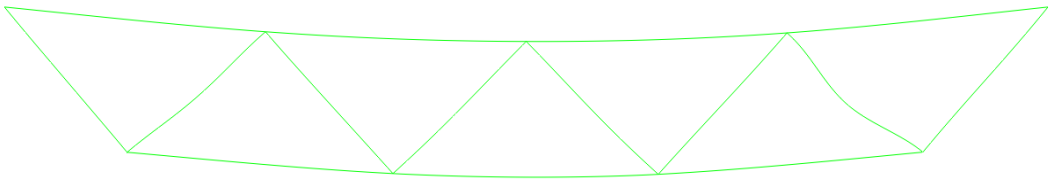

c) Failure Mode using beam elements

Figure 3.20 Comparison of failure modes for test Girder A of Edwards (2004)

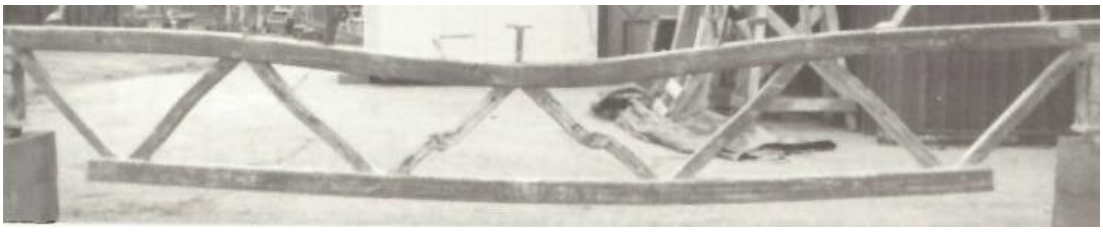

a) Test observation (Edwards, 2004)

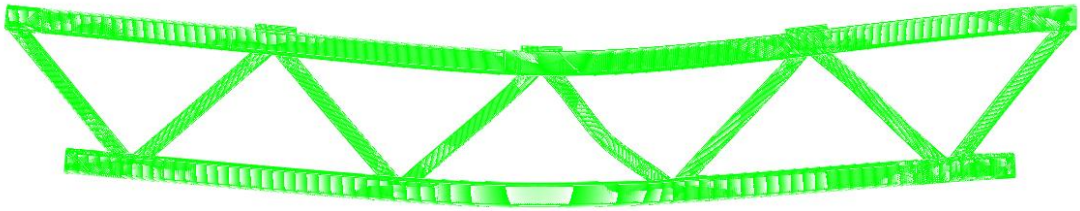

b) Failure Mode using shell elements

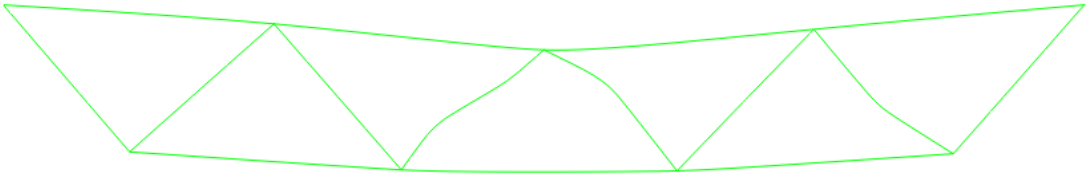

c) Failure Mode using beam elements

Figure 3.21 Comparison of failure modes for test Girder B of Edwards (2004)

3.5 Conclusions

This chapter has presented details of the numerical simulation models generated using the finite element package ABAQUS/Standard for welded tubular joints and trusses at elevated temperatures. The simulation models have been validated by comparisons of the modelling results against the available test results of (Liu et al., 2010 (truss, fire test); Kurobane et al., 1986 (K-joint, ambient temperature); Nguyen et al., 2010 (T-joint, ambient and elevated temperatures) and Edwards, 2004 (truss, fire tests).

Based on the validation study results, the following models can be used for simulations of welded steel tubular joints and trusses.

For welded tubular joints,

- 8-noded thick-shell elements for brace and chord members.
- Quadratic wedge solid elements (C3D15) for the weld.
- Mesh sizes of 10mm and 5 mm respectively for the brace and chord members, and the weld.

For welded tubular trusses,

- 2D line elements for the tubular members.
- Initial imperfections according to the lowest buckling mode and EN 1993-1-1 (CEN, 2005c) for the initial imperfection values.

CHAPTER 4 ELEVATED TEMPERATURE RESISTANCE OF WELDED TUBULAR JOINTS

4.1 Introduction

This chapter presents the results of a parametric study to obtain the ultimate capacity of welded steel tubular joints at elevated temperatures. As explained in Chapter 2, the failure modes of welded steel tubular joints include chord plastification, chord side wall failure, chord shear failure, chord punching shear failure, brace failure and local failure. Except for the chord surface plastification failure mode, the ambient temperature equations for calculating the resistance of welded steel tubular joints can be used to calculated the elevated temperature resistance by simply replacing the steel yield strength at ambient temperature by those at elevated temperatures. For the chord surface plastification mode, this method may not be appropriate because the joint resistance may be affected by the large deformation of the surface. The purpose of this chapter is to find a method that takes into consideration the effects of chord surface deformation on welded tubular joint resistance at elevated temperatures.

Finite Element (FE) simulations of axially loaded tubular joints made of CHS or SHS at different elevated temperatures have been carried out using the commercial Finite Element software ABAQUS v6.10-1. Extensive numerical simulations have been conducted on T-, Y-, X-, N- and non-overlapped K-joints subjected to brace axial compression or tension, considering a wide range of geometrical parameters. The material and geometrical nonlinearities, which have a significant influence on the ultimate strength of tubular joints at elevated temperatures, have been taken into account. Uniform temperature distribution is assumed for both the chord and brace members. At ambient temperature, the load carrying capacity of the joint is defined as the load corresponding to the 3% deformation limit or the maximum load, whichever occurs first. However, a deflection limit is no longer applicable at elevated temperatures in fire. Therefore, in all cases, the structure is considered to have failed if it has reached the peak load.

4.2 Parametric Studies on Welded Tubular Joints in Fire

Figure 4.1 shows the joint configurations investigated in the parametric study, including T-, Y-, X-, N- and non-overlapped K-joints subjected to brace axial compression or tension.

Table 4.1 lists the geometrical parameters considered in the parametric study. Table 4.1 also illustrates the loading and boundary conditions. Details of the case studies are given as follows:

(Case 1) T-joints were analysed under brace compression load in order to examine the effects of global bending of the chord member and large distortions (flattening) at the chord face on the ultimate strength of tubular joints at elevated temperatures. Table 4.2 lists the detailed parameters considered. The investigated parameters include the ratio of brace-to-chord diameter (β), the ratio of chord diameter to thickness (γ) and the tubular section type (CHS or SHS).

(Case 2) X-joints subject to brace axial compression or tension, considering different brace angles, were modelled to exclude the global bending effect. Table 4.3 shows the geometric parameters.

(Case 3) This case is the direct opposite to Case 1. Here the brace member in the T-joints was in tension. Table 4.4 lists the parameters considered.

(Case 4) Table 4.5 lists the parameters for the K-joints. For these joints, one brace member was in tension and the other in compression and the loads were equal in order to eliminate the effects of global bending and flattening of the chord. The brace angles were set at 60^{o}. Furthermore, CHS N-joints (by setting one of the brace members of the K-joint perpendicular to the chord) were performed. Table 4.6 lists the geometrical parameters considered.

(Case 5) Changing the angle of the brace member to the chord member from 90° in the T-joint to different values makes Y-joint. Different values of this angle (θ=30°, 45° and 60°) were simulated to investigate its effect. Table 4.7 lists the geometrical parameters for the Y-joints.

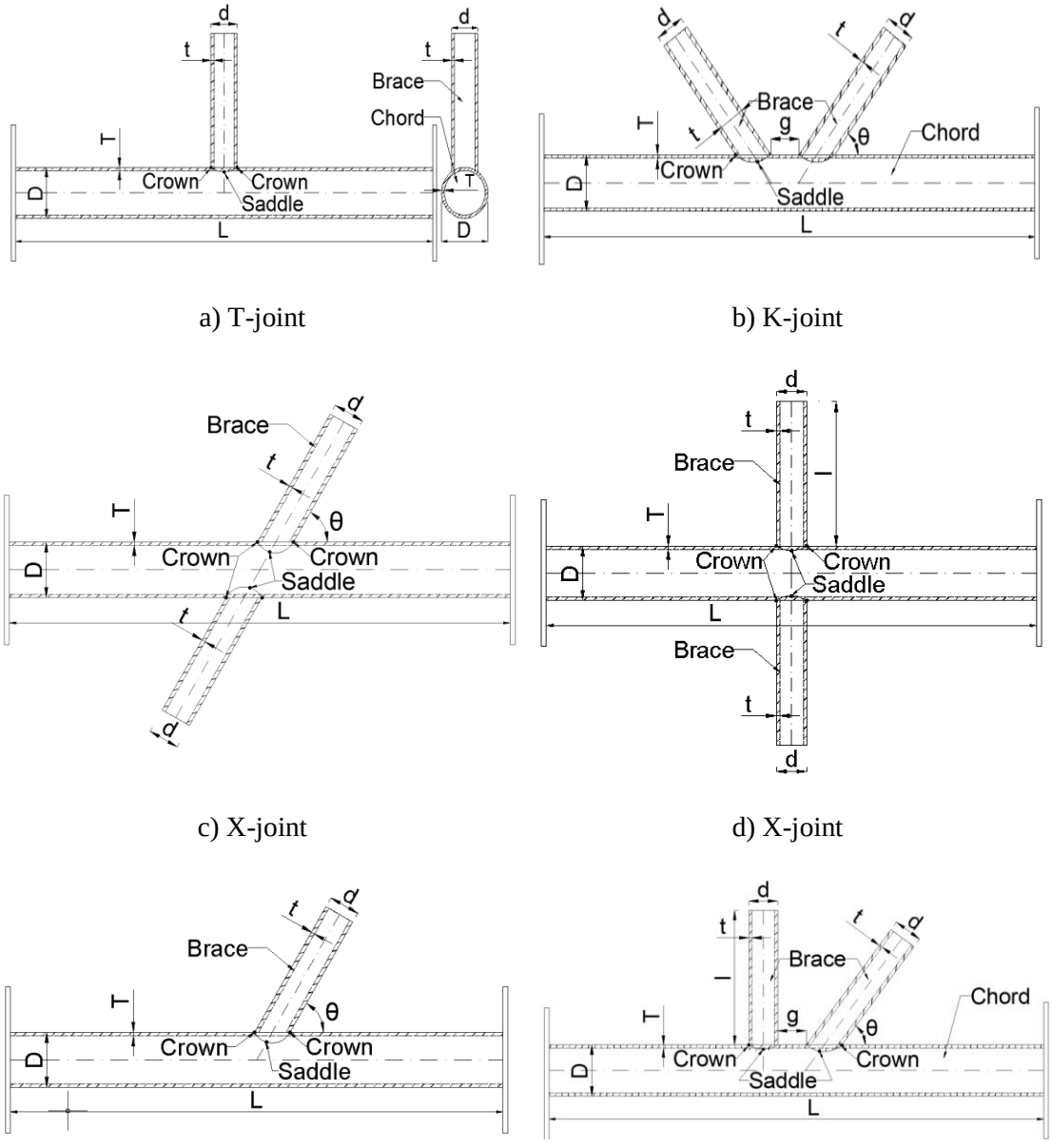

a) T-joint

b) K-joint

c) X-joint

d) X-joint

e) Y-joint

f) N-joint

Figure 4.1 Joint configurations used in the parametric study

Table 4.1 Summary of simulation cases with loading and boundary conditions

Case Studies	Parameters	Boundary and Loading Conditions	
Case 1: T-joints – compressive brace member	➢ β, Ratio of brace diameter to chord diameter (=d/D) ➢ γ, Ratio of chord diameter to twice the chord thickness (=D/2T) ➢ Section type	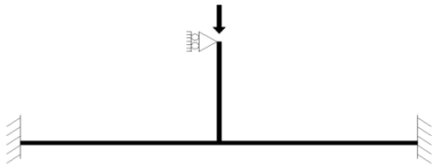	
Case 2: X-joints	➢ θ, Brace-to-chord intersection angle ➢ Brace loading directions	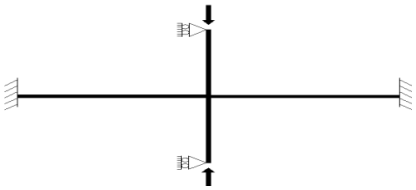	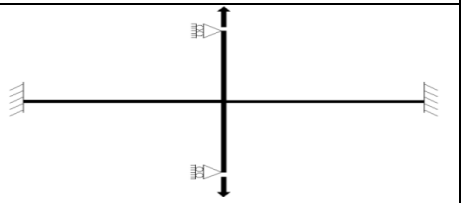
Case 3: T-joints – tensile brace member	➢ β, Ratio of brace diameter to chord diameter (=d/D) ➢ γ, Ratio of chord diameter to twice the chord thickness (=D/2T) ➢ Section type	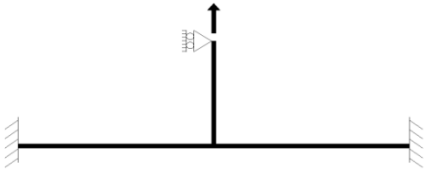	
Case 4: K-joints & N-joints	➢ β, Ratio of brace diameter to chord diameter (=d/D) ➢ θ, Brace-to-chord intersection angle	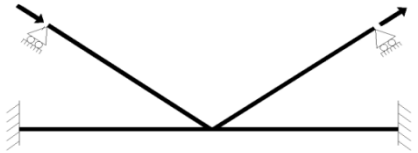	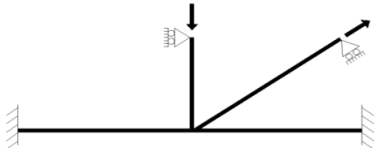
Case 5: Y-joints	➢ θ, Brace-to-chord intersection angle ➢ Brace loading directions	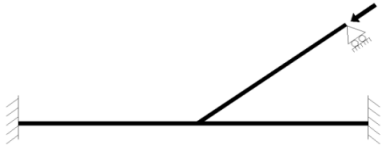	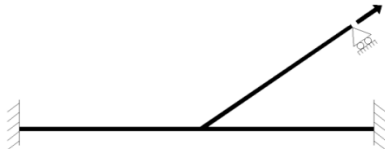

Table 4.2 to Table 4.7 list the parameters considered in each case study respectively. For identification, the name of each joint consists of three letters, the first one (C or S) representing the tubular cross-section shape (CHS or SHS), the second indicating joint type, and the third giving the brace loading direction (Tension or Compression). For example, CTC1 means CHS - T-joint with the brace member subjected to an axial compression load.

Table 4.2 Geometrical parameters for T-joints with compressive brace member (see Case 1 in Table 4.1)

Joint Type	Joint Name	D (mm)	d (mm)	T (mm)	t (mm)	γ(D/2T)	β (d/D)	θ (^{0})
CHS T-joints	CTC1	244.5 (L_c=2200)	168.3 (l_b=1000)	6.3	6.3	19.4	0.69	90
	CTC2	244.5 (L_c=2200)	139.7 (l_b=1000)	6.3	6.3	19.4	0.57	90
	CTC3	244.5 (L_c=2200)	114.3 (l_b=1000)	6.3	6.3	19.4	0.47	90
	CTC4	323.9 (L_c=4000)	193.7 (l_b=1000)	10	10	16.2	0.60	90
	CTC5	323.9 (L_c=3000)	168.3 (l_b=1000)	10	10	16.2	0.52	90
	CTC6	323.9 (L_c=3000)	139.7 (l_b=1000)	10	10	16.2	0.43	90
	CTC7	323.9 (L_c=3000)	114.3 (l_b=1000)	10	10	16.2	0.35	90
	CTC8	323.9 (L_c=4000)	193.7 (l_b=1100)	8	8	20.2	0.60	90
	CTC9	323.9 (L_c=4000)	193.7 (l_b=1100)	12.5	12.5	13.0	0.60	90
	CTC10	323.9 (L_c=4000)	193.7 (l_b=1100)	16	16	10.1	0.60	90
SHS T-joints	STC1	323.9 (L_c=4000)	193.7 (l_b=1100)	10	10	16.2	0.60	90
	STC2	300 (L_c=4000)	200 (l_b=1100)	10	10	15.0	0.67	90
	STC3	300 (L_c=4000)	150 (l_b=1100)	10	10	15.0	0.50	90
	STC4	300 (L_c=4000)	120 (l_b=1100)	10	10	15.0	0.40	90
							TOTAL	162

Table 4.3 Geometrical parameters for X-joints (see Case 2 in Table 4.1)

Joint Type	Joint Name	D (mm)	d (mm)	T (mm)	t (mm)	β (d/D)	θ (^{0})
CHS X-joints	CXC1	323.9 (L_c=4000)	193.7 (l_b=1100)	10	10	0.60	90
	CXT1	323.9 (L_c=4000)	193.7 (l_b=1100)	10	10	0.60	90
	CXC2	323.9 (L_c=4000)	193.7 (l_b=1100)	10	10	0.60	45
	CXT2	323.9 (L_c=4000)	193.7 (l_b=1100)	10	10	0.60	45
	CXC3	323.9 (L_c=4000)	193.7 (l_b=1100)	10	10	0.60	60
	CXT3	323.9 (L_c=4000)	193.7 (l_b=1100)	10	10	0.60	60
SHS X-joints	SXC1	323.9 (L_c=4000)	193.7 (l_b=1100)	10	10	0.60	90
	SXT1	323.9 (L_c=4000)	193.7 (l_b=1100)	10	10	0.60	90
						TOTAL	64

Table 4.4 Geometrical parameters for T-joints with tensile brace member (see Case 3 in Table 4.1)

Joint Type	Joint Name	D (mm)	d (mm)	T (mm)	t (mm)	γ(D/2T)	β (d/D)	θ (^{0})
CHS T-joints	CTT1	323.9 (L_c=4000)	193.7 (l_b=1100)	8	8	20.2	0.60	90
	CTT2	323.9 (L_c=4000)	193.7 (l_b=1100)	12.5	12.5	13.0	0.60	90
	CTT3	323.9 (L_c=4000)	193.7 (l_b=1100)	10	10	16.2	0.60	90
	CTT4	323.9 (L_c=4000)	168.3 (l_b=1100)	10	10	16.2	0.52	90
	CTT5	323.9 (L_c=4000)	139.7 (l_b=1100)	10	10	16.2	0.43	90
	CTT6	323.9 (L_c=4000)	114.3 (l_b=1100)	10	10	16.2	0.35	90
SHS T-joints	STT1	323.9 (L_c=4000)	193.7 (l_b=1100)	10	10	16.2	0.60	90
	STT2	300 (L_c=4000)	200 (l_b=1100)	10	10	15.0	0.67	90
	STT3	300 (L_c=4000)	150 (l_b=1100)	10	10	15.0	0.50	90
	STT4	300 (L_c=4000)	120 (l_b=1100)	10	10	15.0	0.40	90
							TOTAL	80

Table 4.5 Geometrical parameters for K-joints (see Case 4 in Table 4.1)

Joint Type	Joint Name	D (mm)	d (mm)	T (mm)	t (mm)	g (mm)	β (d/D)	θ (^{0})
CHS K-joints	CK1	219.1 (L_c=1500)	193.7 (l_b=1100)	6.3	6.3	30	0.88	60
	CK2	219.1 (L_c=1500)	168.3 (l_b=1100)	6.3	6.3	30	0.77	60
	CK3	219.1 (L_c=1500)	114.3 (l_b=1100)	6.3	6.3	30	0.52	60
SHS K-joint	SK1	300 (L_c=4000)	150 (l_b=1100)	10	10	30	0.5	60
							TOTAL	32

Table 4.6 Geometrical parameters for N-joints (see Case 4 in Table 4.1)

Joint Type	Joint Name	D (mm)	d (mm)	T (mm)	t (mm)	g (mm)	β (d/D)	θ (^{0})
CHS N-joints	CN1	323.9 (L_c=4000)	193.7 (l_b=1000)	10	10	30	0.6	45
	CN2	323.9 (L_c=4000)	168.3 (l_b=1000)	10	10	30	0.52	45
	CN3	323.9 (L_c=4000)	139.7 (l_b=1000)	10	10	30	0.43	45
							TOTAL	24

Table 4.7 Geometrical parameters for Y-joints (see Case 5 in Table 4.1)

Joint Type	Joint Name	D (mm)	d (mm)	T (mm)	t (mm)	γ(D/2T)	β (d/D)	θ (^{0})
CHS Y-joints	CYC1	323.9 (L_c=4000)	193.7 (l_b=1000)	10	10	16.2	0.60	30
	CYC2	323.9 (L_c=4000)	193.7 (l_b=1000)	10	10	16.2	0.60	45
	CYC3	323.9 (L_c=4000)	193.7 (l_b=1000)	10	10	16.2	0.60	60
	CYC4	323.9 (L_c=4000)	193.7 (l_b=1000)	8	8	20.2	0.60	45
	CYC5	323.9 (L_c=4000)	193.7 (l_b=1000)	12.5	12.5	13.0	0.60	45
	CYC6	323.9 (L_c=4000)	193.7 (l_b=1000)	16	16	10.1	0.60	45
	CYT1	323.9 (L_c=4000)	193.7 (l_b=1000)	10	10	16.2	0.60	30
	CYT2	323.9 (L_c=4000)	193.7 (l_b=1000)	10	10	16.2	0.60	45
	CYT3	323.9 (L_c=4000)	193.7 (l_b=1000)	10	10	16.2	0.60	60
							TOTAL	72

To obtain the joint resistance values, steady state analysis was used. In this case, the effect of the temperature was to change the mechanical properties of the steel.

However, the results are applicable to the transient condition as demonstrated by the comparison between the steady state and transient state analysis results in Section 4.5.

4.2.1 Material properties and boundary conditions

In the numerical analyses, the elevated engineering temperature stress-strain curves of the steel were based on EN-1993-1-2, as shown in Figure 4.2 (CEN, 2005a). The yield stress and modulus of elasticity at ambient temperature were 355 N/mm^2 and 210 GPa respectively and the Poisson's ratio was 0.3. Uniform temperature distribution was assumed throughout the joint. Furthermore, the von Mises yield surface criterion and isotropic strain hardening rules were used in order to represent the yielding of steel.

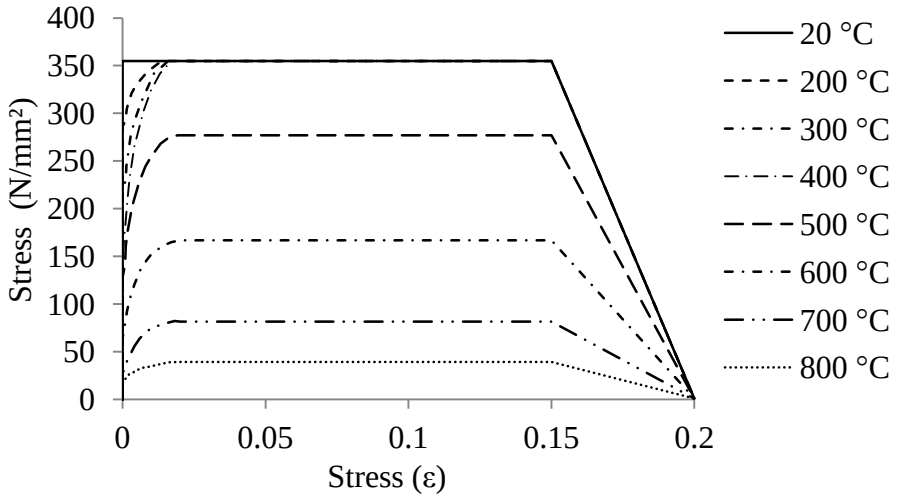

Figure 4.2 Stress-strain relationships at elevated temperatures

The numerical modelling is limited to symmetric geometry where the loading and geometry of the joint are symmetrical. Because of this, the effects of bending in the brace and chord members have not been considered.

4.3 Simulation Results and Discussions

This section presents the five case studies as summarised in Table 4.1. Each case study discusses whether or not the numerical simulation result of joint strength ratio is in accordance with the effective yield strength of steel at elevated temperatures. In the results to be presented, the joint strength ratio (P_θ/P_{20}) is used, being the ratio of the joint strength at elevated temperature θ to that at ambient temperature. The joint strength ratios at different temperatures are compared to the steel strength and

modulus of elasticity reduction factors at elevated temperatures. The chord face plastification, which is the most common failure mode in tubular joints, has been taken into account for all the case studies (see Appendix A). Appendix B presents the load ratios for each joint, based on the numerical results.

4.3.1 Case 1: T-joints with brace member in compression

T-joints were analysed under brace axial compression to understand how the strengths of T-joints vary at different temperatures. Table 4.2 lists the parameters considered. The results are divided into two groups. The first group focuses on the effect of β and γ on the joint strength ratio of (CHS) T-joints. The other group is to understand the effect of section type on the ultimate load ratio.

Figure 4.3 compares the strength ratios with the steel yield strength and modulus of elasticity reduction factors at elevated temperatures. It can be seen that for both CHS and SHS T-joints, the numerical simulation strength ratios are generally lower than the reduction factors for the yield strength of steel at elevated temperatures. The joint strength reduction for SHS joints is higher than for CHS joints.

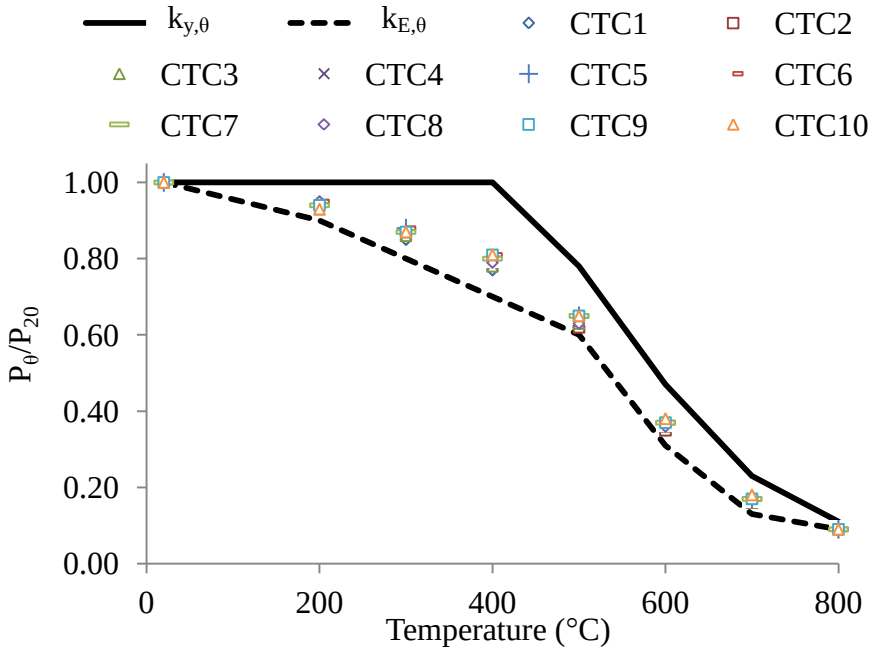

a) CHS T-joints

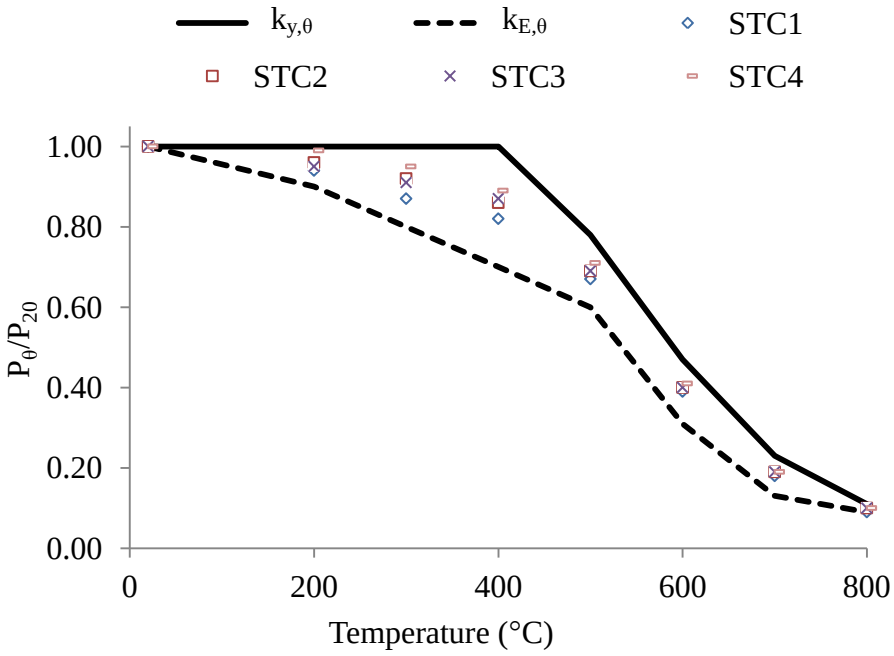

b) SHS T-joints

Figure 4.3 Comparison for T-joints with compressive brace member

Two factors contribute to the higher reduction in joint strength than the reduction in steel yield stress at elevated temperatures. Figure 4.4 shows the deformed shape of a quarter of a CTC5 joint at 700 °C. When a T-joint is under brace compression load, the connected chord wall is in compression from global bending of the chord. This compression force in the chord member produces some additional local bending moment when the chord compression acts on the deformation of the chord face (local P-δ effect). At the same time, the side faces of the chord member experience local bulging (ovalisation) under the brace compression, causing the chord side wall to flatten. Both effects prevent the joint from reaching the yield line capacity of the chord face, which is based on the original undeformed chord face.

At elevated temperatures, both effects increase due to increased deformations as a result of reduced steel stiffness. Therefore, the joint failure loads decrease faster than the steel yield strength at elevated temperatures as shown in Figure 4.3(a) and Figure 4.3(b). Furthermore, the strength reductions at elevated temperatures are greater for CHS joints than for SHS joints because the extent of flattening is much greater in the CHS chord member than in the SHS chord member.

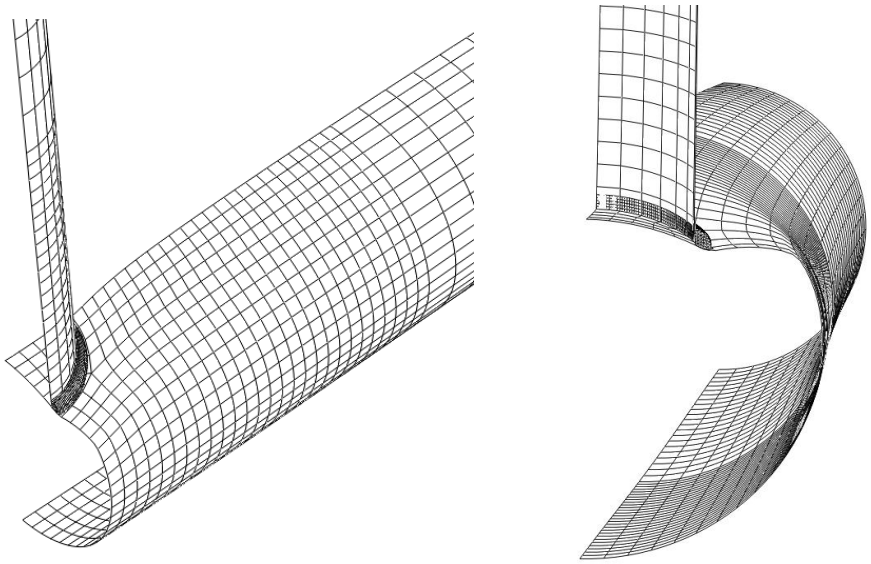

Figure 4.4 Deformations of the CTC5 joint at 700 °C

Detailed examination of the simulation results (Figure 4.3a) reveals that changing the brace-to-chord dimension ratio β (=d/D) or the wall thickness ratio γ has little influence on the elevated temperature effects on joint strength, which is in agreement with the findings of Tan et al. (2012).

These findings suggest that for both (CHS) and (SHS) T-joints under brace compression load, merely changing the ambient temperature yield strength of the steel to that at elevated temperature overestimates the ultimate load carrying capacity of the joint. Since the joint strength reduction is caused by deformation of the chord member, the joint strength reduction should be related to the deformation characteristics of the joint. Based on the above observation that the joint strength reduction is not influenced by the joint geometry and that using the reduction factor for the Young's modulus of steel at elevated temperature gives a close lower bound approximation to the joint strength reduction, it is suggested that for T-joints with the brace member in compression, the joint strength equation be modified by the Young's modulus reduction factor for steel at elevated temperatures.

4.3.2 Case 2: X-joints with the brace members in equal compression or tension

When an X-joint is subject to equal load in the two brace members, there is no global bending in the chord member. Figure 4.5 shows the deformed shape of an eighth of the complete CXC1 joint at 700 °C. Therefore, the abovementioned P-δ effect is eliminated. When the brace members are in tension, the local flattening of the chord

member disappears. Therefore, it is expected that the yield-line equation for calculating the chord face capacity still applies provided the elevated temperature yield stress of the steel is used. The results in Figure 4.6(b) confirm this expectation. However, when the brace members are in compression, the local flattening of the chord member still exists. The results in Figure 4.6(a) suggest that the effect of local flattening is severe. Although the brace-chord angle has some influence, all the simulation results are close and just above the reduction factor for the Young's modulus of steel at elevated temperatures.

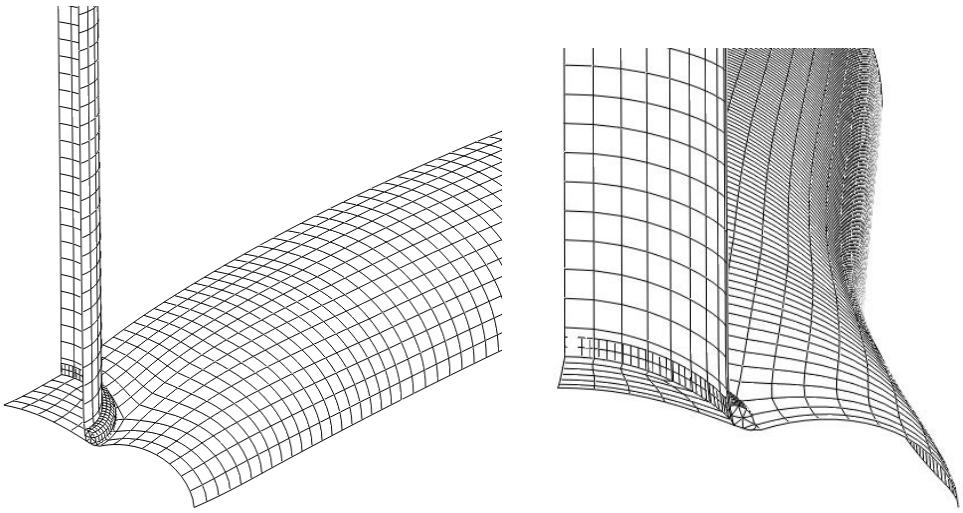

Figure 4.5 Deformations of the CXC1 joint at 700 °C

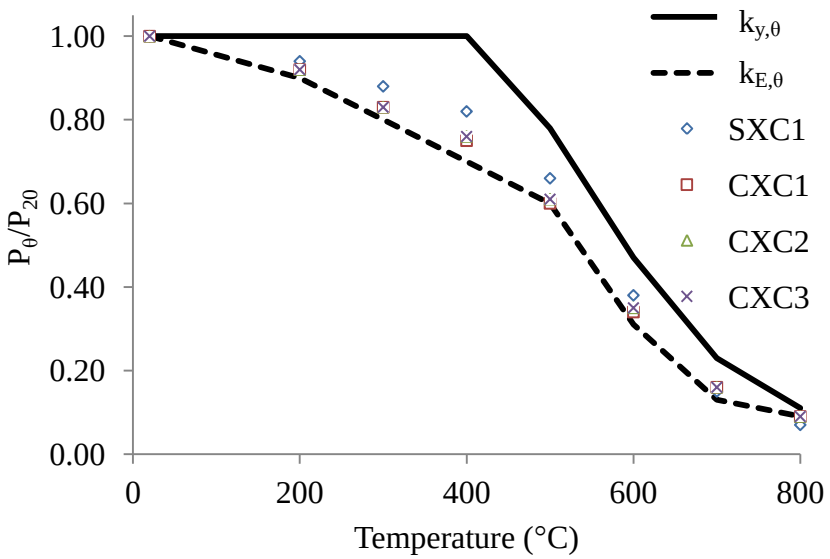

a) Brace in compression

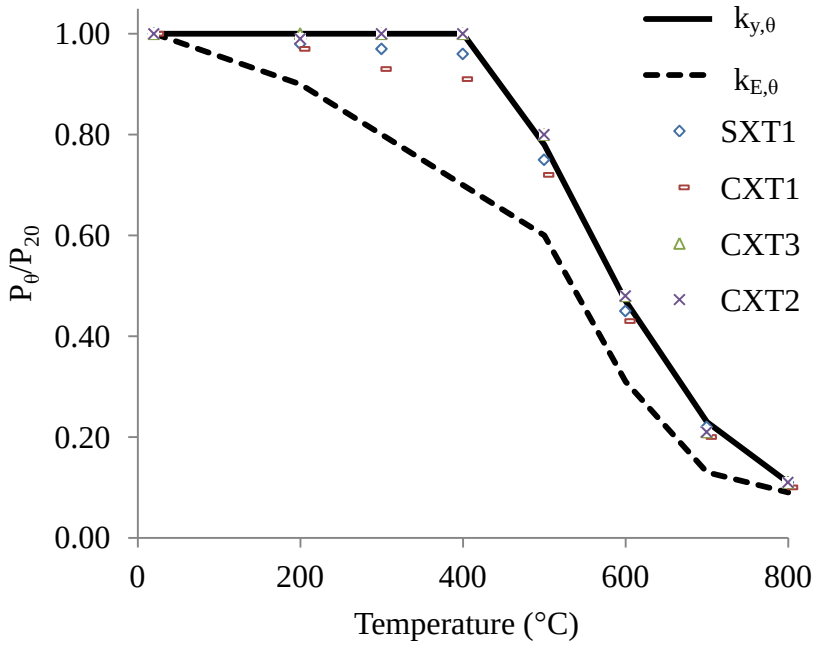

b) Brace in tension

Figure 4.6 Comparison for CHS and SHS X-joints with the brace members in equal compression or tension

4.3.3 Case 3: T-joints with the brace member in tension

When the brace member of a T-joint is in tension, global bending of the chord member induces tension in the connected chord face. Therefore, the local P-δ effect disappears around the brace-to-chord intersection area. Also, there is no longer any flattening of the chord face at the loaded region beneath the brace. This is shown in Figure 4.7. Therefore, it is expected that the joint strength can be calculated using the ambient temperature equation based on the yield-line solution, but modified by the steel yield strength reduction factors at elevated temperatures. The results in Figure 4.8(a) and (b) for both SHS and CHS joints confirm this. This effect is slightly higher for joints with smaller brace-to-chord dimension ratios (β). Nevertheless, this effect is relatively small and it is acceptable to use the yield strength reduction factor for the joint strength reduction at elevated temperatures.

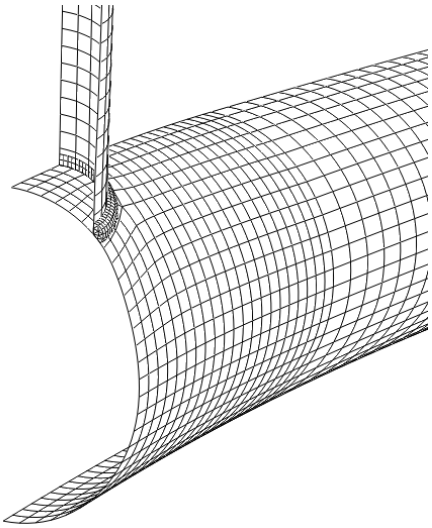

Figure 4.7 Deformations of the CTT5 joint at 700 °C

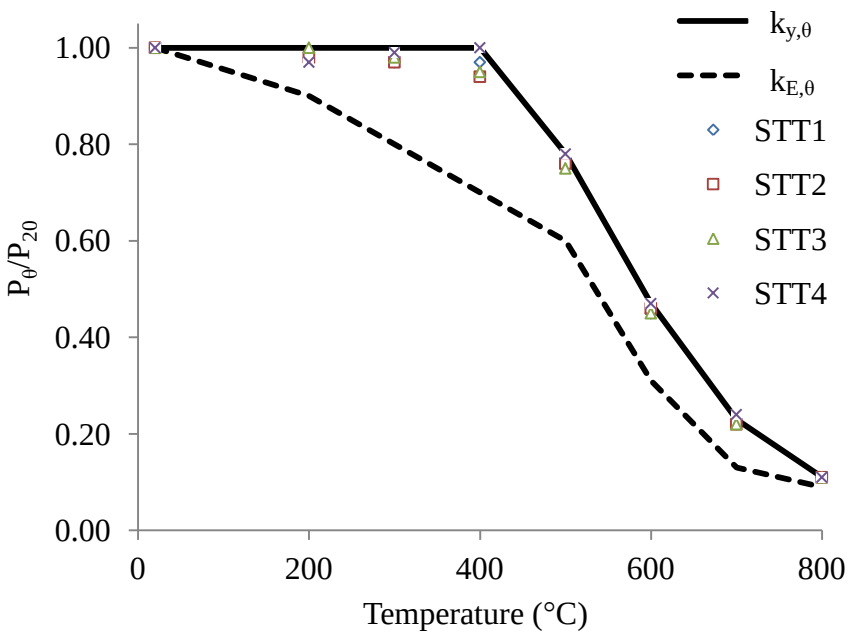

a) SHS T-joints

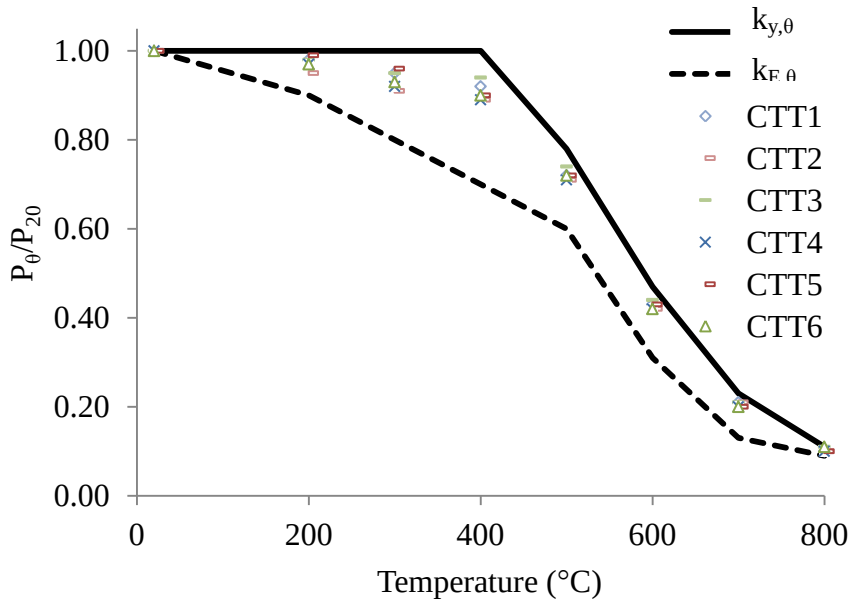

b) CHS T-joints

Figure 4.8 Comparisons for T-joints with the brace member in tension

4.3.4 Case 4: K-joints and N-joints with equal but opposite loads in the brace members

The brace members in a K-joint usually have equal, but opposite, forces. This eliminates global bending as well as local flattening in the chord member as shown in Figure 4.9. The results in Figure 4.11(a) show that in this case, the joint strength can be calculated using the ambient temperature equation and the elevated temperature yield strength of steel.

Due to the different directions of the brace forces, there was some axial force in the chord member. The CK4 joint, which had a long chord length and small brace-to-chord intersection angle ($\theta = 30^{\circ}$, $\beta = 0.60$ and L_c=4000), was selected to investigate the influence of the horizontal components (along the chord members) of the brace forces on the ultimate load carrying capacity of the tubular joints at elevated temperatures. The brace forces would cause the highest tensile stresses in the left chord member and the greatest compressive stresses in the right chord member. Owing to the small magnitude of the brace forces compared to the compressive resistance of the chord members, the failure mode of CK4 was identical to other joints, being local plastification, rather than buckling, of the chord member. The joint

failure loads were according to the effective yield strength reduction factors at elevated temperatures as shown in Figure 4.11(a).

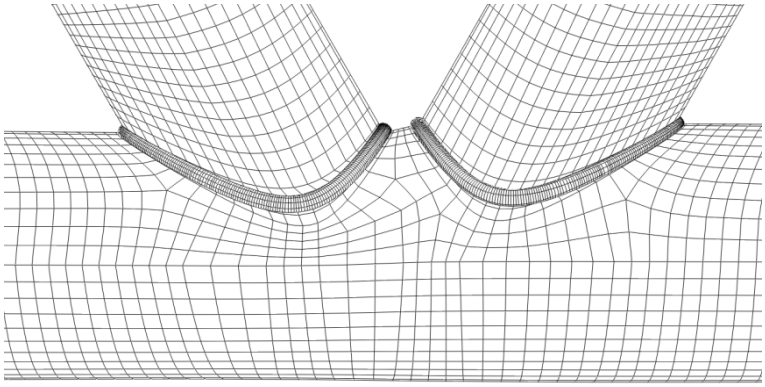

Figure 4.9 Deformations of the CK1 joint at 700 °C

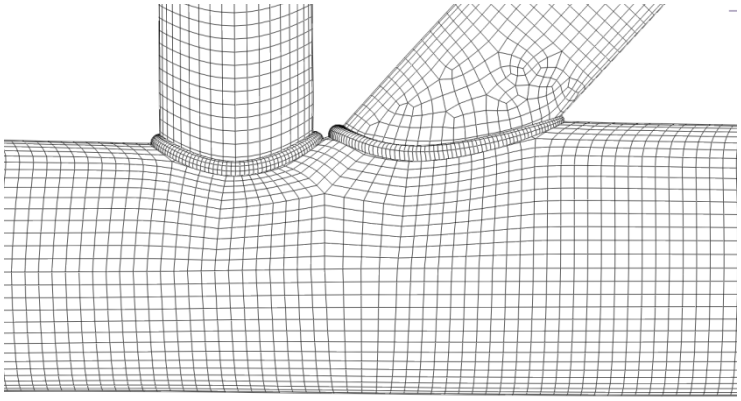

Figure 4.10 Deformations of the CN3 joint at 700 °C

The behaviour of the N-joints (Figure 4.11(b)) is consistent with the K-joints (Figure 4.11(a)) because the global bending and local flattening effects are largely eliminated (Figure 4.10) even though the two brace member loads do not produce exactly opposite effects.

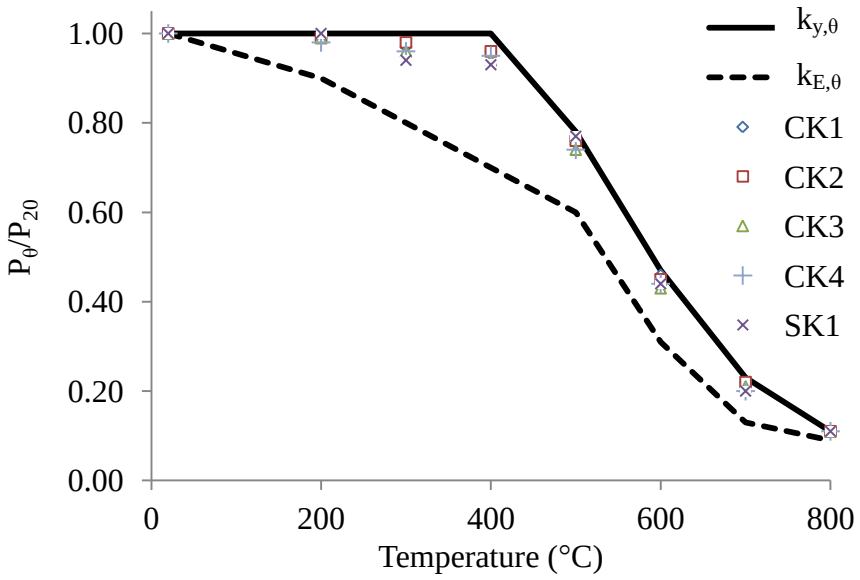

a) K-joints

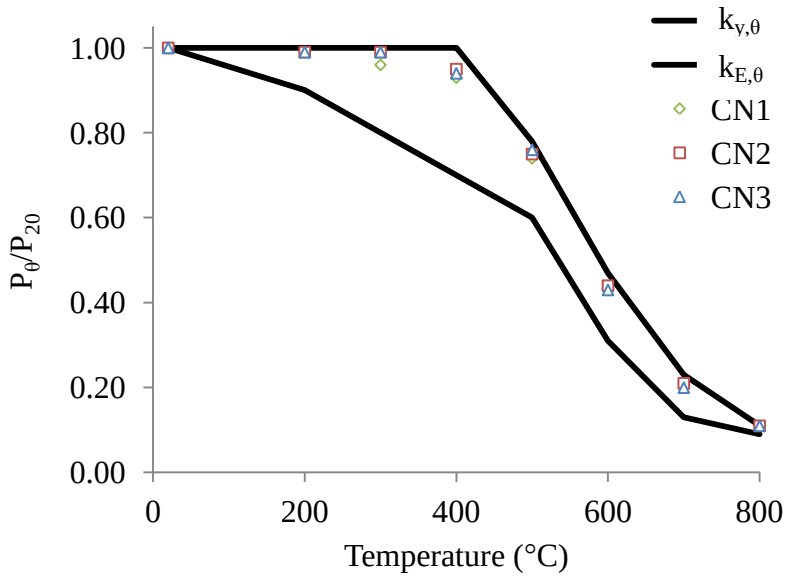

b) N-joints

Figure 4.11 Comparison for K- and N- joints

4.3.5 Case 5: Y-joints

A Y-joint is similar to a T-joint except that the brace member is not perpendicular to the chord member. Therefore, it is expected that elevated temperatures will have the same effect on the joint strength. This is confirmed by the results shown in Figure 4.12(a) and Figure 4.12(b) for Y-joints with the brace member in compression and tension respectively. Also, these figures include the relevant results for the T-joints.

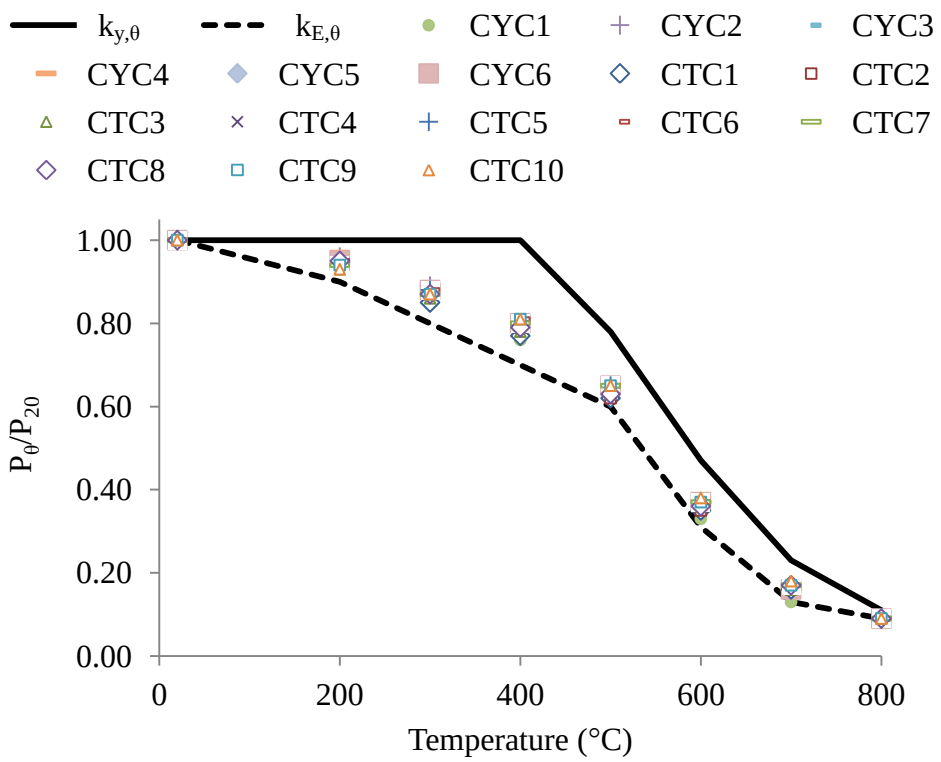

a) Brace in compression

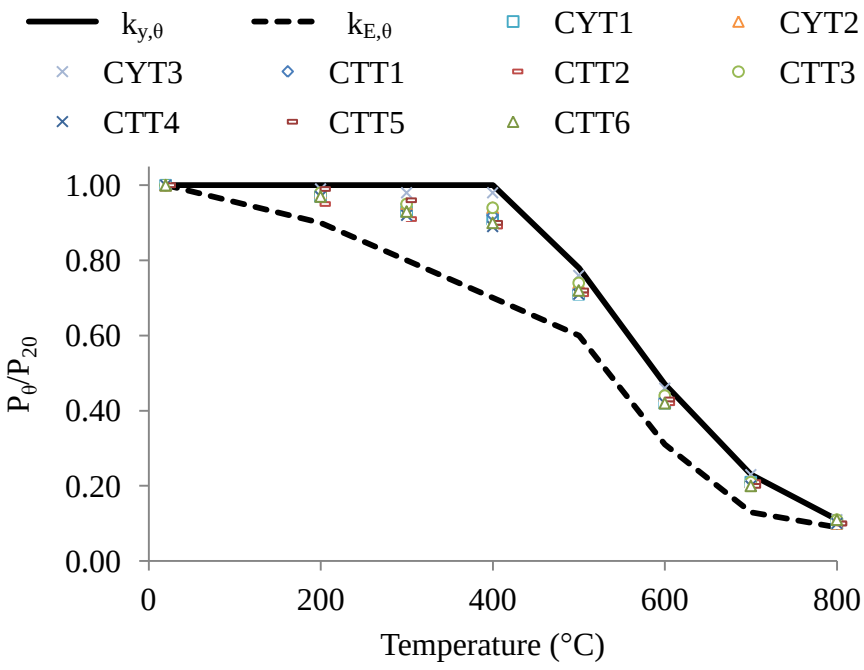

b) Brace in tension

Figure 4.12 Comparison of CHS Y- and T-joints with the brace member in compression or tension

4.3.6 Summary of results

In summary, these results show that due to the deformation of the chord face (flattening of the chord face) at elevated temperatures, failure loads of the T-, Y- and X-joints with the brace member(s) in compression reduce faster than the steel yield strength at high temperatures. Since the deformation of the chord face is caused by the degradation of steel stiffness, it is suggested that for these joints, the strength equation should be modified by the Young's modulus reduction factor for steel at elevated temperatures rather than the yield strength reduction factor.

For T-, Y- and X-joints with the brace member(s) in tension, and for K- and N-joints with the brace members under opposite loads, there is not any local failure in the chord face in fire. Therefore, failure loads of these joints can be calculated using the ambient temperature equations by replacing the yield stress of steel at elevated temperatures.

4.4 Effects of Pre-stress in Chord Member

This section investigates the effects of chord pre-load on the capacity of tubular joints at elevated temperatures. The chord member was subjected to either compression or tension force prior to loading the brace member. The values of chord pre-load ratio ($N_{chord}/N_{pl,chord}$) were 0.3, 0.5, 0.7 and 0.9. Figure 4.13 illustrates the loading conditions of selected joints with the chord member in compression.

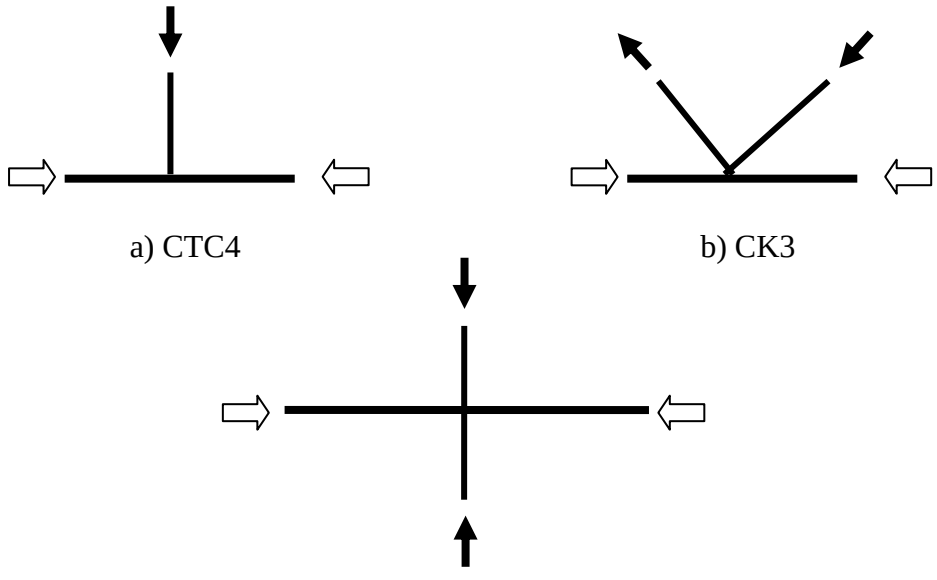

a) CTC4 b) CK3

c) CXC1

Figure 4.13 Loading conditions of T-, K- and X-joints with the chord member in compression

Figure 4.14 (a)-(f) compare the reduction factors, defined as the ratio of joint strength with chord preload ($P_{chord\ pre\text{-}load}$) to that without chord preload ($P_{no\ chord\ pre\text{-}load}$), at elevated temperatures between numerical simulation and calculations using CIDECT (Wardenier et al., 2010a) and EN-1993-1-8 (CEN, 2005b). According to EN-1993-1-8, there is no reduction in joint strength if the preload in the chord member is tension. The results in Figure 4.14 (b), (d) and (f) are in agreement with this design recommendation. In contrast, CIDECT (Wardenier et al., 2010a) suggests substantial reductions in joint strength, depending on the level of tensile pre-stress in the chord member. For compressive preload in chord members, the results in Figure 4.14 (a), (c) and (e) show that the CIDECT design guide is quite accurate. In general, the CIDECT calculation results are slightly lower than the numerical simulation results, indicating that the CIDECT method is safe. Because there is little difference between the results of CIDECT and EN-1993-1-8 (not included in the figures), this means that the EN 1993-1-8 calculation method is also accurate. Appendix B shows a comparison of the reduction factors, for compressive pre-load in the chord member, between the numerical simulation and the calculations using EN-1993-1-8.

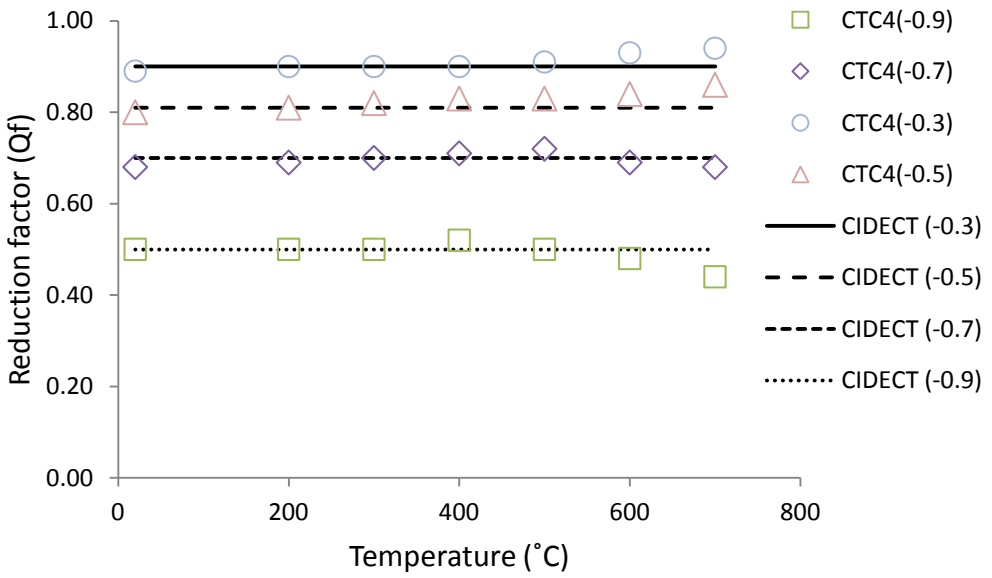

(a) Effects of compressive pre-load in chord member on T-joint strength

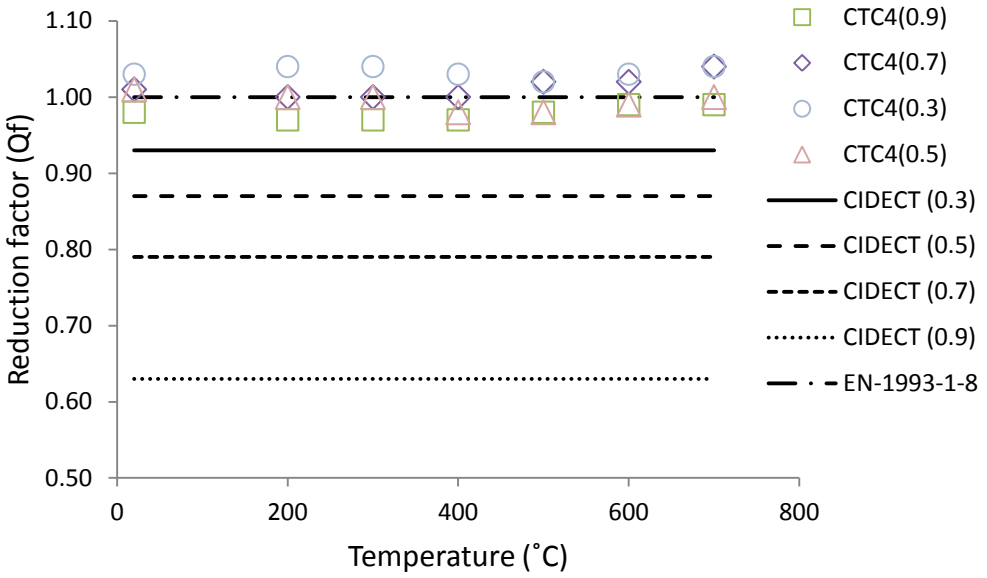

b) Effects of tensile pre-load in chord member on T-joint strength

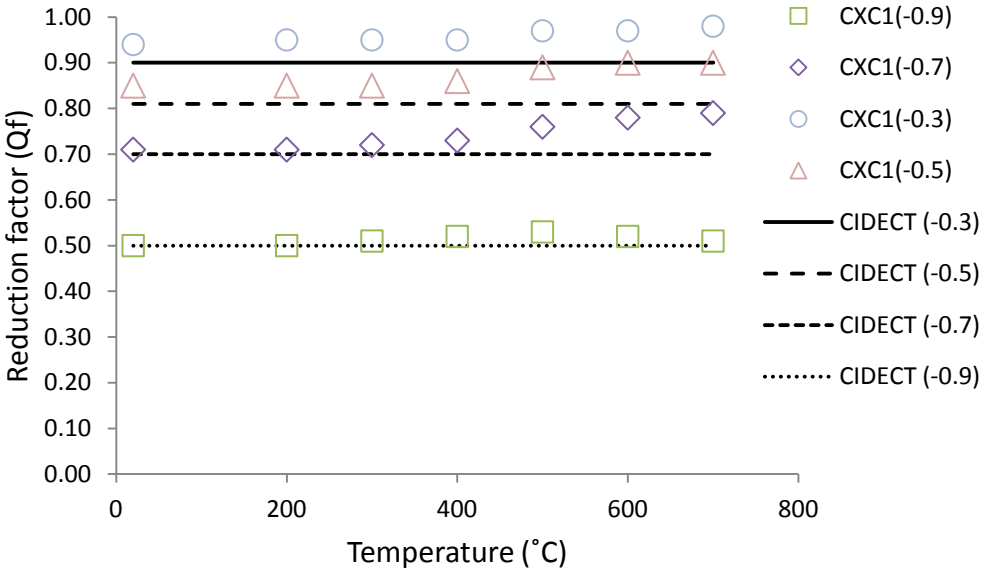

c) Effects of compressive pre-load in chord member on X-joint strength

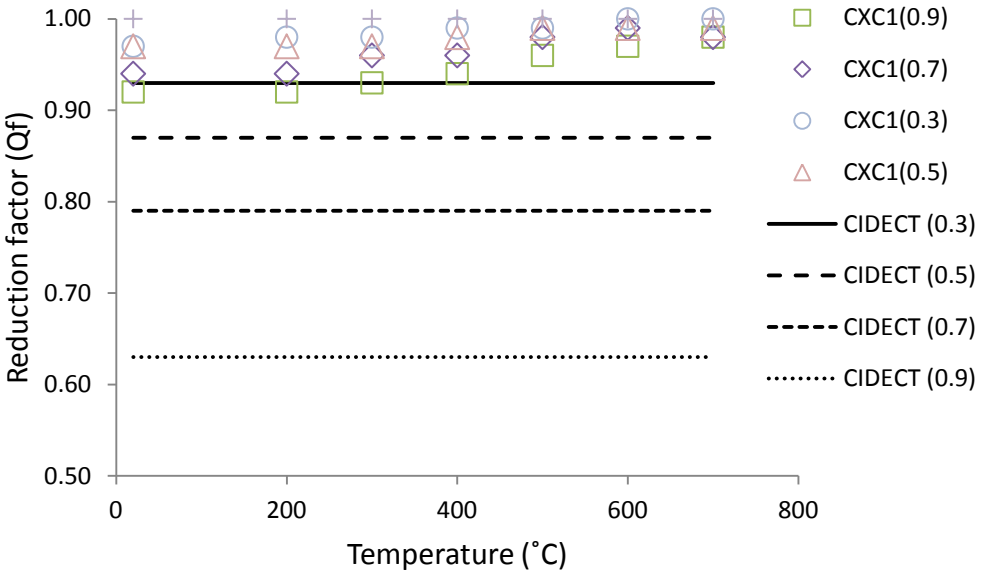

d) Effects of tensile pre-load in chord member on X-joint strength

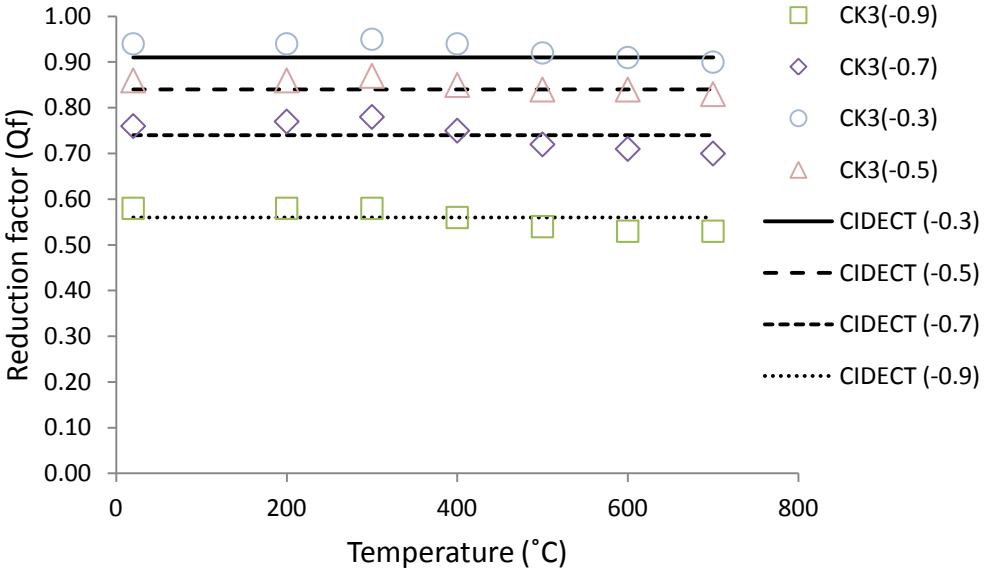

e) Effects of compressive pre-load in chord member on K-joint strength

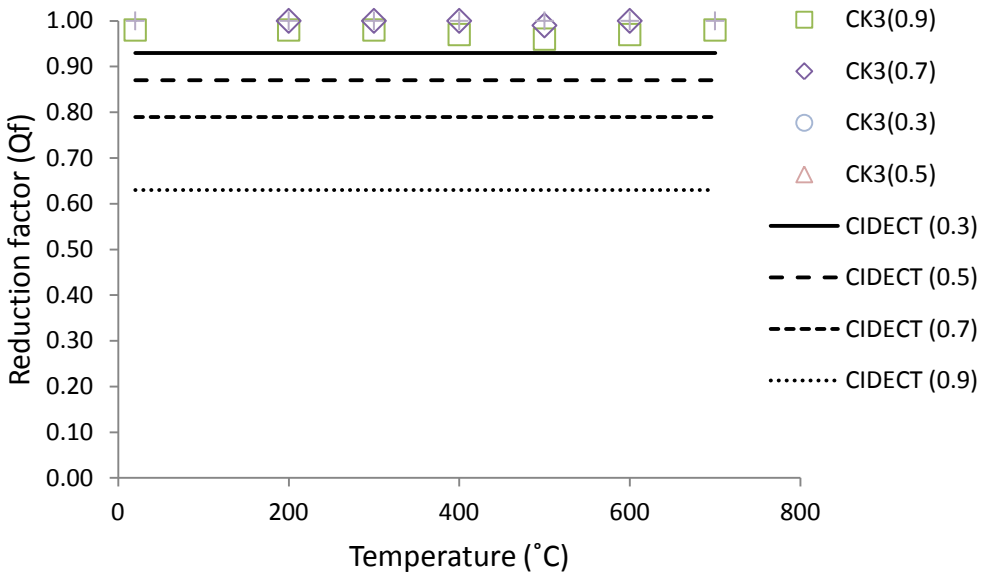

f) Effects of tensile pre-load in chord member on K-joint strength

Figure 4.14 Comparison of joint reduction factors for CHS T-, X- and K-joints with pre-stress in the chord member (either compression or tension) between numerical simulation and design calculations

4.5 Comparison between Steady State and Transient State Analyses

The previous results were obtained from steady state analyses, in which the steel temperatures were increased to the desired level and followed by structural analysis at elevated temperatures. This was done because the analysis directly outputs the joint resistance. In realistic structures, the process is transient, as the load is applied first and then maintained when the temperature is increased. It is necessary to ensure that the steady state results are applicable to the transient condition.

CTC4 and CK3 joints were used as examples to investigate the differences between steady state and transient state analyses. The mechanical loads were applied at ambient temperature, the values being the same as their failure loads from the steady state analysis at the different temperature levels. The transient state analyses were then carried out to ascertain the joint failure temperatures under the different loads.

Table 4.8 Comparison of steady state and transient state failure temperatures for CTC4 and CK3 joints

	Transient failure temperatures (in brackets) at loads (kN) equal to steady state resistances at different temperatures						
Steady state temperature	20 °C	200 °C	300 °C	400 °C	500 °C	600 °C	700 °C
CTC4	561.1 (20 °C)	533.1 (199 °C)	488.2 (297 °C)	448.9 (398 °C)	359.1 (496 °C)	202.0 (595 °C)	95.4 (695 °C)
CK3	301.1 (20 °C)	298.1 (201 °C)	289.1 (302 °C)	283.0 (404 °C)	222.8 (496 °C)	129.5 (598 °C)	63.2 (698 °C)

Table 4.8 compares the steady state and transient state joint failure temperatures for the two example joints. The two sets of failure temperatures are very close, with the maximum difference being 5 °C. This confirms that the steady state results are applicable to the transient state condition.

4.6 Conclusions

This chapter has presented the results of a numerical parametric study to investigate the effects of elevated temperatures on the ultimate load carrying capacity of welded steel tubular joints. In particular, this study has focused on the chord surface plastification failure mode because large deformation of the chord surface has considerable effects on welded tubular strength. Both CHS and SHS sections were considered. The joints investigated include T- and Y- joints with the brace member in tension or compression, X-joints with the two brace members in equal tension or equal compression and K- and N-joints with the two brace members with exactly opposite loads. The parametric study covered a range of different joint geometries for these different joint types. The elevated temperature mechanical properties of steel were based on EN-1993-1-2 (CEN, 2005a). The numerical simulations were carried out under the steady state condition in which the temperature was kept constant while the applied load was increased until joint failure.

Based on comparisons between the joint strength reduction factor with the steel yield stress and Young's modulus reduction factors at elevated temperatures, the following proposals are recommended for calculating joint strengths at elevated temperatures:

(1) For T-, Y- and X-joints with the brace member(s) in tension, and for K- and N-joints with the brace members under opposite loads, the joint strength reduction follows the steel yield strength reduction at elevated temperatures. Therefore, the existing CIDECT (Wardenier et al., 2010a) or EN 1993-1-8 (CEN, 2005b) equations for ambient temperature design can be used, provided the steel yield strength at ambient temperature is replaced by that at elevated temperature.

(2) For T-, Y- and X-joints with the brace member(s) in compression, it is not safe to use the above proposal. However, it is safe to use the joint strength calculation equations developed at ambient temperature, but the joint strength should be modified by the Young's modulus of steel reduction factor at the elevated temperature.

(3) When the chord member is under tensile pre-stress, the joint strength hardly changes. This means that the reduction factor according to CIDECT (Wardenier et al., 2010a) underestimates the joint strength. In contrast, EN-1993-1-8 (CEN, 2005b) proposes no joint strength reduction due to tensile pre-stress in the chord member and the simulation results are in agreement with this recommendation. For chord compressive pre-stress, the simulation results of joint strength are in agreement with both the CIDECT (Wardenier et al., 2010a) and EN 1993-1-8 (CEN, 2005b) results, with the design calculation results being slightly on the safe side. Overall, the recommended method in EN 1993-1-8 for taking into consideration the effects of pre-stress in the chord member can be extended to elevated temperatures.

(4) The steady state results are applicable to the transient design condition.

CHAPTER 5 UNIFORMLY HEATED TRUSSES

5.1 Introduction

This chapter presents the results of a numerical investigation into the behaviour of uniformly heated welded steel tubular trusses at elevated temperatures.

Under fire conditions, the current method for truss member design involves calculating the member force using static analysis at ambient temperature and then finding the critical temperature, defined as the maximum temperature at which the member can resist the applied load, using the ambient temperature member force. The member force – critical temperature relationship can be evaluated using design methods such as those in BS 5950 Part 8 (BSI, 2003) and EN 1993-1-8 (CEN, 2005b). However, the member force obtained from truss static analysis at ambient temperature may not be correct at elevated temperatures due to large deformations of the truss.

This chapter will examine whether the current method of calculating truss member limiting temperature, based on considering each individual truss member and using the member force from ambient temperature analysis, is suitable. The simulated trusses are subjected to constant mechanical loads and then increasing temperatures until failure. In all cases, the structure is considered to have failed if it has reached the peak temperature. The elevated temperature stress-strain curves are based on EN-1993-1-2 (CEN, 2005a). Initial geometrical imperfections are included, based on the lowest buckling mode from eigenvalue analysis.

The numerical parametric study examines the effects of truss type, joint type, truss span-to-depth ratio, critical member slenderness, applied load ratio, number of brace members, initial imperfection and thermal elongation on critical temperatures of the critical truss members.

These critical temperatures, obtained considering whole truss behaviour, are then compared with the member-based critical temperatures, which are numerically calculated using ABAQUS but using the member force values obtained from ambient temperature structural analysis, as will be the case in the current design method.

ABAQUS simulations of individual truss members are used to obtain the member limiting temperatures to eliminate any inaccuracy of the design code limiting temperature – load ratio relationships.

Wherever the member-based fire resistance design approach is not safe, a new method will be developed to modify the member-based method to take into consideration whole truss behaviour.

5.2 Influential Factors on Structural Behaviour of Truss at Elevated Temperature

The behaviour of a truss at elevated temperatures is affected by many design factors as well as design assumptions. The parametric study in section 5.3 of this chapter will investigate, in detail, the effects of different design factors. This section presents the results of a number of numerical investigations to examine the effects of different design assumptions. This study is based on the Warren truss type as shown in Figure 5.1. These assumptions are:

(1) Joints: the welded truss joint may be considered to be rigid (Figure 5.1(a)), pinned (Figure 5.1(c)) or semi-rigid (where the chord members are continuous, but the brace members are pinned, Figure 5.1(b));

(2) Restraint to differential thermal elongations of the members due to certain temperature differences may have some effect on the truss member critical temperatures.

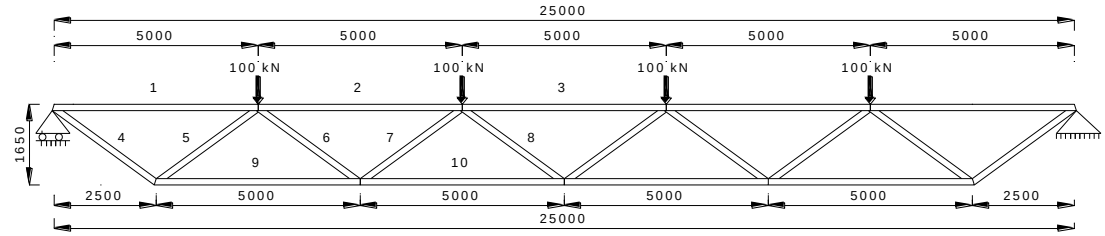

(a) Rigid joints

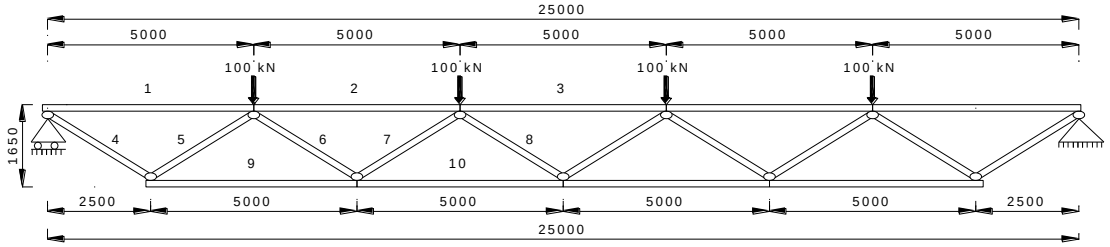

(b) Semi-rigid joints

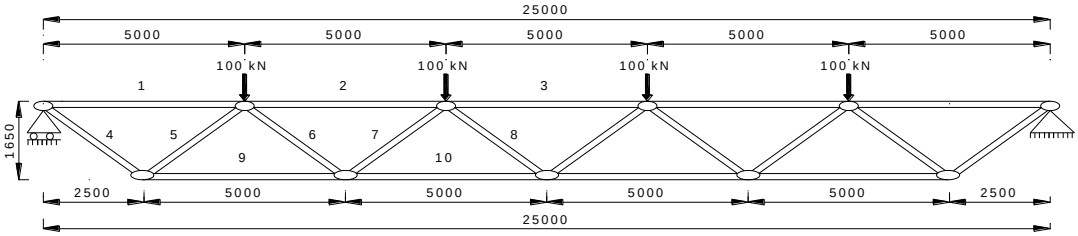

(c) Pin-jointed members

Figure 5.1 Truss configurations used in numerical analyses (dimensions in mm)

Figure 5.1 illustrates the joint and boundary conditions of the trusses. Table 5.1 lists the truss member dimensions. The material strength of steel is f_y = 355 N/mm^2 f_u = 450 N/mm^2. The elastic modulus of steel is assumed to be 210 GPa. The elevated temperature stress-strain curves and the thermal expansion coefficient of steel are based on EN-1993-1-2 (CEN, 2005a).

Table 5.1 Truss member dimensions

Member Type	Dimensions (mm)
Bottom and top chords	Φ 323.9x8
Outer bracings (Member 4 and 5)	Φ 193.7x4
Inner bracings (Member 6, 7 and 8)	Φ 114.3x5

For comparison, ABAQUS simulations of the individual truss members were carried out to obtain the critical temperatures of all the members according to the current member based design method. In these analyses, the member force values were the

same as those at 20 °C. Table 5.2 summarises the critical temperatures of the individual members.

Table 5.2 Critical temperatures of the individual members of the Warren truss in Figure 5.1(c)

Member no	1	2	3	4	5	6	7	8	9	10
Critical temperature (°C)	780	652	624	577	573	640	558	635	679	624

In the following truss simulations, the rates of temperature increase of all the members were assumed to be in proportion to their individual critical temperatures in Table 5.2.

The failure temperatures of the trusses with rigid, semi-rigid and pinned joints are 535 °C, 529 °C and 523 °C respectively. The failure temperatures of the trusses without thermal expansion are 541 °C for rigid joints and 533 °C for semi-rigid joints. Whether or not thermal expansion was considered, the truss failure temperatures were almost identical. This indicates that any differential thermal elongation due to different truss members being heated to different temperatures had a negligible effect on the failure temperature of the trusses.

Since assuming pinned joints gives the lowest truss failure temperature, it is suggested that this assumption may be made in the fire resistant design of the truss. Therefore, in the further investigation of this chapter, only statically determinate, pin-jointed trusses will be considered. However, even assuming pin-joints, the member-based calculation method of using the ambient temperature forces may not be safe. For example, for the truss in Figure 5.1, the member-based critical temperature of member 7 of the truss, obtained numerically using ABAQUS, was 558 °C. This is higher than the actual critical temperature (535 °C) of the member in the rigid truss.

The reason for this difference is due to the increased member force in the member in truss analysis when the truss deflection is high. To confirm this, static structural analysis was performed using the deformed configuration of the truss. The initial member forces, the member force at truss failure (523 °C) and the member force

from static analysis based on the deformed shape of the truss were 184.4 kN, 213.6 kN and 213.6 kN respectively.

The ABAQUS model of member 7 was rerun, in this case using the final member forces (213.6 kN). The failure temperature was 523 °C, exactly the same as the failure temperature of the member in the pin-jointed truss.

The following parametric study will investigate how the member forces change and also the effects of this change on member critical temperatures. In the investigations, the trusses will be assumed to be pin-jointed.

5.3 Parametric Study

Figure 5.2 shows the different types of truss being investigated and the following explains the rationale for selecting the different parameters:

- Case 1, span-to-depth ratio (Warren truss, see Figure 5.3): different span-to-depth ratios will give different chord axial force values and different diagonal member angles.
- Case 2, member slenderness, λ (varying from 48 to 89, Warren and Pratt trusses): to investigate different member failure modes.
- Case 3, applied load ratio, (Warren truss with a span of 25 metres and Pratt truss with a span of 12 metres): to investigate the effect of changing chord force.
- Case 4, truss span: Warren truss, spans of 4.5 metres, 12 metres and 25 metres.
- Case 5, truss configurations: Warren, Howe and Pratt trusses (see Figure 5.2).
- Case 6, number of braces: Warren truss with a span of 12 metres. Three different configurations were modelled as shown in Figure 5.6. The total applied load and angle between brace and chord members were constant.
- Case 7, failure location: Pratt truss with a span of 100 metres. The dimensions of the outer and inner brace members were changed to move the location of the critical member.

Appendix C gives the cross-sectional dimensions used in the simulations.

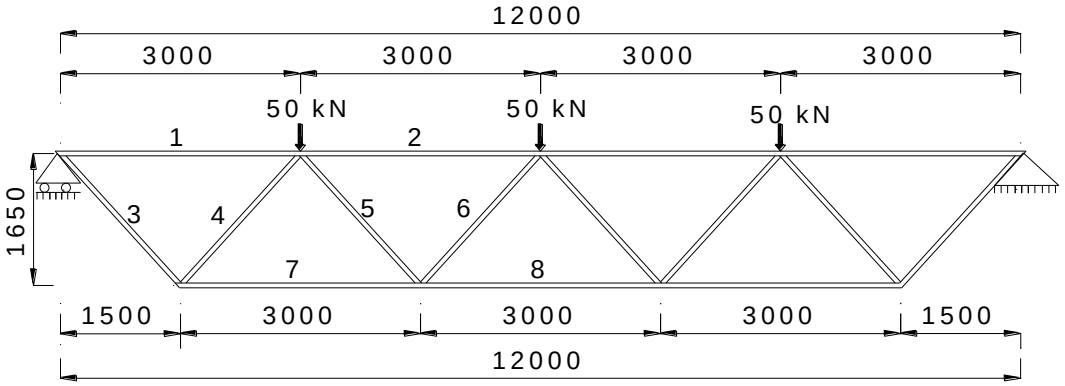

a) Warren truss (WT1)

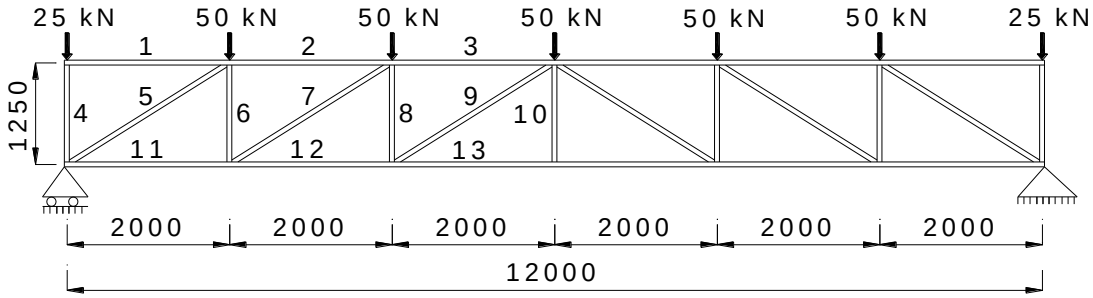

b) Howe truss (HT1)

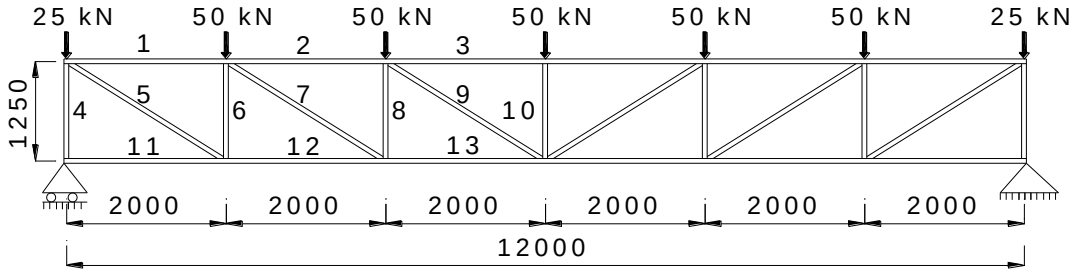

c) Pratt truss (PT1)

Figure 5.2 Truss configurations used in parametric study (dimensions in mm)

5.3.1 Case 1: Effect of span-to-depth ratio

Figure 5.3 illustrates the geometric configurations of the Warren trusses with different span-depth ratios. Appendix C summarises the member dimensions of the trusses used in the parametric study and Table 5.3 provides a summary of the simulation results. In Table 5.3, P_θ / $P_{20°C}$ is the ratio of the member force at elevated temperature (P_θ) from truss analysis to that at ambient temperature ($P_{20°C}$). In all cases, failure was initiated in member 7. The member-based analysis gives a critical

temperature of more than 30 °C higher than truss analysis for a truss span-to-depth ratio of 18.

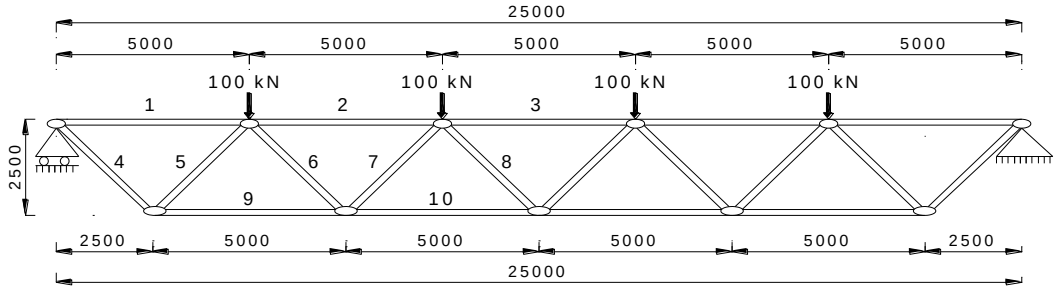

a) Span/depth ratio = 1 / 10 (WT2)

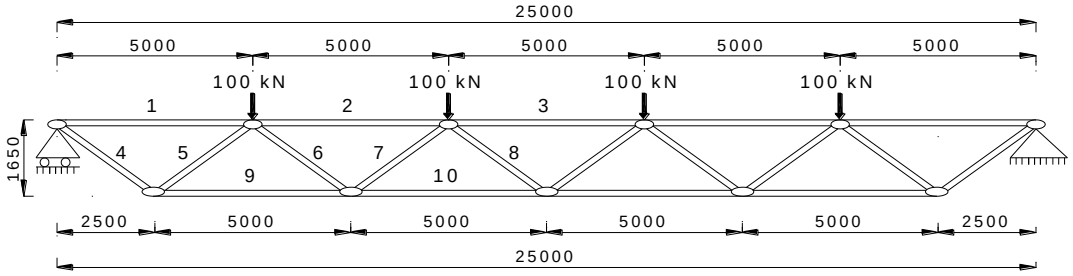

b) Span/depth ratio = 1 / 15 (WT3)

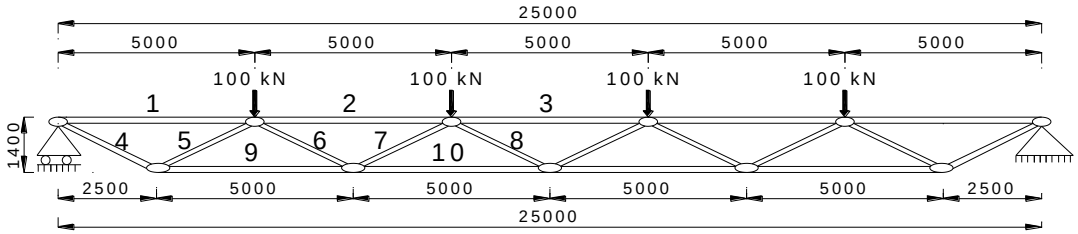

c) Span/depth ratio = 1 / 18 (WT4)

Figure 5.3 Warren trusses with different span/depth ratios (dimensions in mm)

As the span-to-depth ratio increases, the angles between the chord and brace members become smaller. As will be shown in Section 5.4, which presents a method to calculate the increased member force in a compressive diagonal member, it is the vertical component of the chord force in the deformed truss that increases the compression force in the diagonal brace members. This increase is in an inverse relationship to the angle between the diagonal brace member and the chord member. A smaller angle (for a large truss span-to-depth ratio) leads to a higher increase in the brace member force.

Table 5.3 Effect of truss span-to-depth ratio on critical temperature

		Isolated Member 7	Heated Truss
Depth Ratio : 1/10	Critical temperature	556 °C	540 °C
	Maximum displacement	-	389mm
	Member force ratio ($P_\theta/P_{20°C}$)	1.00	1.07
Depth Ratio : 1/15	Critical temperature	558 °C	523 °C
	Maximum displacement	-	587mm
	Member force ratio ($P_\theta/P_{20°C}$)	1.00	1.19
Depth Ratio : 1/18	Critical temperature	541 °C	509 °C
	Maximum displacement	-	663mm
	Member force ratio ($P_\theta/P_{20°C}$)	1.00	1.22

5.3.2 Case 2: Effect of member slenderness (λ)

This case used the Warren truss shown in Figure 5.3(a) and the Pratt truss shown in Figure 5.2(c). The influence of different slenderness values for the Warren truss (λ = 89, 78 and 62) was examined by changing the cross-section of critical member 7 (Φ101.6x6.3, Φ 114.3x5 and Φ139.7x3 respectively for the above slenderness values). In the case of the Pratt truss, the critical member was member 10 and the member size was ϕ76.1x2.5, ϕ60.3x3.6 and ϕ48.3x5 to give slenderness values of λ =48, 62 and 81 respectively.

Table 5.4 and Table 5.5 summarise the simulation results for the Warren and Pratt trusses respectively. Because the overall geometry of the trusses was unchanged, the truss member forces were similar in all cases. However, a comparison between Table 5.4 and Table 5.5 shows that the increase in member force in the Pratt truss is greater. This is expected because the increase in the compression force (due to the vertical component of the compression chord force in the deformed position of the truss) of the brace is shared by two diagonal members in the Warren truss but resisted by only one single member in the Pratt truss.

Table 5.4 Effect of member slenderness on Warren truss critical temperature

		Isolated Member 7	Heated Truss
$\lambda = 89$	Critical temperature	532 °C	508 °C
	Maximum displacement	-	563mm
	Member force ratio ($P_\theta/P_{20°C}$)	1.00	1.16
$\lambda = 78$	Critical temperature	558 °C	523 °C
	Maximum displacement	-	587mm
	Member force ratio ($P_\theta/P_{20°C}$)	1.00	1.19
$\lambda = 62$	Critical temperature	547 °C	518 °C
	Maximum displacement	-	574mm
	Member force ratio ($P_\theta/P_{20°C}$)	1.00	1.16

Table 5.5 Effect of member slenderness on Pratt truss critical temperature

		Isolated Member 10	Heated Truss
$\lambda = 81$	Critical temperature	602 °C	579 °C
	Maximum displacement	-	210mm
	Member force ratio ($P_\theta/P_{20°C}$)	1.00	1.23
$\lambda = 62$	Critical temperature	650 °C	618 °C
	Maximum displacement	-	222mm
	Member force ratio ($P_\theta/P_{20°C}$)	1.00	1.26
$\lambda = 48$	Critical temperature	656 °C	609 °C
	Maximum displacement	-	260mm
	Member force ratio ($P_\theta/P_{20°C}$)	1.00	1.30

5.3.3 Case 3: Effect of applied load ratio

For this investigation, the Warren truss in Figure 5.3(a) and the Pratt truss in Figure 5.2(c) were used. Each point load was 50 kN. Table 5.6 presents the simulation results. The member forces change similarly as discussed in the previous section.

However, the effect of the same change in the member compression force is different at different load ratios. For the Pratt truss with a high load ratio (applied load = 100 kN), the reduction of truss critical temperature from the member-based analysis is nearly 60 °C.

Table 5.6 Effects of applied load ratio on Warren and Pratt truss critical temperatures

		Warren Truss		Pratt Truss	
		Isolated Member 7	Heated Truss	Isolated Member 10	Heated Truss
Applied load : 50 kN	Critical temperature	655 °C	630 °C	656 °C	609 °C
	Maximum displacement	-	630mm	-	260mm
	Member force ratio ($P_\theta/P_{20°C}$)	1.00	1.18	1.00	1.30
Applied load : 100 kN	Critical temperature	558 °C	523 °C	556 °C	498 °C
	Maximum displacement	-	587mm	-	240mm
	Member force ratio ($P_\theta/P_{20°C}$)	1.00	1.19	1.00	1.29

5.3.4 Case 4: Effect of truss span

In this investigation, the span of a Warren truss was changed but the span-to-depth ratio was kept constant at 20.8. Figure 5.4 shows the truss dimensions.

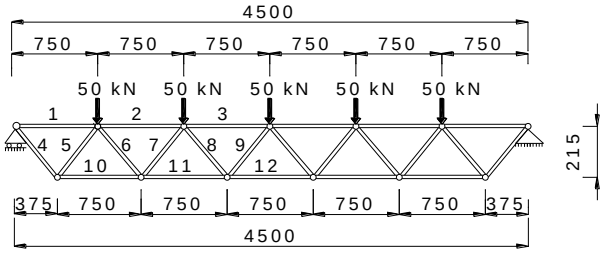

a) Short span: 4.5 metres (WT5)

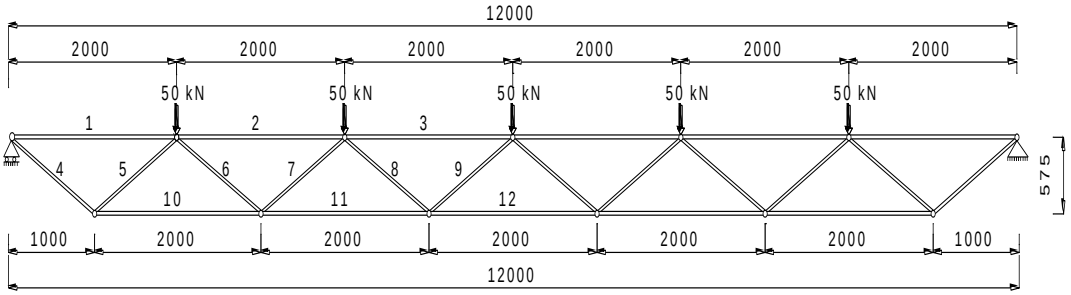

b) Span 12 metres (WT6)

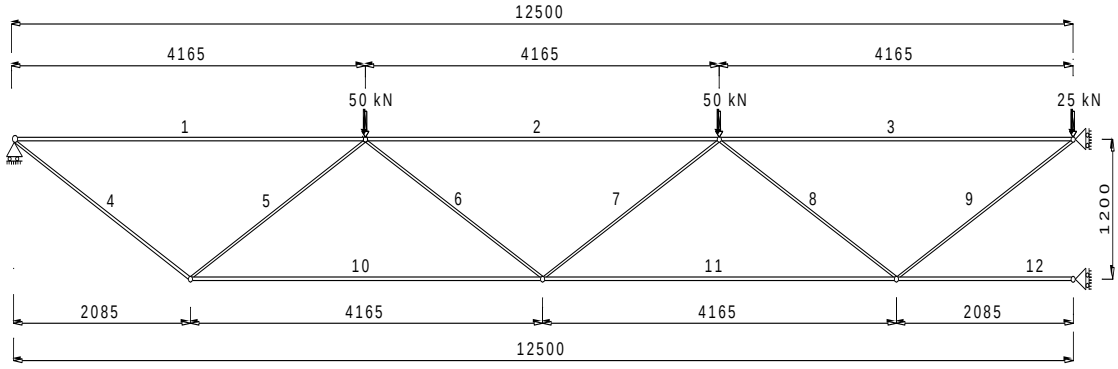

c) Span 25 metres (a half span) (WT7)

Figure 5.4 Dimensions of Warren trusses with different spans (dimensions in mm)

Table 5.7 compares the simulation results. Since the span-to-depth ratio was constant, the member forces experienced very similar changes. Due to the shallow truss depth, the increase in member force was quite high, resulting in truss critical temperatures much lower (by as much as 76 °C) than those from the member-based analysis.

Table 5.7 Effect of truss span with constant span to depth ratio

	Span: 4.5 metres		Span: 12 metres		Span: 25 metres	
	Isolated Member 9	Heated Truss	Isolated Member 9	Heated Truss	Isolated Member 9	Heated Truss
Critical temperature	635 °C	586 °C	647 °C	571 °C	624 °C	575 °C
Maximum displacement	-	97 mm	-	221 mm	-	532 mm
Member force ratio ($P_\theta/P_{20°C}$)	1.00	1.33	1.00	1.35	1.00	1.32

5.3.5 Case 5: Effect of truss configuration

Warren, Howe and Pratt trusses of the same span, the same span-to-depth ratio and the same load level were simulated. Figure 5.2 shows the truss dimensions.

Table 5.8 compares the simulation results. Figure 5.5 shows the members that experienced an increase in their compression forces to resist the vertical component of the chord forces in the deformed condition. As expected, more brace members involved in sharing the load (Howe truss > Warren truss > Pratt truss) results in a lower increase in the compression force of each member.

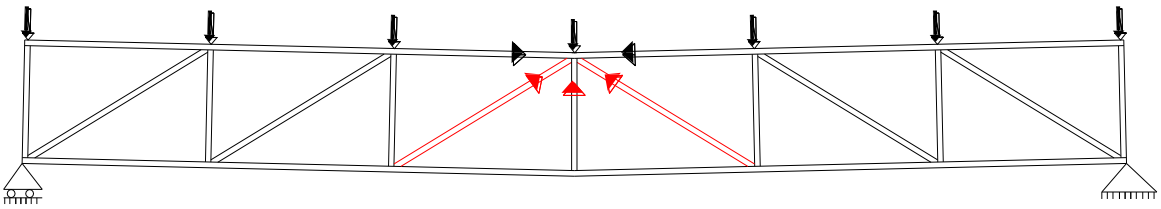

a) Howe Truss

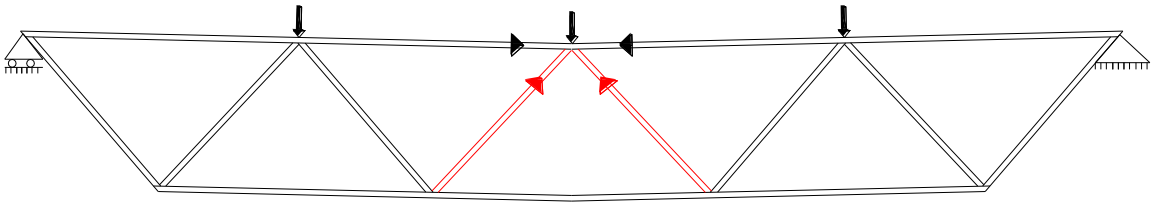

b) Warren Truss

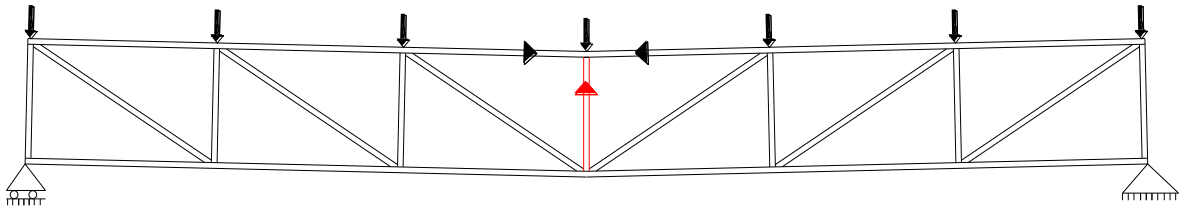

c) Pratt Truss

Figure 5.5 Deformed shape of truss

The results of this investigation show that the effect of increased member force may be ignored for Howe trusses. In the case of increased member forces, Pratt truss analysis revealed a more significant effect on the failure temperature compared to Warren trusses. This effect should be considered for fire resistance analysis of both Warren and Pratt trusses when failure takes place in the middle brace members.

Table 5.8 Effects of truss configuration

	Warren Truss		Howe Truss		Pratt Truss	
	Isolated Member 9	Heated Truss	Isolated Member 9	Heated Truss	Isolated Member 9	Heated Truss
Critical temperature	652 °C	636 °C	644 °C	640 °C	656 °C	609 °C
Maximum displacement	-	168 mm	-	378 mm	-	260 mm
Member force ratio ($P_\theta/P_{20°C}$)	1.00	1.12	1.00	1.03	1.00	1.30

5.3.6 Case 6: Effect of number of braces

For this investigation, the trusses in Figure 5.6 were used. The number of brace members was different, all other dimensions being equal. The total load was 500 kN.

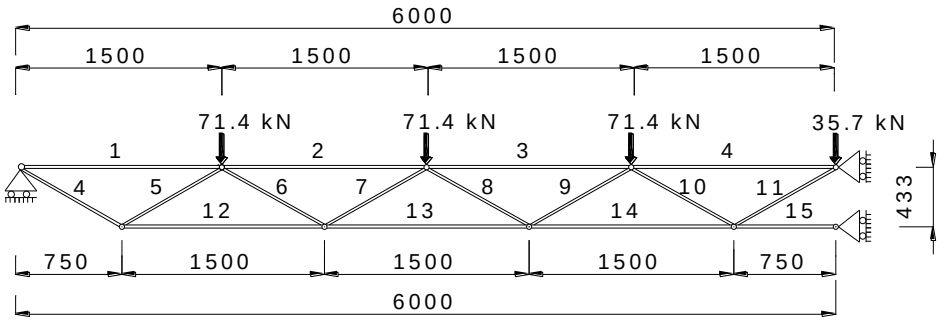

a) Truss A (WT8)

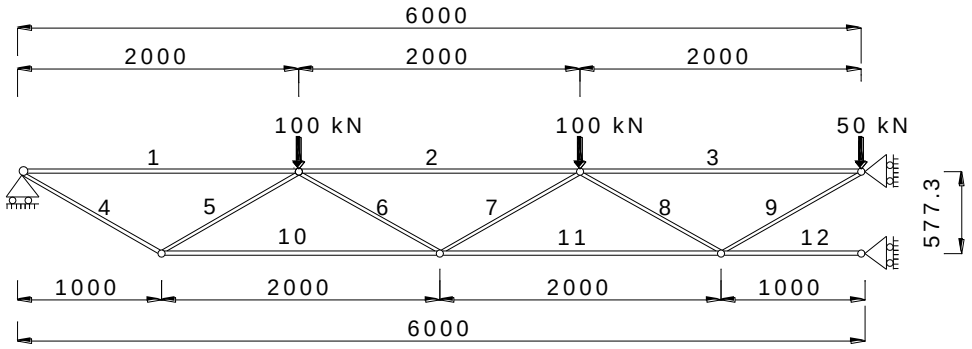

b) Truss B (WT9)

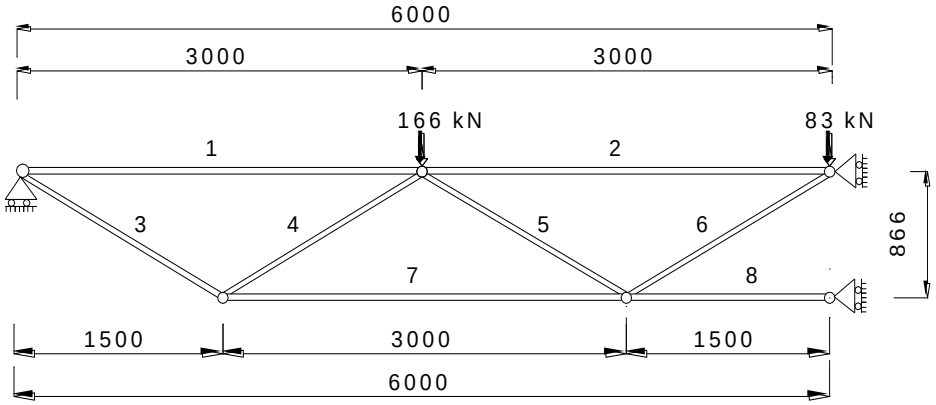

c) Truss C (WT10)

Figure 5.6 Dimensions of Warren Trusses (half span, dimensions in mm)

Table 5.9 compares the simulation results. Changing the number of brace members in a truss changes the maximum chord compression force. As the number of brace members increases, the chord compression force at the truss centre increases. This increase in the chord compression force results in a higher increase in the brace compression force. For truss A, which is sensibly proportioned, the brace compression force at truss failure more than doubled the initial compression force. This resulted in a truss critical temperature of more than 100 °C lower than the member-based result, which did not include this increase in the brace force.

Table 5.9 Effects of number of brace members

	Truss A		Truss B		Truss C	
	Isolated Member 11	Heated Truss	Isolated Member 9	Heated Truss	Isolated Member 6	Heated Truss
Critical temperature	746 °C	642 °C	692 °C	623 °C	597 °C	542 °C
Maximum displacement	-	183 mm	-	227 mm	-	218 mm
Member force ratio ($P_\theta/P_{20°C}$)	1.00	2.07	1.00	1.70	1.00	1.36

5.3.7 Case 7: Effect of failure location

In the previous cases, failure of the truss was initiated in the brace near the centre of the truss. In this simulation, failure of the truss was forced to start from the brace member near the support by reducing the size of this member. A Pratt truss with a span of 100 metres was used and Figure 5.7 shows the truss dimensions.

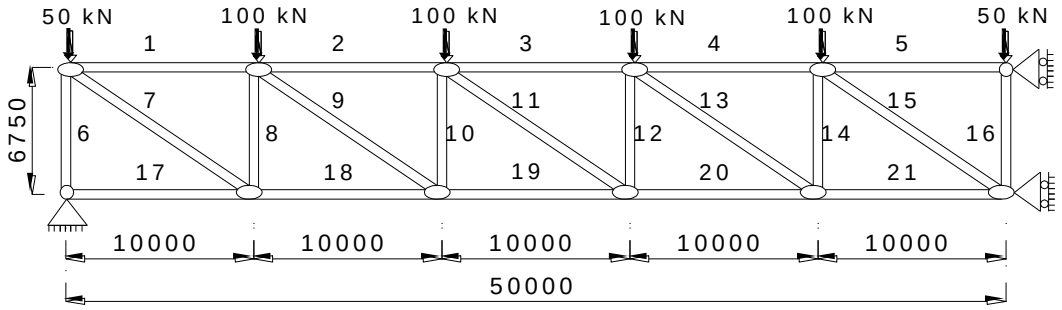

Figure 5.7 Dimensions of a Pratt truss (half span shown, dimensions in mm), (PT2)

Table 5.10 compares the results between the two failure locations. When the failure is near the support, using truss analysis gave the same results as the member-based analysis. This is because the increase in the brace force was very small, a result of the small chord compression force and a small change in the line of action in the chord compression force (as will be explained in Section 5.4).

Table 5.10 Effects of the failure location

	Inner brace failure		Outer brace failure	
	Isolated Member 16	Heated Truss	Isolated Member 6	Heated Truss
Critical temperature	566 °C	515 °C	585 °C	590 °C
Maximum displacement	-	1417 mm	-	3033 mm
Member force ratio ($P_\theta/P_{20°C}$)	1.00	1.40	1.00	0.99

5.3.8 Summary of results

In summary, these results show that due to truss undergoing large displacements at elevated temperatures, some truss members (compression brace members near the truss centre) experience large increases in member forces. Therefore, when calculating the member critical temperatures, it would not be safe to use the member forces from ambient temperature structural analysis. Using the ambient temperature member force may overestimate the truss member critical temperature (based on truss analysis) by 100 °C.

The influence of slenderness on the truss member forces can be ignored owing to the unchanged overall geometry of the trusses. Also, the span of the trusses had no effect on the critical temperature as long as the span-to-depth ratio was constant.

As will be explained in the next section, the changes in forces in the top chord, bottom chord and tension brace members of Howe, Pratt and Warren trusses are small at high temperatures. However, the effect of the deformed shape of Pratt and Warren trusses at elevated temperatures on the compression brace members is considerable. Furthermore, the angle between diagonal member and chord member has a significant influence on failure temperature of the trusses.

5.4 Development of Simple Method

The lower truss critical temperatures from truss analysis compared to member-based analysis are a result of increased brace compression force. Two methods will be developed in this section to calculate this force increase. This increase is a result of the large deflection of the truss. As shown in Table 5.11, the maximum truss deflection ranged from 0.014 to 0.03 of the truss span (span to deflection ratios of 71

and 33 respectively). In the fire protection industry, a deflection limit of span/30 is often used (BSI, 2009) to determine fire resistance. For simplicity and for safety, this value will be used in developing the calculation methods.

Table 5.11 Maximum truss deflections

Member No.	δ_{max} (mm)	L (mm)	δ_{max} / L
WT1	168	12000	0.014
WT2	389	25000	0.016
WT3-A	587	25000	0.024
WT3-B	563	25000	0.023
WT3-C	574	25000	0.023
WT3-D	630	25000	0.025
WT4	663	25000	0.027
WT5	97	4500	0.022
WT6	221	12000	0.018
WT7	523	25000	0.021
WT8	183	12000	0.015
WT9	227	12000	0.019
WT10	218	12000	0.018
PT1-A	210	12000	0.018
PT1-B	222	12000	0.019
PT1-C	260	12000	0.022
PT1-D	240	12000	0.02
PT2-A	1417	100000	0.014
PT2-B	3033	100000	0.03
PT3	638	25000	0.026

5.4.1 Method 1: Analytical method

To enable detailed comparison for forces in different truss members between calculation using the proposed analytical method and truss analysis results, results for the Warren and Pratt trusses shown in Figure 5.8 are used.

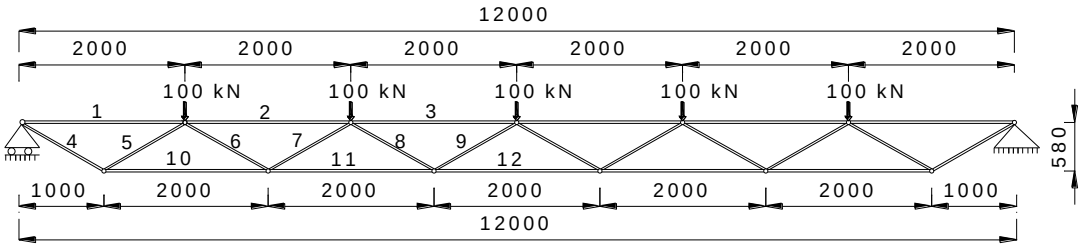

a) Warren Truss (WT9)

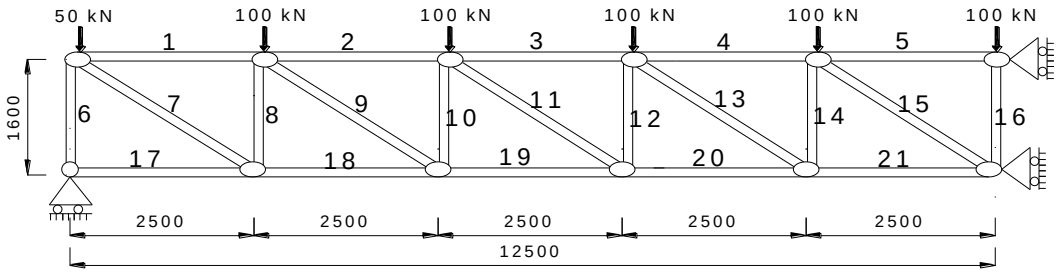

b) A half of Pratt Truss (PT3)

Figure 5.8 Dimensions of trusses used for detailed comparison of additional forces (dimensions in mm)

The critical temperature of the Warren truss was 623 °C, due to buckling of brace member 9 in compression. At truss failure, the maximum truss deflection was 293 mm. Table 5.12 and Table 5.13 compare the truss member forces with their initial values at 20 °C. For the Pratt truss, the critical temperature was 617 °C, reached due to failure of member 16. At the failure temperature, the maximum truss deflection was 638 mm.

Table 5.12 Comparison of the member forces for the Warren truss in Figure 5.8 (units in kN)

Member No.	ABAQUS		
	$F_{20°C}$	$F_{max, Abaqus}$	Ratio ($F_{max, Abaqus}$ / $F_{20°C}$)
1	-433.0	-416.2	0.96
2	-1125.8	-1107.8	0.98
3	-1472.0	-1462.7	0.99
4	500.0	501.6	1.00
5	-500.0	-512.4	1.02
6	300.0	274.4	0.91
7	-300.0	-345.5	1.15
8	100.0	57.6	0.58
9	**-100.0**	**-167.1**	**1.67**
10	866.0	878.7	1.01
11	1385.6	1414.5	1.02
12	1558.8	1608.4	1.03

Table 5.13 Comparison of the member forces for the Pratt truss in Figure 5.8 (units in kN)

Member No.	ABAQUS		
	$F_{20°C}$	$F_{max, Abaqus}$	Ratio ($F_{max, Abaqus}$ / $F_{20°C}$)
1	-703.1	-713.0	1.01
2	-1250.0	-1267.5	1.01
3	-1640.6	-1655.3	1.01
4	-1875.0	-1891.1	1.01
5	-1953.1	-1987.0	1.02
6	-500.0	-498.8	1.00
7	834.8	851.4	1.02
8	-450.0	-453.7	1.01
9	649.3	658.1	1.01
10	-350.0	-365.4	1.04
11	463.8	460.6	0.99
12	-250.0	-284.1	1.14
13	278.2	279.1	1.00
14	-150.0	-186.0	1.24
15	92.8	92.5	1.00
16	**-100.0**	**-189.6**	**1.90**
17	0.0	23.7	-
18	703.1	732.4	1.04
19	1250.0	1278.2	1.02
20	1640.6	1660.0	1.01
21	1875.0	1892.3	1.01

The results in Table 5.12 and Table 5.13 reveal the following trend clearly:

- Forces in the tension brace members decrease. Therefore, for these members, the current member-based design method is on the safe side;
- The changes in forces in the chord members are small. Therefore, the current member-based design method is acceptable;

- The large percentage change in forces occurs in the compression brace members near the centre of the truss. Away from the truss centre, the change in compression force in the brace members rapidly diminishes.

5.4.1.1 Maximum increase in compression brace force at centre of truss

Referring to Figure 5.9, which shows the deformed geometry at the joint at the centre of the truss, the increase in compression force in the compression brace members (member 9) is to resist the vertical components of the compression chords (member 3).

Assuming the maximum truss deflection is δ_{max}, the angle between the straight line drawn from the support to the maximum deformed position of the compression chord is $\alpha=\delta_{max}/(L/2)$, where L is the total span of the truss. The angle between the deformed compression chord and the horizontal is approximately $\alpha/2$. Based on the above assumptions, the additional vertical force from one of the two chord members with the maximum compression force (chord member 3) can be calculated as:

$$F_{maximum\ chord\ compression} * \frac{\delta_{max}}{L/2} * \frac{1}{2} = F_{maximum\ chord\ compression} * \frac{\delta_{max}}{L} \quad 5.1$$

Therefore, the maximum increase in compression force in the brace member (member 9) can be calculated as follows:

$$\Delta F_{truss\ centre} = \frac{F_{maximum\ chord\ compression} * \frac{\delta_{max}}{L}}{\sin\theta} \quad 5.2$$

where θ is the angle between the compression brace member at the truss centre (member 9) and the horizontal.

The total compressive force in the brace member at the truss centre (member 9) is:

$$F_{truss\ centre} = F_{truss\ centre,0} + \frac{F_{maximum\ chord\ compression} * \frac{\delta_{max}}{L}}{\sin\theta} \quad 5.3$$

5.4.1.2 Increase in compression brace force away from the centre of truss

Away from the centre of truss, the increase in force in the compression brace members decrease rapidly for three reasons: (1) the chord compression forces are lower; (2) the additional vertical force from one of the two chord members with the

higher compression force are shared by two brace members; (3) as shown in Figure 5.9(c), the relative chord rotation (γ) between two adjacent members is much smaller than the angle $\alpha/2$ to the horizontal at the centre of the truss (Figure 5.9(b)). Because the percentage increases in forces in these members are small, gross approximation is acceptable when calculating the force increase in these members. Assuming the chord compression force decreases linearly from at the truss centre to 0 at support, and assuming that the relative rotation of the chord members at each node is $\alpha/2$, the increase in compression force in compression brace members not at the centre of the truss can be approximately calculated as:

$$\Delta F_{other\ brace\ member} = \frac{1}{2} * \Delta F_{truss\ centre} * \frac{d}{L/2} \quad 5.4$$

where d is the distance from the support to the node connecting the compression brace member whose force is calculated.

$$F_{other\ brace\ member} = F_{other\ brace\ member,0} + \frac{1}{2} * \Delta F_{truss\ centre} * \frac{d}{L/2} \quad 5.5$$

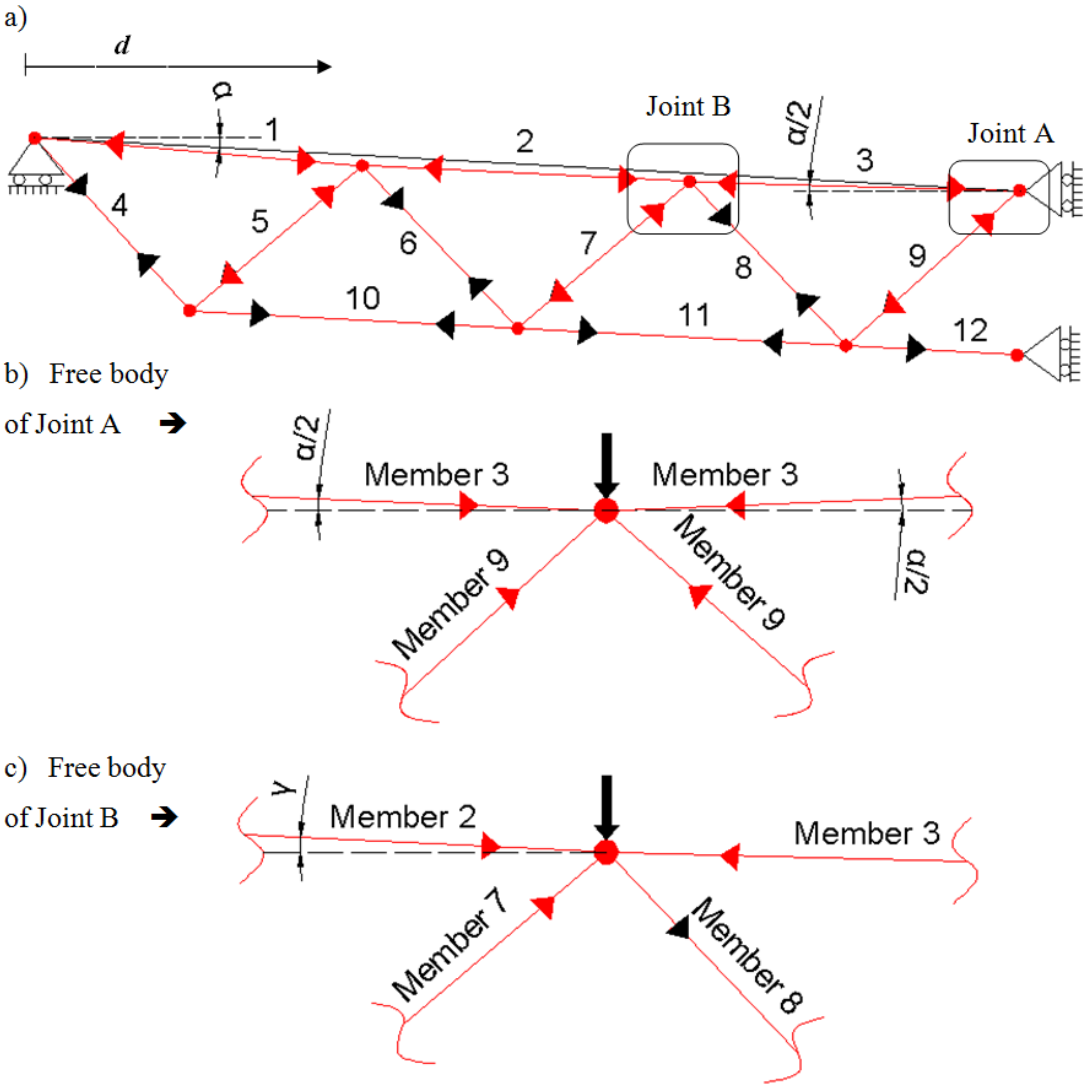

Figure 5.9 Deformed shape and free body diagrams for a Warren truss

For the Pratt truss, as shown in Figure 5.8, because there is only one vertical member at the centre, the additional compressive force is doubled as given in Equation 5.2, and θ=90°. Therefore:

$$\Delta F_{truss\ centre} = 2 * F_{maximum\ chord\ compression} * \frac{\delta_{max}}{L} \qquad 5.6$$

The increase in compression force in the members away from the centre can be calculated using Equation 5.5 for the same reasoning as for the Warren truss.

Table 5.14 and Table 5.15 compare the compression brace forces from truss analysis ($F_{max,\ Abaqus}$) with those calculated using Equations 5.3, 5.5 and 5.6 for the two trusses, one for the actual maximum truss deflection at failure (F_{max}) and one for the assumed maximum truss deflection of L/30 ($F_{assumed}$). As can be seen from the tables

below, the predicted forces in compression brace members are slightly higher, but reasonably close to the member forces based on truss numerical simulations.

Table 5.14 Comparison of compressive member forces for the Pratt truss in Figure 5.8 (units in kN)

Member No.		ABAQUS	EQUATIONS 5.5 and 5.6			
	$F_{20°C}$	$F_{max, Abaqus}$	ΔF_{max}	F_{max}	$\Delta F_{assumed}$	$F_{assumed}$
8	-450.0	-453.7	-3.6	-453.6	-4.7	-454.7
10	-350.0	-365.4	-12.8	-362.8	-16.7	-366.7
12	-250.0	-284.1	-25.1	-275.1	-32.8	-282.8
14	-150.0	-186.0	-38.3	-188.3	-50.0	-200.0
16	**-100.0**	**-189.6**	**-99.7**	**-199.7**	**-130.2**	**-230.2**

Table 5.15 Comparison of compressive member forces for the Warren truss in Figure 5.8 (units in kN)

Member No.		ABAQUS	EQUATIONS 5.3 and 5.5			
	$F_{20°C}$	$F_{max, Abaqus}$	ΔF_{max}	F_{max}	$\Delta F_{assumed}$	$F_{assumed}$
WT9-M5	-500.0	-508.0	-5.5	-505.5	-9.6	-509.6
WT9-M7	-300.0	-330.2	-28.4	-328.4	-32.7	-332.7
WT9-M9	**-100.0**	**-169.6**	**-55.7**	**-155.7**	**-98.1**	**-198.1**

The accuracy of the proposed analytical method has been checked against all the simulation trusses used in the parametric study. Figure 5.10 compares the maximum compression brace forces at the centre of the trusses from truss analysis with those calculated using Equations 5.3 and 5.6 for two maximum truss deflections: the maximum truss deflection at failure from ABAQUS analysis and the assumed maximum truss deflection of L/30. Also, original truss member forces at 20 °C ($F_{20°C}$) are included in Figure 5.10. The results in Figure 5.10 indicate that the proposed calculation method can produce very accurate results if the actual maximum deflection of truss is used. If a value of L/30 is used for the maximum deflection, the calculation results are reasonably close to the ABAQUS simulation

results, and are on the safe side. In contrast, using the ambient temperature forces can greatly underestimate the member forces and produce unsafe design.

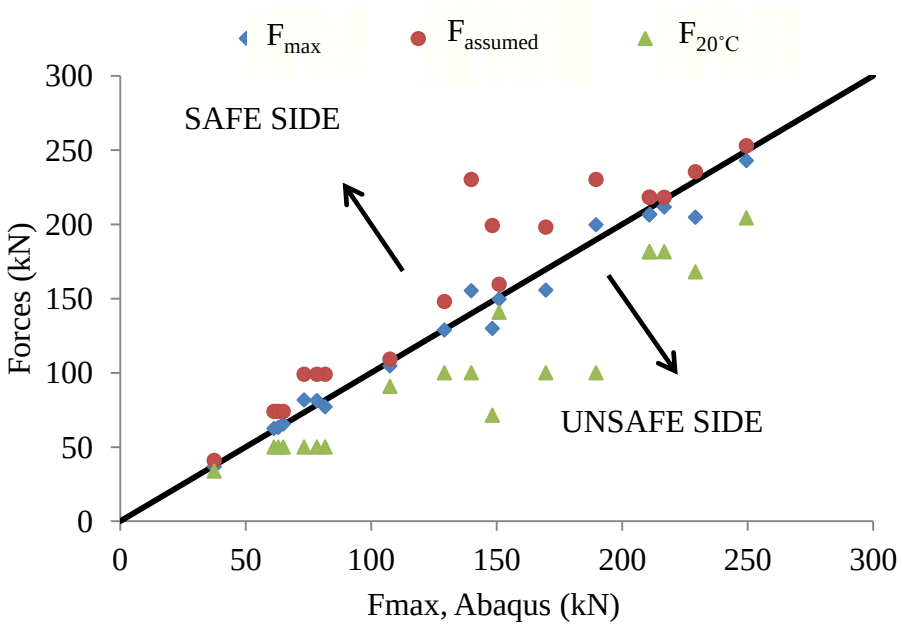

Figure 5.10 Comparison of forces in critical members of Warren and Pratt trusses between analytical calculations, ABAQUS simulation results and ambient temperature values

Figure 5.11 illustrates the same comparisons for other compression brace members. Because the ambient temperature forces are high and the associated chord member forces are small, the changes in these member forces are much smaller than for the critical members shown in Figure 5.10. Therefore, the three sets of results are much closer to each other than shown in Figure 5.10. Nevertheless, using the ambient temperature member forces is unsafe in certain cases. Since the proposed calculation method is simple to use and the calculation results are in good agreement with the ABAQUS simulation results, it is recommended to use the proposed analytical method.

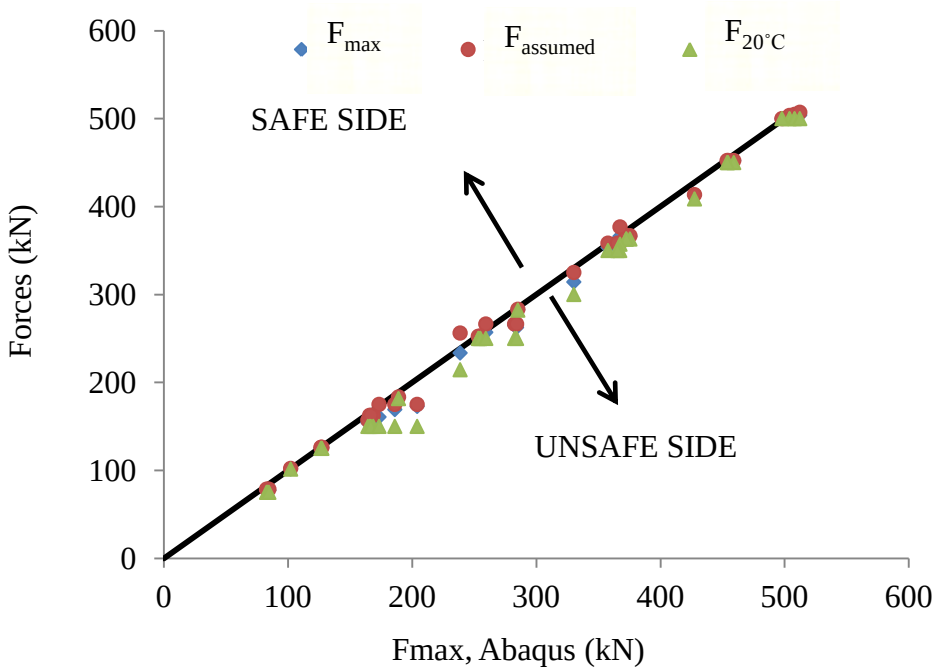

Figure 5.11 Comparison of forces in compression brace members of Warren and Pratt trusses between analytical calculations, ABAQUS simulation results and ambient temperature values

5.4.2 Method 2: Static analysis of truss with large displacement

In the previous section, an analytical method has been developed to calculate the increases in brace member compressive forces due to the large truss deflection. This force increase is a result of the truss configuration being different from the initial condition, which has no deflection. This section will investigate whether these force changes can be obtained directly from second-order, static elastic analysis of the truss at the proposed large deflection of span/30. The rationale behind this alternative method is twofold: (1) assumptions were made in the previous section on the change of angles between two adjacent chord segments; (2) structural engineers are familiar with static elastic truss analysis and it would be easy to continue the static elastic truss analysis until the deflection limit of span/30 was reached.

The Warren and Pratt trusses shown in Figure 5.8 will be reanalysed. The procedure for obtaining the new design member forces, due to the effect of large truss deflection, is as follows:

(1) Perform second-order, elastic static analysis of the truss with increasing load until the maximum truss deflection reaches span/30.
(2) Using the loads above, perform linear elastic static analysis of the truss.

(3) The ratios of member forces from step (1) to step (2) are the required results reflecting the effects of large truss deflection on member forces.

Table5.16 and Table 5.17 compare the force ratios in all truss members for the two trusses shown in Figure 5.8, between the results of static analysis ($F_{max,L/30}/F_{20°C}$), with the elevated temperature simulation results ($F_{Elevated} / F_{20°C}$) and the analytical method of the previous section ($F_{max,proposed}/F_{20°C}$).

For all members, the three different methods give close results. Bold type in these tables indicates compression members. These members experience increased forces due to large truss deflection and these increased forces should be included in truss fire resistance design.

Table 5.16 Comparison of force ratios for all members of the Warren truss in Figure 5.8

Member No.	ABAQUS		Equation 5.3 and 5.5
	$\frac{F_{Elevated}}{F_{20°C}}$	$\frac{F_{max,L/30}}{F_{20°C}}$	$\frac{F_{max,proposed}}{F_{20°C}}$
1	0.94	0.92	
2	0.98	0.95	
3	0.99	0.97	
4	1.00	0.97	
5	**1.02**	**1.00**	**1.02**
6	0.91	0.87	
7	**1.10**	**1.11**	**1.17**
8	0.44	0.64	
9	**1.97**	**2.01**	**1.98**
10	1.01	0.98	
11	1.03	0.99	
12	1.05	1.03	

Table 5.17 Comparison of force ratios for all members of the Pratt truss in Figure 5.8

Member No.	ABAQUS		Equation 5.5 and 5.6
	$\frac{F_{Elevated}}{F_{20°C}}$	$\frac{F_{max,L/30}}{F_{20°C}}$	$\frac{F_{max,proposed}}{F_{20°C}}$
1	1.01	0.97	
2	1.01	0.98	
3	1.01	0.98	
4	1.01	0.98	
5	1.01	1.00	
6	1.00	0.96	
7	1.02	0.86	
8	**1.01**	**0.98**	**1.01**
9	1.01	0.97	
10	**1.04**	**1.01**	**1.05**
11	0.99	0.97	
12	**1.14**	**1.13**	**1.13**
13	1.00	0.96	
14	**1.24**	**1.29**	**1.33**
15	1.00	1.38	
16	**1.90**	**2.44**	**2.30**
17	-	-	
18	1.04	1.02	
19	1.02	0.99	
20	1.01	0.99	
21	1.01	0.98	

Table 5.18 compares the calculated load ratios using second-order static truss analysis of this section, the calculation results using the analytical method of the previous section and the elevated temperature simulation results, for the critical members of all the trusses investigated in the previous section. The agreement between the three sets of results is excellent, confirming that both approximate methods may be used to calculate the increased brace compression force due to the large truss deflections.

Table 5.18 Comparison of forces in the critical brace members of all the Warren and Pratt trusses studied in section 5.3 between ABAQUS elevated temperature simulation results, ABAQUS ambient temperature second-order elastic simulation, and analytical calculation

Member No.	Elevated Temperature Analysis	Second-order Elastic Analysis	Analytical Method (Equation 5.3 and 5.5)
	$\frac{F_{Elevated}}{F_{20°C}}$	$\frac{F_{max,L/30}}{F_{20°C}}$	$\frac{F_{max,proposed}}{F_{20°C}}$
WT4-M7	1.22	1.16	1.19
WT5-M9	1.95	2.06	1.98
WT6-M9	2.04	2.18	1.98
WT7-M9	1.96	2.10	1.98
WT8-M11	2.38	2.55	2.53
WT9-M9	1.97	2.01	1.98
WT10-M6	1.36	1.59	1.40
PT1-A-M10	1.42	1.50	1.48
PT3-M16	1.90	2.44	2.30

Table 5.19 further compares the three sets of results for the compressive brace members next to the critical members. Again, the results confirm the accuracy of the two approximate methods.

Table 5.19 Comparison of forces in the compression brace members of all the Warren and Pratt trusses studied in section 5.3 between ABAQUS elevated temperature simulation results, ABAQUS ambient temperature second-order elastic simulation, and analytical calculation

Member No.	Elevated Temperature Analysis	Second-order Elastic Analysis	Analytical Method (Equation 5.3 and 5.5)
	$\frac{F_{Elevated}}{F_{20°C}}$	$\frac{F_{max,L/30}}{F_{20°C}}$	$\frac{F_{max,proposed}}{F_{20°C}}$
PT1-A-M8	1.11	1.10	1.05
PT1-A-M6	1.02	1.04	1.01
PT3-M14	1.24	1.29	1.33
PT3-M12	1.14	1.13	1.13
PT3-M10	1.04	1.01	1.05
PT3-M8	1.01	0.98	1.01
WT4-M5	1.04	1.02	1.01
WT5-M7	1.13	1.15	1.09
WT5-M5	1.02	1.02	1.01
WT6-M7	1.11	1.13	1.17
WT6-M5	1.01	1.02	1.02
WT7-M7	1.11	1.16	1.17
WT7-M5	1.02	1.03	1.02
WT8-M9	1.22	1.28	1.39
WT8-M7	1.07	1.10	1.11
WT8-M5	1.01	1.01	1.01
WT9-M7	1.10	1.11	1.08
WT9-M5	1.02	1.00	1.02
WT10-M4	1.02	1.01	1.01

5.5 Conclusions

This chapter has presented the results of a numerical investigation into the behaviour of welded steel tubular trusses at elevated temperatures. Finite Element (FE) simulations were carried out for Circular Hollow Section (CHS) trusses using the commercial Finite Element software ABAQUS v6.10-1 (2010).

The focus of this study was truss behaviour and how truss action can be taken into account when calculating the truss member critical temperatures. It has been found that when calculating truss member critical temperatures, the joints between the truss members may be safely simplified as pin joints. This simplification allows us to ignore the effects of any differential thermal expansion in different truss members.

The main conclusion of the parametric study on truss behaviour was that the member-based calculation method for calculating member critical temperatures, in which the ambient temperature truss member forces are used, may not be safe. The critical temperature from the present member-based calculation method can overestimate the truss critical temperature by as much as 100 °C. The reason for this is that compression brace members experience increases in their forces at large truss deflections. The increase in compression brace member force is highest at the centre of the truss and rapidly decreases towards the supports. The increase in compression brace member force is higher in a Pratt truss than in a Warren truss.

The author has developed two approximate methods to calculate the increases in the truss compressive brace member forces due to increased truss deflection: an analytical method, and another method based on second-order elastic truss analysis at ambient temperature. In both methods, the maximum truss deflection is span L/30; a value that is familiar to fire protection engineers. Both approximate methods have been shown to produce revised truss member results, due to the effects of large truss deflections, which are in reasonably good agreement with ABAQUS elevated temperature simulation results and are generally on the safe side.

CHAPTER 6 BEHAVIOUR AND DESIGN OF LOCALLY HEATED TRUSSES

6.1 Introduction

This chapter examines the effects of thermal restraint on failure temperatures of the critical members of trusses when the truss is subjected to localised fire. In such a truss, the truss member nearest to the fire will experience the highest temperature, with reduced temperatures in the nearby members. The number of nearby truss members being heated and their temperatures will affect the failure temperature of the critical truss member with the highest temperature. The aim of this chapter is to investigate these effects and how they should be considered in fire safety design.

The critical member in a truss with localised heating behaves as a thermally restrained member whose behaviour is shown in Figure 6.1. Because the thermal elongation of the critical member with the highest temperature is restrained, additional compressive force is generated in the member (stage A). This results in the critical member experiencing premature failure (point A) because the member force is higher than the initial member force at ambient temperature. After this premature failure, the force in the critical member is relieved (stage B). Depending on the restraint stiffness of the surrounding structure, the critical member may still be able to sustain forces greater than the initial force at ambient temperature. For the purpose of this study, the truss member failure temperature is defined as the temperature at which the force in the critical member returns to the initial value at ambient temperature (point B). This definition of the failure temperature of thermally restrained members has been used by a number of studies including those of Franssen (2000), Wang (2004) and Wang et al. (2010).

In order to develop a method to calculate the failure temperature, as defined above, of the critical member of the truss subjected to localised heating, it is necessary to address the following three issues:

(1) To quantify the level of axial restraint to the critical member, afforded by the surrounding structure;
(2) To calculate the failure temperature of the axially restrained member;

(3) To develop a method to account for the effects of the surrounding members being heated.

Sections 6.2, 6.3 and 6.4 will deal with the above three issues respectively.

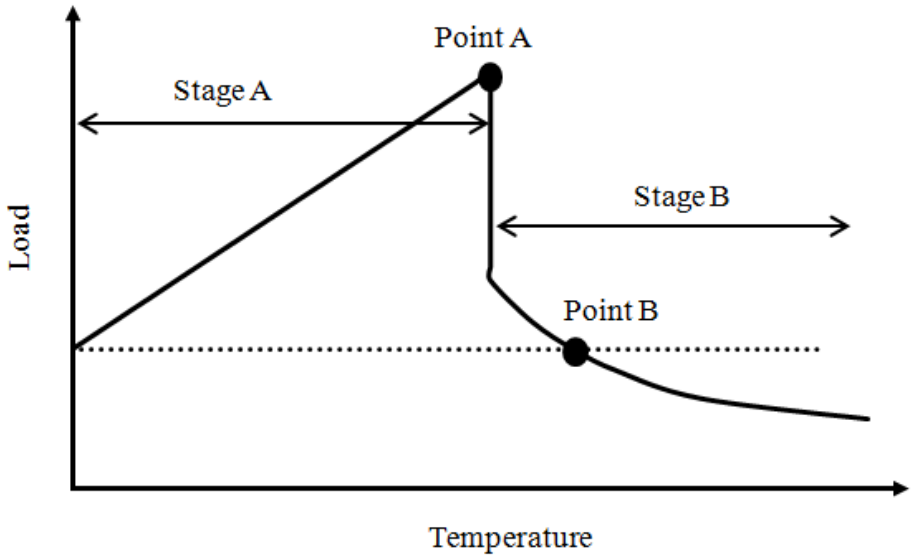

Figure 6.1 Load – temperature behaviour of restrained compression member

This study will be based on numerical simulations using the general purpose Finite Element software ABAQUS v6.10-1. In any typical truss, because the chord members have large section sizes relative to the brace members, the effect of thermal restraint to the chord members is small. Therefore, this study will focus on the brace members. In the numerical simulations, the truss is assumed to have continuous chord members and pin-joined brace members, as shown in Figure 6.2. The continuous chord members impose axial restraint on the brace members. In contrast, there would be no additional compression force if the truss is pinned and statically determinate. Furthermore, pin-joints between the brace and chord members are assumed to ensure that the results are on the safe side. Furthermore, initial imperfections are assumed in the critical truss members. However, to reduce complexity, the other members are assumed straight.

The truss member temperature distributions will be assumed, however, since the developed design method will be generally applicable, this assumption is not a problem because the purpose of the truss simulation results is to provide data to validate the developed design method. The simulations will be carried out to examine the influences of the following design parameters:

- Load ratio, ρ_N
- Slenderness, λ
- Axial restraint ratio, β_l

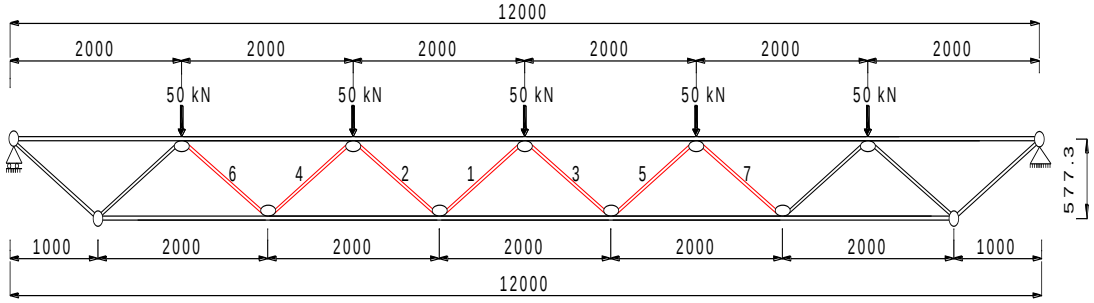

(a) Warren Truss (WT-M1)

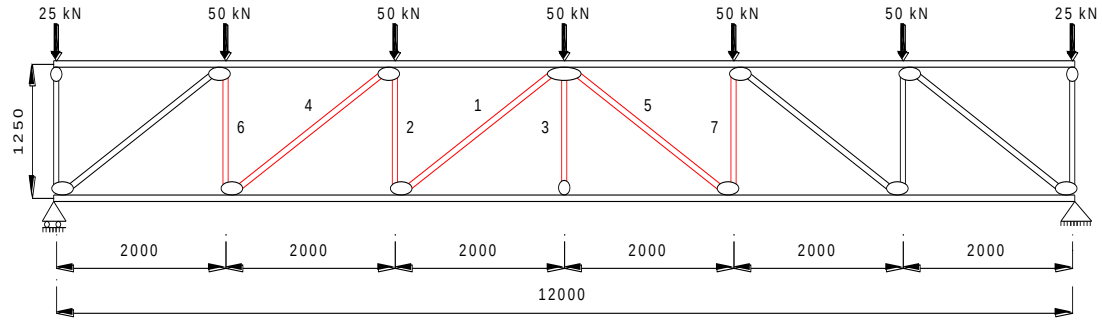

(b) Howe Truss (HT-M1)

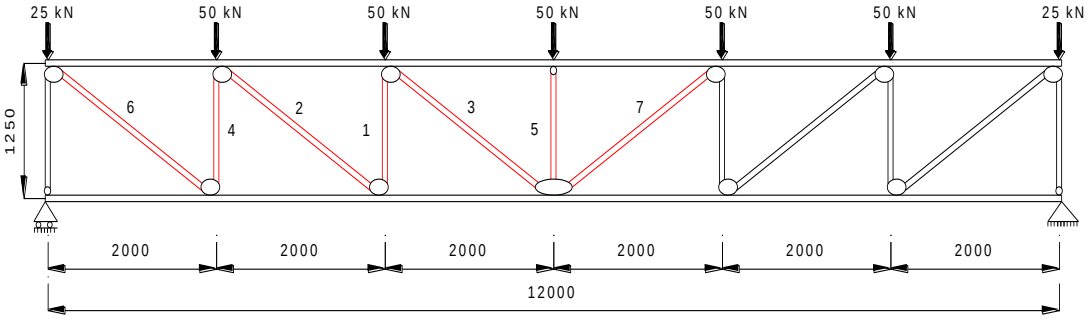

(c) Pratt Truss (PT-M1)

Figure 6.2 Truss configurations (dimensions in mm)

6.2 Behaviour of Single Heated Brace Member in Truss

When a brace member in a truss is heated, it behaves as an axially restrained member with restrained thermal expansion. In analysing an axially restrained compression member, a spring is used to represent the restraint. In the truss, the restraint to the

heated member comes from the surrounding structure. It is necessary to calculate the equivalent restraint stiffness and to ensure that the correct restraint stiffness is used. This section will compare the behaviour of brace members in trusses with their representations of a single member with an attached axial spring.

Figure 6.3(a) shows an isolated truss brace member, with the springs at each end representing the surrounding structures.

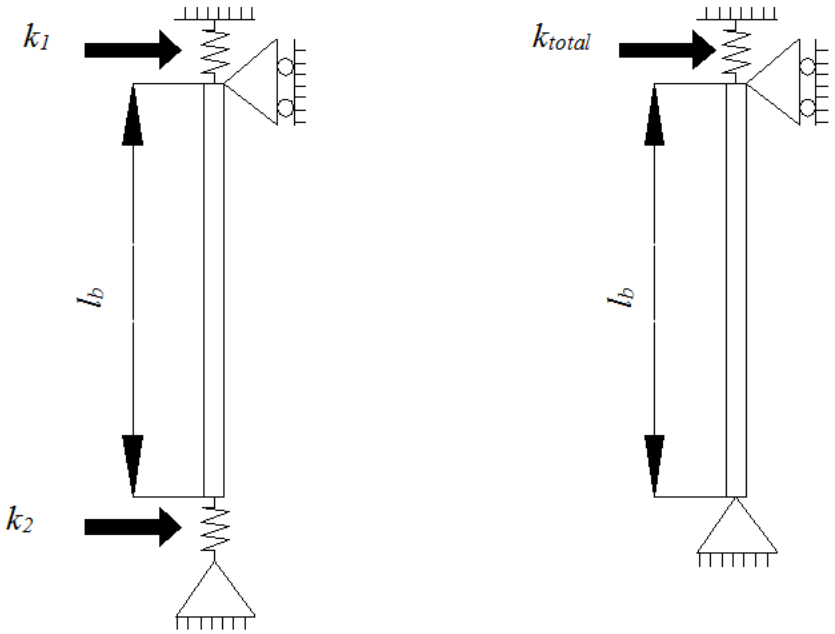

a) Spring at both ends b) Single spring

Figure 6.3 Mechanical model of a restrained steel truss member

This member can be represented by the member shown in Figure 6.3 (b) with one spring stiffness, which is often the model used in analysing axially restrained compressive members. The equivalent one spring stiffness can be calculated as follows:

$$\frac{1}{k_{total}} = \frac{1}{k_1} + \frac{1}{k_2} \qquad 6.1$$

The equivalent one spring stiffness can be calculated based on static analysis of the truss. Take the truss shown in Figure 6.4 as an example. The critical member is

removed and replaced by equal compression forces applied at the two end joints. The overall stiffness k_{total} is simply P divided by the total separation of the two joints.

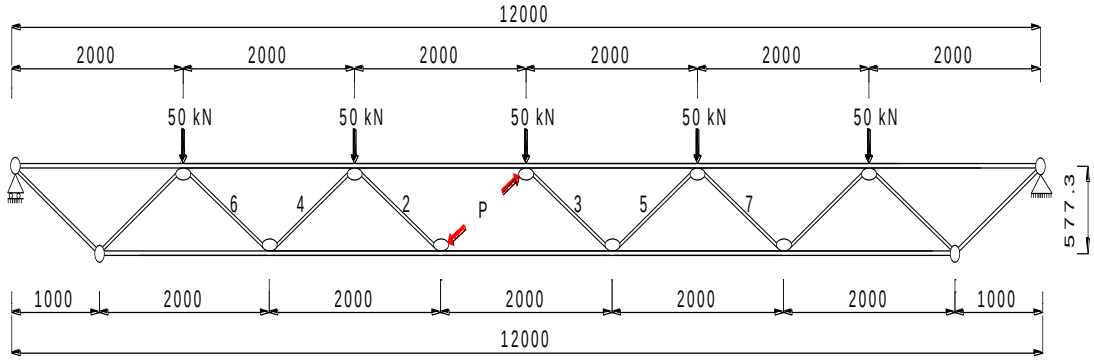

Figure 6.4 Model to determine the restraint stiffness to a heated member

In the numerical simulations, the axially restrained compressive member is modelled using 2D line elements of type B31 with a spring element as shown in Figure 6.3 (b). Initial geometrical imperfections should be included, based on the lowest buckling mode from eigenvalue analysis.

A number of trusses have been modelled, using both member analysis (Figure 6.3 (b)) and truss analysis where only one member is heated. Figure 6.2 shows the different simulated trusses and the heated members, with only one of the members being heated in each simulation.

In these simulations, different levels of load ratio, ρ_N, were considered by changing the applied load. The section size of both the top and bottom chord members was changed to vary the restraint stiffness. Appendix D gives the cross-sectional dimensions used in the simulations.

Table 6.1 lists the comparison cases, for three different truss types, different load ratios, different critical member slendernesses and different axial restraint ratios. For identification, the name of each truss consists of the truss type (Warren (WT), Howe (HT) and Pratt (PT)), the truss number (such as WT1, WT2, PT2, etc.) and the heated member number (e.g. M1 refers to member 1 being heated). For example, WT2-M1 refers to brace member 1 of Warren truss number 2 being heated.

The axial restraint ratio is expressed as follows:

$$\beta_l = \frac{k_{total}}{k_b} \quad 6.2$$

$$k_b = \frac{EA}{l} \quad 6.3$$

where k_b is the brace member stiffness.

Table 6.1 Simulation models with different parameters

Simulation case	Load Ratios (ρ_N)	Slenderness (λ)	Axial Restraint Ratios (β_l)
WT1-M1	0.20	57	0.17
WT2-M1	0.44	57	0.17
WT3-M1	0.58	57	0.17
WT4-M1	0.47	57	0.12
WT5-M1	0.26	57	0.12
WT6-M1	0.68	84	0.08
WT7-M1	0.22	57	0.23
WT8-M1	0.47	84	0.24
WT9-M1	0.36	84	0.19
WT10-M1	0.65	44	0.14
WT11-M1	0.40	44	0.14
PT1-M5	0.40	49	0.01
PT2-M5	0.46	92	0.03
PT3-M1	0.60	33	0.05
HT1-M1	0.38	93	0.11

Figure 6.5 compares selective force – temperature curves between the member and truss based analyses. It is clear that the agreement is excellent throughout all the different phases of the restrained truss member behaviour.

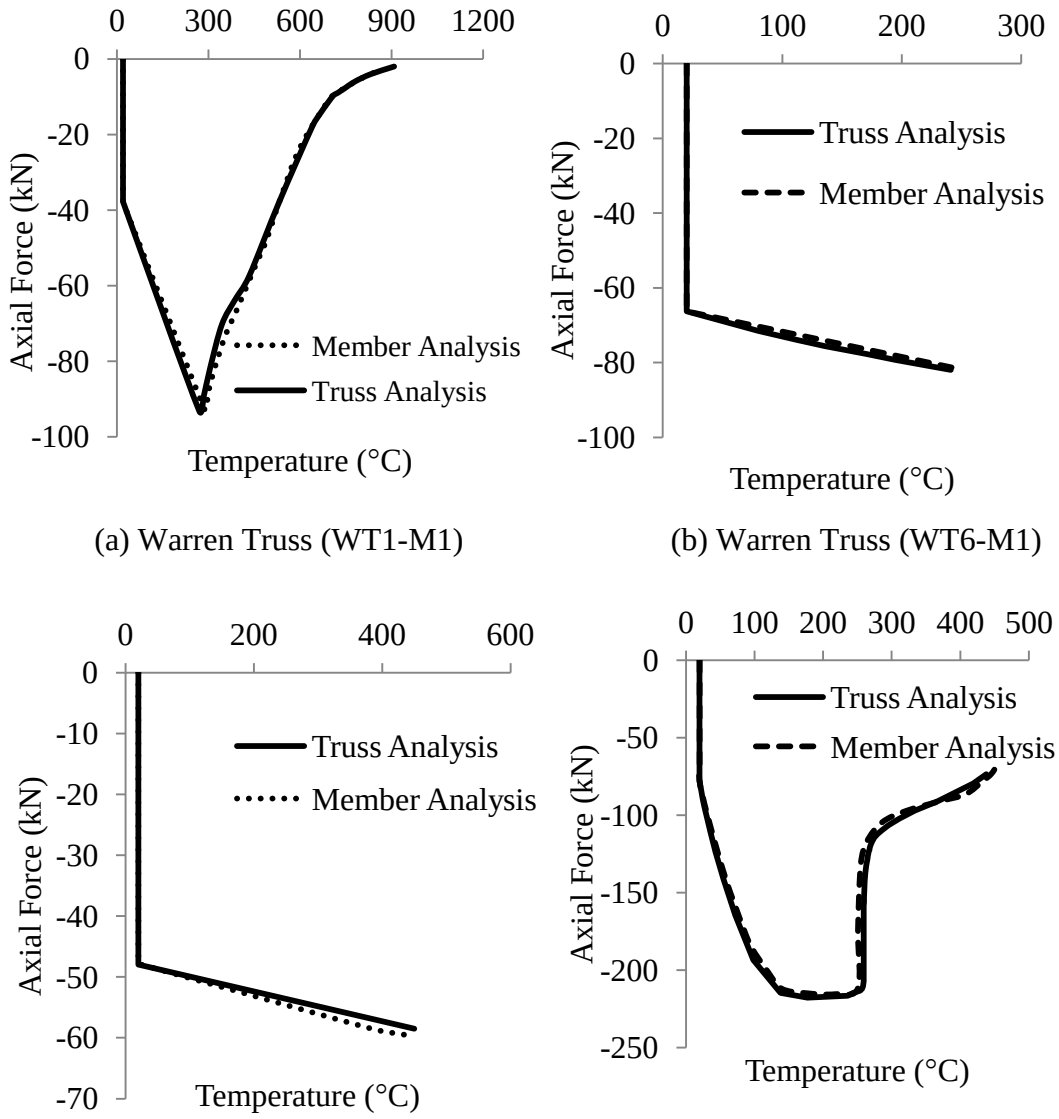

(a) Warren Truss (WT1-M1)

(b) Warren Truss (WT6-M1)

(c) Pratt Truss (PT1-M5)

(d) Howe Truss (HT1-M1)

Figure 6.5 Comparison of force – temperature curves between member and truss analyses

Table 6.2 compares the truss member failure temperatures between the truss member analyses with or without axial restraint, and truss simulations. Results are given for both the load ratio ($P_\theta/P_{20°C}$), which is the ratio of the member force at failure temperature (P_θ) from truss analysis to that at ambient temperature ($P_{20°C}$), and the member failure temperatures. Table 6.2 clearly shows that there is excellent agreement between the truss analysis results and the member analysis results with axial restraint. The member analysis results without restraint can give considerable overestimation of the restrained member failure temperatures.

This comparative study (both Figure 6.5 and Table 6.2) clearly confirms that the single member based analysis, with axial restraint, is adequate to represent the behaviour of the single heated truss member in the truss. Also, it is important that the effects of the axial restraints, in reducing the restrained truss member failure temperature, are included in fire resistant design.

Table 6.2 Comparison between failure temperatures of single heated truss members and changes in their forces

Truss	Member Analysis (without restraint)	Truss Analysis	Member Analysis (with restraint)	P_θ / $P_{20°C}$
WT1-M1	688 °C	532 °C	533 °C	2.44
WT2-M1	578 °C	322 °C	328 °C	1.70
WT3-M1	526 °C	231 °C	235 °C	1.35
WT4-M1	598 °C	368 °C	378 °C	1.72
WT5-M1	657 °C	510 °C	520 °C	2.10
WT6-M1	470 °C	241 °C	245 °C	1.26
WT7-M1	679 °C	546 °C	549 °C	3.81
WT8-M1	543 °C	233 °C	233 °C	1.71
WT9-M1	586 °C	345 °C	347 °C	2.00
WT10-M1	575 °C	323 °C	329 °C	1.79
WT11-M1	620 °C	470 °C	477 °C	1.54
PT1-M5	520 °C	440 °C	450 °C	1.25
PT2-M5	571 °C	315 °C	320 °C	1.99
PT3-M1	528 °C	415 °C	423 °C	1.27
HT1-M1	644 °C	418 °C	433 °C	2.80

6.3 Method of Calculating Failure Temperatures of Axially Restrained Compressive Tubular Members

Wang et al. (2010) have conducted extensive numerical simulations of axially restrained steel columns at elevated temperatures and have proposed a method, based on regression analysis of their simulation results, to calculate the reduction in the column failure temperature from columns without axial restraint. Their studies were for H-section columns. This section checks whether their calculation method is applicable to tubular members. For this check, numerical simulations were carried

out for axially restrained members in compression with a range of load ratios, levels of axial restraint, and slendernesses. These three parameters govern the retrained column behaviour. A WT4 truss (see in Figure 6.2(a)) was used, considering different load ratios, slendernesses and axial restraints.

The calculation equations of Wang et al. (2010) have been presented in section 2.3.2.2.

6.3.1 Case 1: Effect of load ratio, (ρ_N)

Table 6.3 compares the simulation results for different load ratios. In Table 6.3, $T_{20°C}$ and T_θ refer to the failure temperature from individual member analysis without restraint (using the 20 °C member force) and with axial restraint respectively. ΔT_{ABAQUS} (= $T_{20°C}$-T_θ) is the reduction in the member failure temperature due to restrained thermal expansion, from the ABAQUS simulation model. $\Delta T_{Wang\ et\ al.}$ is the reduction in the failure temperature calculated according to the regression equations of Wang et al. (2010). For these members, the axial restraint ratio and the slenderness were 0.17 and 57 respectively.

Table 6.3 Reduction in member failure temperatures for different load ratios

Load Ratios (ρ_N)	$T_{20°C}$	T_θ	ΔT_{ABAQUS}	$\Delta T_{Wang\ et\ al.}$
0.14	733 °C	607 °C	126 °C	125 °C
0.24	688 °C	533 °C	155 °C	171 °C
0.34	636 °C	440 °C	196 °C	213 °C
0.44	578 °C	308 °C	270 °C	246 °C
0.52	547 °C	278 °C	269 °C	268 °C
0.60	520 °C	243 °C	277 °C	285 °C

The agreement between the ABAQUS results and the calculated results using the Wang et al. (2010) equations is very good.

6.3.2 Case 2: Effect of axial restraint ratio, (β_l)

For this case, two different load ratios, 0.24 and 0.55, were applied while the slenderness was kept constant at 57.

Table 6.4 (a) and 6.4 (b) present the comparisons of the results for these two load ratios.

The ABAQUS simulation results in Table 6.4 (a) indicate that there is a cap in reduction in the restrained member failure temperature as the restraint stiffness increases. This finding correlates with the simulation results of Franssen (2000). This happens when the member force is relatively low and the restraint stiffness is high. The restrained member can resist further temperatures after initial failure at the maximum load and the restrained member behaves very similarly during the phase when the member force returns to the initial force of ambient temperature. This is shown in Figure 6.6. The calculation equations of Wang et al. (2010) do not predict this effect. Nevertheless, the rate of change in the reduction in failure temperature slows down as the restraint stiffness increases. Furthermore, the calculation results using the Wang et al. (2010) equations are on the safe side.

Table 6.4 Comparison of failure temperatures of restrained tubular members (load ratio=0.24)

(a) Load ratio: ρ_N =0.24

Axial Restraint Ratio (β_l)	$T_{20°C}$	T_θ	ΔT_{ABAQUS}	$\Delta T_{Wang\ et\ al.}$
0.02	688 °C	654 °C	34 °C	39 °C
0.08	688 °C	540 °C	148 °C	122 °C
0.12	688 °C	540 °C	148 °C	151 °C
0.17	688 °C	540 °C	148 °C	173 °C
0.30	688 °C	540 °C	148 °C	192 °C

(b) Load ratio ρ_N =0.55

Axial Restraint Ratio (β_l)	$T_{20°C}$	T_θ	ΔT_{ABAQUS}	$\Delta T_{Wang\ et\ al.}$
0.02	537 °C	507 °C	30 °C	61 °C
0.08	537 °C	316 °C	221 °C	194 °C
0.12	537 °C	293 °C	244 °C	238 °C
0.17	537 °C	264 °C	273 °C	271 °C
0.30	537 °C	241 °C	296 °C	302 °C

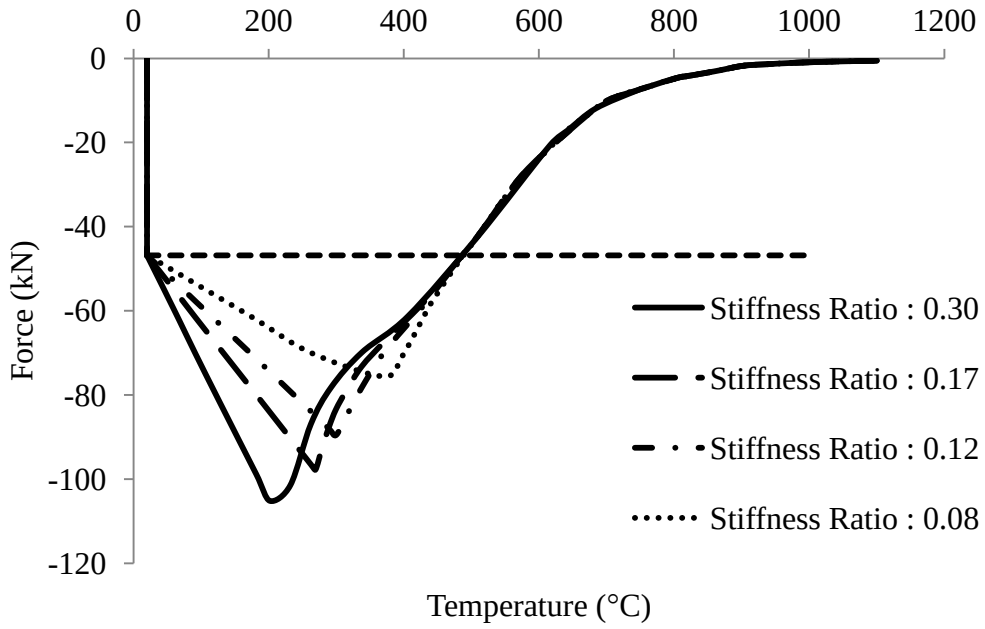

Figure 6.6 Force – temperature curves of axially restrained members (load ratio: 0.24)

6.3.3 Case 3: Effect of slenderness, (λ)

For this case, different cross sections (ϕ76.1x3, ϕ60.3x3, ϕ48.3x4 and ϕ42.4x4) were used. The load ratio and the axial restraint were kept constant at values of 0.55 and 0.17 respectively and Table 6.5 compares the results. These results show very large reductions in column failure temperatures due to axial restraint and that the regression equations of Wang et al. (2010) give good predictions for tubular columns.

Table 6.5 Comparison of restrained member failure temperatures for different member slenderness

Member Slenderness (λ)	$T_{20°C}$	T_θ	ΔT_{ABAQUS}	$\Delta T_{Wang\ et\ al.}$
44	604 °C	337 °C	267 °C	242 °C
57	537 °C	264 °C	273 °C	271 °C
74	507 °C	238 °C	269 °C	303 °C
84	513 °C	245 °C	268 °C	318 °C

In summary, the failure temperature of an axially restrained tubular member in compression will be lower than that without thermal expansion. The reduction in the column failure temperature depends on the load ratio, the axial restraint ratio and the slenderness of the member. It is important that the restraint effect is considered in the

fire safety design of trusses under localised heating. The method proposed by Wang et al. (2010) for calculating the reduction in the failure temperature of axially restrained columns is suitable for tubular members.

6.4 Effects on Critical Member with Multiple Truss Members being Heated

When a single truss member is heated, it is relatively easy to convert this member into an axially restrained compression member, as outlined in section 6.3. When additional members adjacent to the critical member are also heated under localised fire, the behaviour of the critical member is affected. The thermal elongations of the adjacent members will affect the movements at the ends of the critical member, thereby affecting the additional compressive force generated in the critical member. This section develops a method to quantify this change.

6.4.1 Temperature distributions

Figure 6.7 shows different temperature distributions. The truss dimensions are the same as those of WT4 in Figure 6.2(a). The critical member is number 1, being exposed to the highest temperature, T_{max}. Figure 6.7(a), (b), (c) and (d) illustrate heating only the critical member, heating the critical member plus the two adjacent members (one on each side), heating the critical member plus the four adjacent members (two on each side), and heating the critical member plus the six adjacent members (three on each side) respectively. The adjacent members are heated to $3/4T_{max}$ (members 2 and 3), $T_{max}/3$ (members 4 and 5) and $T_{max}/4$ (members 6 and 7) respectively.

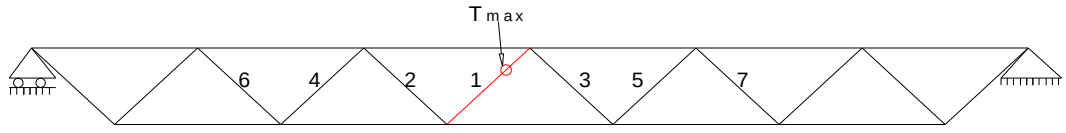

a) Single (critical) member being heated

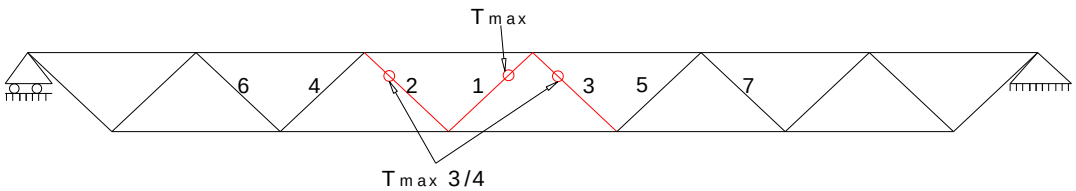

b) Critical member (1) plus two adjacent members (2&3) being heated

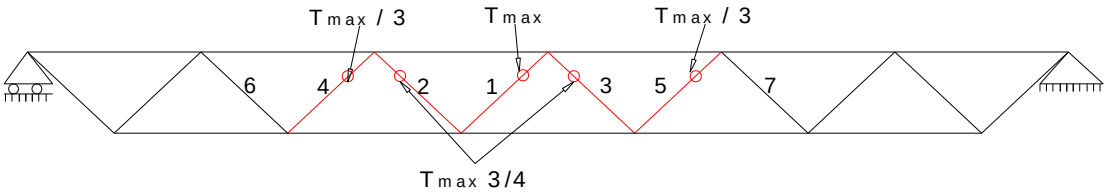

c) Critical member (1) plus four adjacent members (2&3, 4&5) being heated

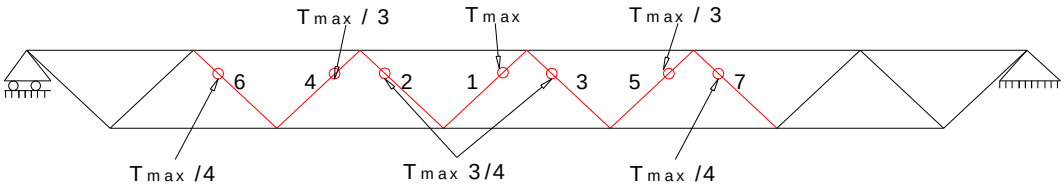

d) Critical member (1) plus six adjacent members (2&3, 4&5, 6&7) being heated

Figure 6.7 Different scenarios of localised heating of a Warren truss

6.4.2 Effects of heating the adjacent members on the critical member

Figure 6.8 compares the temperature–force curves for the different heating scenarios in Figure 6.7 for the critical member (member 1). The rates of increase in the critical member force are lower when multiple members are heated than when only the critical member is heated. Therefore, it would be on the safe side when only considering the critical member being heated in fire resistant design. However, the calculation results would be too conservative. Moreover, there is a negligible effect on the failure temperature of the critical member when the adjacent heated members are three or more members away from the critical member. This is indicated by the closeness of the results in Figure 6.8 between heating 5 members (heated members being 2 members away from the critical member) and 7 members (heated members being 3 members away from the critical member). Therefore, it is only necessary to consider up to two adjacent members on each side of the critical member.

The reduction in the rate of force increase in the critical member due to the adjacent member being heated may be explained by referring to Figure 6.9. When the adjacent members next to the critical member are heated, the joints at both ends of the critical member (Joints A and B in Figure 6.9) are pushed away from each other, thus relieving the thermal elongation of the critical member, reducing the unrestrained thermal expansion of the critical member.

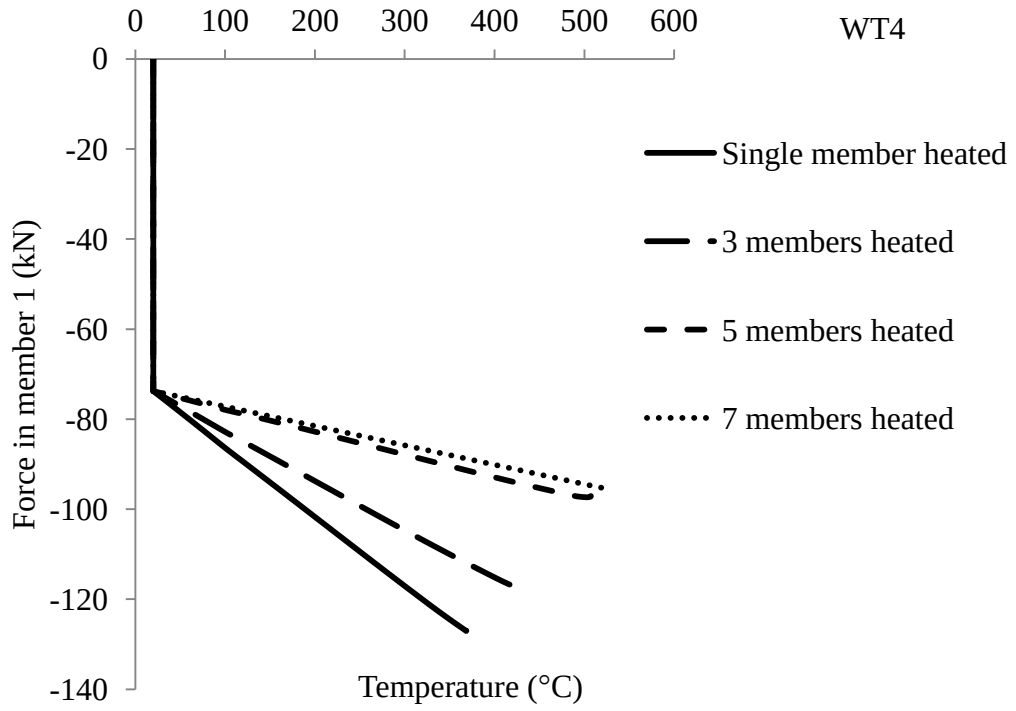

Figure 6.8 Comparison of temperature – force curves for different heating scenarios

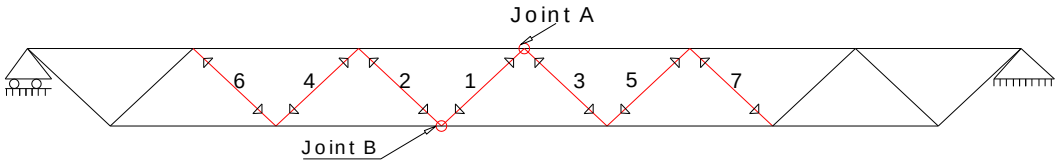

Figure 6.9 Effects of adjacent members being heated on the critical member

6.4.3 Method for analysis and design

The results in Figure 6.8 indicate that the effect of heating the adjacent members is to reduce the rate of compression force increase in the critical member. This is equivalent to reducing the restraint stiffness. This section will develop a method to calculate this reduction.

If only one member is heated, the initial rate of increase in the compression force of the member can be calculated using Equation 6.4 (Wang and Moore 1994a, b) if the modulus of elasticity is assumed to be unchanged with a small temperature change.

$$\Delta F_{single\ member} = \frac{k_{total} k_b}{k_{total} + k_b} \alpha_{th} \Delta T_{max} l_b \qquad 6.4$$

Where α_{th} is the coefficient of thermal elongation of steel and ΔT_{max} is the temperature increase in the critical member.

When the adjacent members are heated, the increase in the compression force of the critical member is given by:

$$\Delta F_{multiple\ members} = \frac{k_{total}k_b}{k_{total}+k_b}\alpha_{th}\Delta T_{max}l_b - \sum_{i=1}^{n} F_{cric,i} \quad 6.5$$

where $F_{cric,i}$ is the increase in the tension force of the critical member when the i^{th} adjacent member is heated to a temperature corresponding to a rise in temperature of ΔT_{max} in the critical member.

Using the format of Equation 6.4 for only the critical member being heated, the equation for calculating the increase in compression force for multiple members being heated can be written as:

$$\Delta F_{multiple\ members} = k_f \frac{k_{total}k_b}{k_{total}+k_b}\alpha_{th}\Delta T_{max}l_b \quad 6.6$$

where n is the number of heated adjacent members and

$$k_f = \frac{\Delta F_{multiple\ members}}{\Delta F_{single\ member}} \quad 6.7$$

therefore:

$$\beta_l = \frac{k_{total}}{\frac{k_b + k_{total}}{k_f} - k_{total}} \quad 6.8$$

The above equivalent stiffness ratio should be used in the regression equations of Wang et al. (2010) when calculating the temperature reduction of the critical member.

Static truss analysis at ambient temperature can be employed to calculate force, $F_{cric,i}$. This force change is caused by the additional force ($F_{i,i}$) in member "i" when its own thermal expansion is restrained. $F_{i,i}$ can be calculated by using Equation 6.4, but substituting the stiffness terms associated with the critical member with those associated with member i, and also the temperature increase in member "i" corresponds to the temperature increase of ΔT_{max} in the critical member. Replacing member "i" with force $F_{i,i}$, a static analysis at ambient temperature is carried out. The resulting force in the critical member is the sought after value $F_{crit,i}$. It should be

pointed out that only a nominal value (say 1 °C) for ΔT_{max} is necessary in this calculation.

6.4.4 Comparison of failure temperature between numerical and analytical results

The accuracy of the proposed analytical method has been checked against the different trusses used in the parametric study presented in section 6.2. Table 6.6 compares the failure temperatures of the trusses under different fire scenarios between ABAQUS truss analysis and analytical solutions of the modified restraint stiffness ratio in the regression equations of Wang et al. (2010). The results of member analysis without axial restraint are included in Table 6.6. Not including the effects of axial restraint will be unsafe, but will grossly overestimate the truss member failure temperatures. Including the effects of heating three members adjacent to the critical member (Members 1-7 in the table) has very little influence compared to heating only the two adjacent members (Members 1-5 in the table). The results in Table 6.6 indicate that the proposed analytical method can give reasonably close predictions compared to the ABAQUS truss simulation results, with the analytical results being on the safe side.

Table 6.6 Comparison of critical member failure temperatures between the analytical results and numerical simulation results

Truss ID	Number of heated members, and modification factor for axial restraint ratio	ABAQUS member analysis without axial restraint	Analytical Method	ABAQUS truss analysis
WT1-M1	Member 1, k_f = 1.00	688 °C	535 °C	532 °C
WT1-M3	Members 1-3, k_f = 0.73		552 °C	563 °C
WT1-M5	Members 1-5, k_f = 0.46		582 °C	597 °C
WT1-M7	Members 1-7, k_f = 0.44		585 °C	597 °C
WT2-M1	Member 1, k_f = 1.00	578 °C	332 °C	322 °C
WT2-M3	Members 1-3, k_f = 0.74		358 °C	362 °C
WT2-M5	Members 1-5, k_f = 0.45		409 °C	415 °C
WT2-M7	Members 1-7, k_f = 0.44		412 °C	415 °C

WT4-M1	Member 1, $k_f = 1.00$	598 °C	375 °C	368 °C
WT4-M3	Members 1-3, $k_f = 0.74$		407 °C	428 °C
WT4-M5	Members 1-5, $k_f = 0.45$		462 °C	507 °C
WT4-M7	Members 1-7, $k_f = 0.41$		470 °C	519 °C
WT5-M1	Member 1, $k_f = 1.00$	657 °C	499 °C	510 °C
WT5-M3	Members 1-3, $k_f = 0.74$		522 °C	532 °C
WT5-M5	Members 1-5, $k_f = 0.46$		558 °C	555 °C
WT5-M7	Members 1-7, $k_f = 0.45$		560 °C	556 °C
WT6-M1	Member 1, $k_f = 1.00$	470 °C	222 °C	241 °C
WT6-M3	Members 1-3, $k_f = 0.73$		269 °C	276 °C
WT6-M5	Members 1-5, $k_f = 0.47$		328 °C	378 °C
WT6-M7	Members 1-7, $k_f = 0.45$		333 °C	380 °C
WT7-M1	Member 1, $k_f = 1.00$	679 °C	504 °C	546 °C
WT7-M3	Members 1-3, $k_f = 0.75$		516 °C	562 °C
WT7-M5	Members 1-5, $k_f = 0.48$		542 ˚C	585 ˚C
WT7-M7	Members 1-7, $k_f = 0.46$		545 ˚C	585 ˚C
WT8-M1	Member 1, $k_f = 1.00$	543 °C	219 °C	233 °C
WT8-M3	Members 1-3, $k_f = 0.74$		243 °C	267 °C
WT8-M5	Members 1-5, $k_f = 0.53$		274 °C	326 °C
WT8-M7	Members 1-7, $k_f = 0.53$		274 °C	325 °C
WT10-M1	Member 1, $k_f = 1.00$	575 °C	329 °C	323 °C
WT10-M3	Members 1-3, $k_f = 0.73$		366 °C	346 °C
WT10-M5	Members 1-5, $k_f = 0.39$		440 °C	424 °C
WT10-M7	Members 1-7, $k_f = 0.37$		446 °C	436 °C

WT11-M1	Member 1, $k_f = 1.00$	620 °C	428 °C	470 °C
WT11-M3	Members 1-3, $k_f = 0.72$		453 °C	493 °C
WT11-M5	Members 1-5, $k_f = 0.43$		500 °C	526 °C
WT11-M7	Members 1-7, $k_f = 0.42$		501 °C	530 °C
PT1-M1	Member 1, $k_f = 1.00$	610 °C	569 °C	583 °C
PT1-M3	Members 1-3, $k_f = 0.10$		610 °C	614 °C
PT2-M1	Member 1, $k_f = 1.00$	544 °C	443 °C	387 °C
PT2-M3	Members 1-3, $k_f = 0.14$		536 °C	537 °C
PT3-M1	Member 1, $k_f = 1.00$	528 °C	415 °C	451 °C
PT3-M3	Members 1-3, $k_f = 0.47$		469 °C	492 °C
PT3-M5	Members 1-5, $k_f = 0.20$		505 °C	517 °C
HT1-M1	Member 1, $k_f = 1.00$	644 °C	412 °C	418 °C
HT1-M3	Members 1-3, $k_f = 0.93$		421 °C	461 °C
HT1-M5	Members 1-5, $k_f = 0.93$		421 °C	461 °C
HT1-M7	Members 1-7, $k_f = 0.93$		421 °C	461 °C

6.5 An Example

An example is provided in this section to illustrate application of the procedure to calculate the failure temperature of a critical member in a truss with multiple heated members.

Referring to Figure 6.7 (d), which shows the temperature distributions of the members closest to the fire source, the WT4 truss was chosen for this example. Calculate the failure temperature of the critical member (member 1, the member with the highest temperature).

Step 1:

Assume the critical member temperature to be 180 °C. The actual temperature value is not important because the stiffness modification factor will be independent of this temperature. Use Equation 6.4 to calculate the additional compression force ($F_{i,i}$) in each of the heated members, and the temperature increase in the other members according to the temperature distribution in Figure 6.7 (d) corresponding to T_{max}=180 °C in the critical member (member 1). Table 6.7 shows the analytical results and compares the analytical results with the ABAQUS simulation results, demonstrating excellent agreement.

Table 6.7 Additional compression forces in members 1, 2, 3, 4, 5 when one member is heated to the temperature corresponding to T_{max}=180 °C, and comparison with ABAQUS simulation results

Member No.	EQUATION 6.4	ABAQUS
Member 1 ($F_{1,1}$)	25871 N	25106 N
Members 2 & 3 ($F_{2,2}$ & $F_{3,3}$)	18233 N	18633 N
Member 4 ($F_{4,4}$)	6788 N	6681 N
Member 5 ($F_{5,5}$)	6194 N	6372 N
Members 6 & 7 ($F_{6,6}$ & $F_{7,7}$)	3871 N	3933 N

The relative displacement of the critical member when being heated alone is 2.04 mm. This gives the restraint stiffness to the critical member of 25106/2.04 = 12307 N/mm.

Step 2:

Replace the adjacent members one by one with the corresponding force in Table 6.7 and perform a static analysis of the truss at ambient temperature. Obtain the resulting force in the critical member ($F_{cric,i}$). For example, Figure 6.10 shows the truss in static analysis in order to obtain $F_{cric,4}$ (the force in the critical member (1) when member 4 is replaced by a load of 6788N). These values are listed in Table 6.8.

Table 6.8 Comparison of change in force

Heated Member No.	Force in the critical member (member 3) (N, tension positive)
2 ($F_{cric,2}$)	593
3 ($F_{cric,3}$)	6099
4 ($F_{cric,4}$)	4017
5 ($F_{cric,5}$)	3589
6 ($F_{cric,6}$)	483
7 ($F_{cric,7}$)	492

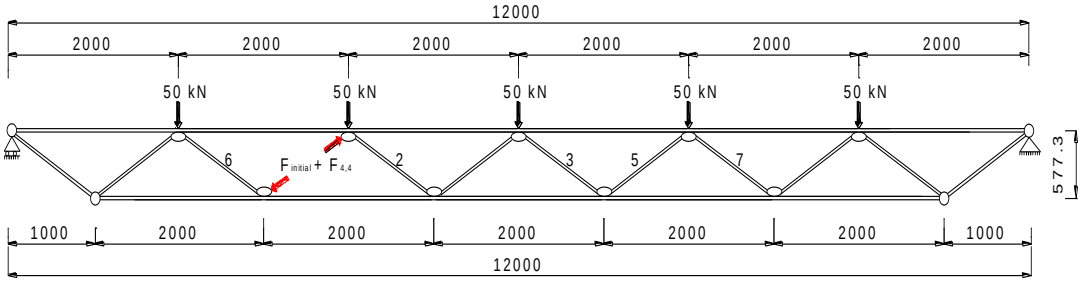

Figure 6.10 Truss static analysis model to obtain $F_{cric,4}$ (member 4 replaced by a force of 6788N in compression)

Step 3:

Use Equation 6.6 to calculate the total increase in compression force of the critical member. The total increase in compression force can then be used in Equation 6.7 to calculate the restraint stiffness modification factor. Table 6.9 summarises the calculation results.

Table 6.9 Final compression forces in the critical member with different adjacent members being heated, and resulting stiffness modification factors

Members being heated	Compression on force (Equation 6.5)	Stiffness modification factor (Equation 6.7) (k_f)
Member 1	25871 N	1.00
Members 1, 2 & 3	19179 N	0.74
Members 1, 2, 3, 4 & 5	11573 N	0.45
Members 1, 2, 3, 4, 5, 6 & 7	10598 N	0.41

Step 4:

Use the regression equations of Wang et al. (2010) to calculate the reduction in failure temperature of the critical member. The calculation results are presented in Table 6.10. Also shown in Table 6.10 are the critical member failure temperatures without considering restraint and from the ABAQUS truss simulation. The proposed analytical method gives excellent results.

Table 6.10 Comparison of the critical member failure temperatures for different number of the adjacent members being heated

Heated members	Member analysis without restraint	ABAQUS truss analysis	Analytical method
Member 1	598 °C	368 °C	375 °C
Members 1-3		428 °C	407 °C
Members 1-5		507 °C	462 °C
Members 1-7		519 °C	470 °C

6.6 Conclusions

This chapter has presented the results of a numerical investigation of the behaviour of welded steel tubular trusses under localised heating that results in non-uniform temperature distribution in different truss members. The simulations were carried out for Circular Hollow Section (CHS) trusses using the commercial Finite Element software, ABAQUS v6.10-1 (2010). Based on the numerical simulation results, an analytical method has been developed to calculate the failure temperature of the critical member (the member with the highest temperature).

Based on the study, the following conclusions can be drawn:

(1) It is important to consider the effects of restrained thermal expansion when a truss is non-uniformly heated. Not including this effect in fire safety design would grossly overestimate the failure temperatures of the critical members.

(2) The behaviour of a single heated brace member in a truss can be represented by an isolated member with axial restraint. The regression equations of Wang et al. (2010), originally developed for axially restrained columns with H cross-sections, are applicable to tubular members.

(3) When the critical member and some of the adjacent members are heated, heating the adjacent members alleviates the effects of restrained thermal expansion of the critical member: the increase in the compression force of the critical member is smaller when under multiple member heating than when under single member heating.

(4) Static truss analyses at ambient temperature can be performed to obtain the change in force in the critical member due to heating of any single adjacent member. Superposition can be used to obtain the total change in force in the critical member by summing up all the force changes due to heating the different members. For simplification, it is not necessary to consider the effects of the adjacent member being heated if the adjacent member is three or more members away from the critical member. This assumption is on the safe side.

(5) An equivalent restraint stiffness can be calculated based on the force change in the critical member due to multiple members being heated. Using this equivalent restraint stiffness in the regression equations of Wang et al. (2010), the critical temperature of the critical member can be calculated.

Comparisons between the analytical results and the numerical simulation results have confirmed that the analytical method is on the safe side and sufficiently accurate for design.

CHAPTER 7 CONCLUSIONS AND FUTURE RESEARCH

7.1 Introduction

This project is undertaken to evaluate the behaviour of welded tubular trusses at elevated temperatures and to develop simple and safe design methods for fire engineers. It is important to investigate both joint and member behaviours and to develop methods for their fire safety design. This thesis has used the commercial Finite Element software ABAQUS v6.10-1 as the research tool.

This research has addressed the following main issues:

- Validation of the numerical simulation models for both welded tubular joints and trusses at elevated temperatures.
- Ultimate strength of welded steel tubular joints at elevated temperatures of CHS or SHS tubular joints with axially loaded brace members at different elevated temperatures.
- Elevated temperature behaviour of tubular trusses exposed to uniform heating, considering different truss configurations and design parameters.
- Simple design method for uniformly heated truss, taking into consideration additional forces in compression brace members due to large truss deformations at high temperatures.
- Behaviour of welded steel tubular trusses exposed to localised fire.
- Simple design method to calculate failure temperatures of critical members for non-uniformly heated trusses.

The following is a summary of the main conclusions of this research.

7.2 Finite Element Modelling Methodology

7.2.1 For welded joints

Validation of the simulation model for tubular joints at elevated temperatures was checked by comparing simulation results against the elevated temperature tests of Nguyen et al. (2010), who tested T-joints at elevated temperatures, and the ambient temperature tests of Kurobane et al. (1986) on the K-joint. Comparisons were made for joint load-displacement curve, deformed joint shape and failure mode. Future

simulation of welded steel tubular joints may consider adopting the following methodology:

- Use 8-noded thick-shell elements with 5 integration points for both the brace and chord members in order to achieve short computational time and accurate results.
- Use quadratic wedge solid elements (C3D15) for the weld.
- Use mesh sizes of 10mm and 5 mm respectively for the brace and chord members, and the weld.

7.2.2 For tubular trusses

Comparisons of numerical simulation results against the fire tests of Edwards (2004) (two girders) and the elevated temperature tests of Liu et al. (2010) (part of a truss) were used as evidence of validation of the simulation model. The main conclusions with regard to modelling methodology are:

- Either 2D line elements or 3D shell elements are suitable for simulating tubular members in fire. 2D line elements were used in the author's parametric study to save on computational time.

7.3 Elevated Temperature Behaviour of Welded Steel Tubular Joints

The results of a comprehensive literature review on joints revealed extensive research on welded steel tubular joints at ambient temperature, but little existing research on elevated temperature behaviour of welded steel tubular joints. Welded tubular joints have many failure modes and it was reasoned that only the chord plastification failure mode would require additional investigation because the joint behaviour at elevated temperatures may be different from that at ambient temperature when the chord surface deformation is small. Extensive parametric simulations were carried out to investigate this failure mode for many types of CHS and SHS joints (T-, K-, X-, Y-, N-joints) with either tension or compression brace members. Uniform temperature distribution was assumed for both the chord and brace members and the numerical simulations were conducted under the steady state condition in which the temperature was kept constant and then the mechanical load was applied until failure. Nevertheless, further numerical

simulations have been carried out to compare the steady state and transient state simulation results in section 4.5.

The main findings and design recommendations are:

- The steady state results are applicable to the transient design condition.
- For T-, Y- and X-joints with the brace member(s) in tension, and for K- and N-joints with the brace members under opposite loads, it is safe to use the existing CIDECT (Wardenier et al., 2010a) or EN 1993-1-8 (CEN, 2005b) equations for ambient temperature design, although the ambient temperature yield strength of steel should be replaced by those elevated temperatures.
- For T-, Y- and X-joints with the brace member(s) in compression, it is not safe to use the design method suggested above because large ovalisation of the chord face (flattening) reduces the yield line resistance. However, it is acceptable to use the same ambient temperature calculation equations, but modifying the joint strength at ambient temperature by the elevated temperature reduction factor for the Young's modulus for steel instead of that for yield strength.
- When the chord member is under either tensile or compressive pre-stress, the recommendations in EN-1993-1-8 (CEN, 2005b) can be applied to elevated temperatures. The reduction factor for chord tension pre-stress in the CIDECT (Wardenier et al., 2010a) design guide underestimates the joint strength.

7.4 Elevated Temperature Truss Behaviour and Design Method

7.4.1 Uniformly heated truss

The parametric study investigated the effects of truss type, joint type, truss span-to-depth ratio, critical member slenderness, applied load ratio, number of brace members and thermal elongation on critical temperatures of the critical truss members. The main conclusions and design recommendations are:

- It is safe to assume the truss joints to be pin joints. Because of this simplification, it is not necessary to consider the effects of any differential

thermal expansion due to slightly different temperatures in different truss members.

- The present member-based calculation method can overestimate the truss critical temperature due to the fact that compression brace members experience increases in their forces compared to the ambient temperature values at large truss deflections. The present member-based approach does not include this effect because it uses the ambient temperature static analysis values when calculating the member limiting temperatures.
- The maximum truss deflection may be assumed to be span/30. Using this truss deflection, two design methods have been proposed to calculate the increased compressive force in brace members: an analytical method and an ambient temperature elastic static, second-order truss analysis method. These methods were developed to ensure there is no need for the user to have specialist knowledge to conduct elevated temperature structural analysis. Comparisons between the proposed methods and the elevated temperature simulation results using ABAQUS have shown good agreement. The recommended design methods are presented in sections 5.4.1 and 5.4.2.

7.4.2 Non-uniformly heated truss

The purpose of this study was to deal with the problem of trusses exposed to localised fire. The main issues were to quantify the increased compressive force in brace members due to restrained thermal expansion and to calculate the reduced brace member limiting temperature. Extensive parametric studies were conducted to investigate the effects of different design parameters, including the number of truss members being heated on failure temperature of the critical member (the member with the highest temperature).

The following conclusions have been reached:

- The additional compressive force due to restrained thermal expansion in a non-uniformly heated truss (localised fie exposure) results in a lower limiting temperature of the critical member compared to a uniformly heated truss.
- The behaviour of one brace member being heated in a truss is the same as an isolated member with axial restraint. Wang et al.'s (2010) equations to calculate the reduced limiting temperatures, which were developed for axially

restrained columns with an H cross-section, can also be used for hollow tubular sections.

- When the member with the highest temperature (closest to localised fire, also referred to as the critical member) and some of the adjacent truss members are heated, the adjacent members mitigate the effect of only the critical member being heated because heating the adjacent members is equivalent to reducing the free thermal expansion of the critical member.
- Ambient temperature, linear elastic, static truss analysis can be performed to obtain the changes in compression force in the critical member due to heating the critical member and any of the adjacent members when only one member is heated. This is done by replacing the heated member by a compression force in static truss analysis. This compressive force corresponds to the temperature increase in the member when the temperature increase in the critical member is 1 $^{\circ}$C. Summation of all the forces gives the total compressive force increase in the critical member when its temperature increases by 1 $^{\circ}$C. For simplification, it is not necessary to consider the effects of an adjacent member being heated if the adjacent member is the third member or further away from the critical member. This method was developed to ensure that the method can be used by users who do not have specialist training in elevated temperature structural analysis.
- Using the compressive force increase in the critical member at a temperature increase of 1 $^{\circ}$C, the critical member is converted into a single axially restrained member. Its critical temperature can be calculated by the approximate method of Wang et al. (2010).

7.5 Recommendations for Future Work

This research has achieved its intended objectives of thoroughly understanding the behaviour of welded tubular joints and welded tubular truss members at elevated temperatures and to develop simple and safe design methods. However, there are limitations to the scope of this research and further research studies can be pursued to develop a more complete understanding of truss behaviour in fire. The following further research studies may be considered:

- Different types of joints, such as plated joints to chord members can be studied.

- This research has focused on joints under axial load only. It would be interesting to assess the effects of in-plane and out-plane bending.
- This research used circular and square truss members. Whilst it is expected that the findings would also be applicable to using rectangular truss members, some further studies are necessary to confirm this suggestion. Furthermore, elliptic tubes are being used, which would require further studies.
- This research has only considered 2D trusses. Further research is required for 3D, space frame trusses.
- This research has assumed static behaviour of the simulated trusses. However, it is possible for dynamic response to occur in the trusses after failure of the individual members. This would require further research.
- This research is based on numerical simulations. Although the author has done as best as can be done to validate the numerical simulation model, there is a severe shortage of fire and elevated temperature testing data. Many more tests are necessary.

APPENDIX A : WELDED TUBULAR JOINTS

CTC5 tubular joint was taken as an example.

Appendix A.1 : Cross Section Classification

To avoid premature failure at brace member due to local buckling, section under compression should satisfy the requirements for Class 1 or Class 2 (CEN, 2005b).

Since steel grade S355 is used, $f_y = 355\ N/mm^2$ (for $t \leq 40mm$) and therefore $\varepsilon = \sqrt{235/355}$ = 0.81. Class 1 is limited to $c/t \leq 50\varepsilon = 40.5$ and Class 2 is limited to $c/t \leq 70\varepsilon = 56.7$.

Chord member

$$\frac{c}{t} = \frac{d_0 - 3.t_0}{t_0} \qquad \text{A.1}$$

$$\frac{c}{t} = \frac{323.9 - 3x10.0}{10.0} = \ 29.39 \leq 40.5 \qquad \textbf{Class 1}$$

Brace member

$$\frac{c}{t} = \frac{d_1 - 3.t_1}{t_1} \qquad \text{A.2}$$

$$\frac{c}{t} = \frac{168.3 - 3x10.0}{10.0} = \ 10.83 \leq 40.5 \qquad \textbf{Class 1}$$

Hence, the chord and brace members are Class 1 sections.

Appendix A.2 : Range of Validity

Table A.1 and A.2 summarise the range of validity in CIDECT (Wardenier et al., 2010a) and EN 1993-1-1 (CEN, 2005c) respectively.

Table A.1 Limit states criteria for axially loaded CHS (Wardenier et al., 2010b)

Range of validity			
General	$0.2 \leq \frac{d_i}{D} \leq 1.0$	$t_i \leq T$	$\frac{e}{D} \leq 0.25$ $f_y \leq 0.8 f_u$ $f_y \leq 460\ N/mm^2$
	$\theta_i \geq 30^0$	$g \geq t_1 + t_2$	$f_{yi} \leq f_{y0}$
Chord	**Compression**	class 1 or 2 and $2\gamma \leq 50$ (for X joints: $2\gamma \leq 40$)	
	Tension	$2\gamma \leq 50$ (for X joints: $2\gamma \leq 40$)	
Braces	**Compression**	class 1 or 2 and $d_i/t_i \leq 50$	
	Tension	$d_i/t_i \leq 50$	

Table A.2 Maximum d_i/t_i ratios for CHS in compression (CEN, 2005c)

	Maximum d_i/t_i ratios			
Steel grade	S235	S275	S355	S460
Yield stress f_y	235 N/mm^2	275 N/mm^2	355 N/mm^2	460 N/mm^2
Class 1	50	42	33	25
Class 2	70	59	46	35

Check for CIDECT (Wardenier et al., 2010b):

- $d_i/D = 168.3/323.9 = 0.52\ and\ 0.2 \leq d_i/D \leq 1.0$
- $t_i = 10.0, t_0 = 10.0\ and\ t_i \leq t_0$
- $\theta_i = 90^0\ and\ \theta_i \geq 30^0$
- $f_{yi}355 \leq f_{y0} and\ f_{yi} \leq f_{y0}$
- $2\gamma = 2 * 16.2 = 32.4\ and\ 2\gamma \leq 50$
- $d_i/t_i = 168.3/10.0 = 16.8\ and\ d_i/t_i \leq 50$
- Both the chord and brace members are Class 1.

Therefore, CTC5 tubular joint is in the range of validity based on CIDECT design guide.

Check for EN 1993-1-1 (CEN, 2005c):

- $d_i/t_i = 168.3/10.0 = 16.8\ and\ d_i/t_i \leq 33$
- Both the chord and brace members are Class 1.

Therefore, CTC5 tubular joint is in the range of validity based on EN 1993-1-1.

Appendix A.3 Resistance of CTC5 joint at ambient temperature

Check for local buckling resistance of brace member (168.3x10.0):

i = 56.1 mm

A = 4970 mm^2

I = 1564 cm^4

The effective length factor is taken as 0.85 according to BS5950 (BSI, 2003). Therefore;

$$\lambda_1 = 93.9\varepsilon \quad \text{A.3}$$

Coefficient depending on f_y $\varepsilon = \sqrt{\frac{235}{f_y}} = \sqrt{\frac{235}{355}} = 0.81$ A.4

$$\lambda_1 = 93.9\ x\ 0.81 = 76.1$$

Non-dimensional slenderness $\bar{\lambda} = \sqrt{\frac{Af_y}{N_{Cr}}} = \left(\frac{L_{cr}}{i}\right)\left(\frac{1}{\lambda_1}\right)$ A.5

Critical buckling load $N_{cr} = \frac{\pi^2 EI}{L_{cr}}$ A.6

$$\bar{\lambda} = 0.26$$

Imperfection factor for CHS steel grade S355 based on EN 1993-1-1 (CEN, 2005c) is taken as α = 0.21.

Reduction factor for the relevant buckling curve $\chi = \frac{1}{\phi + \sqrt{\phi^2 - \bar{\lambda}^2}}$ but $\chi \leq 1.00$ A.7

Where the value to determine the reduction factor is $\phi = 0.5\left[1 + \alpha\left(\bar{\lambda} - 0.2\right) + \bar{\lambda}^2\right]$

Therefore, χ =0.99

The ultimate compressive load is given as below:

$$N_{b,Rd} = \frac{\chi A f_y}{\gamma_{M1}} = \frac{0.99x4970x355}{1.00} = 1746kN$$

Check for chord plastification**:**

Chord face failure for T-Joints

$$N_{1,Rd} = Q_f \frac{f_{y0} t_0^2}{\sin \theta_1} 2.6(1 + 6{,}8\,\beta^2)\gamma^{0.2} \quad \text{A.8}$$

$$N_{1,Rd} = 1\ x\ \frac{355\text{x}10^2}{\sin 90} 2.6(1 + 6{,}8\ x\ 0.68^2)19.4^{0.2} = 692\ kN$$

Check for punching shear resistance of the joint**:**

$$N_1 = \pi . d . t_0 . \frac{f_{y0}}{\sqrt{3}} \quad \text{A.9}$$

$$N_1 = \pi . 168.3\ x\ 10\ x\ \frac{355}{\sqrt{3}} = 1083\ kN$$

Check of required weld size**:**

$$a \geq a_{req} = \sqrt{2}\ x \frac{f_y}{f_u}\ x \beta_w\ x \frac{\gamma_{M2}}{\gamma_{M0}} x\ t_i \quad \text{A. 10}$$

Correlation factor β_w = 0.9

Yield strength f_y = 355 N / mm^2

Ultimate strength f_u = 470 N / mm^2

Weld size a = 11 mm

Required weld size a_{req} = 10 mm

Therefore, failure of CTC5 joint is owing to chord plastification.

APPENDIX B : LOAD RATIOS FOR TUBULAR JOINTS

Appendix B.1 : Case 1: T-joints with brace member in compression

Table B.1: FE results for CHS T-joints

Temperature	CHS									
	CTC1	CTC2	CTC3	CTC4	CTC5	CTC6	CTC7	CTC8	CTC9	CTC10
20 °C	1.00	1.00	1.00	1.00	1.00	1.00	1.00	1.00	1.00	1.00
200 °C	0.94	0.94	0.93	0.95	0.94	0.95	0.94	0.95	0.94	0.93
300 °C	0.85	0.87	0.86	0.87	0.88	0.88	0.87	0.87	0.87	0.87
400 °C	0.77	0.79	0.78	0.80	0.80	0.81	0.80	0.79	0.81	0.81
500 °C	0.62	0.62	0.63	0.64	0.65	0.65	0.65	0.63	0.65	0.65
600 °C	0.35	0.35	0.36	0.36	0.37	0.37	0.37	0.36	0.37	0.38
700 °C	0.16	0.16	0.16	0.17	0.17	0.17	0.17	0.17	0.17	0.18
800 °C	0.09	0.09	0.09	0.09	0.09	0.09	0.09	0.09	0.09	0.09

Table B.2 : FE results for SHS T-joints

Temperature	SHS				EN 1993-1-2	
	STC1	STC2	STC3	STC4	$k_{y,\theta}$	$k_{E,\theta}$
20 °C	1.00	1.00	1.00	1.00	1.00	1.00
200 °C	0.94	0.96	0.95	0.99	1.00	0.90
300 °C	0.87	0.92	0.91	0.95	1.00	0.80
400 °C	0.82	0.86	0.87	0.89	1.00	0.70
500 °C	0.67	0.69	0.69	0.71	0.78	0.60
600 °C	0.39	0.40	0.40	0.41	0.47	0.31
700 °C	0.18	0.19	0.19	0.19	0.23	0.13
800 °C	0.09	0.10	0.10	0.10	0.11	0.09

Appendix B.2 : Case 2: X-joints with the brace members in equal compression or tension

Table B.3: FE results for X-joints

Temperature	SHS		CHS					
	SXC1	SXT1	CXC1	CXT1	CXC2	CXT2	CXC3	CXT3
20 °C	1.00	1.00	1.00	1.00	1.00	1.00	1.00	1.00
200 °C	0.94	0.98	0.92	0.97	0.92	0.99	0.92	1.00
300 °C	0.88	0.97	0.83	0.93	0.83	1.00	0.83	1.00
400 °C	0.82	0.96	0.75	0.91	0.76	1.00	0.76	1.00
500 °C	0.66	0.75	0.60	0.72	0.61	0.80	0.61	0.80
600 °C	0.38	0.45	0.34	0.43	0.35	0.48	0.35	0.48
700 °C	0.15	0.22	0.16	0.20	0.16	0.21	0.16	0.21
800 °C	0.07	0.11	0.09	0.10	0.09	0.11	0.09	0.11

Appendix B.3 : Case 3: T-joint with the brace member in tension

Table B.4: FE results for SHS T-joint under tension load

Temperature	SHS				EN 1993-1-2	
	STT1	STT2	STT3	STT4	$k_{y,\theta}$	$k_{E,\theta}$
20 °C	1.00	1.00	1.00	1.00	1.00	1.00
200 °C	0.98	0.98	1.00	0.97	1.00	0.90
300 °C	0.97	0.97	0.98	0.99	1.00	0.80
400 °C	0.97	0.94	0.95	1.00	1.00	0.70
500 °C	0.76	0.76	0.75	0.78	0.78	0.60
600 °C	0.45	0.46	0.45	0.47	0.47	0.31
700 °C	0.22	0.22	0.22	0.24	0.23	0.13
800 °C	0.11	0.11	0.11	0.11	0.11	0.09

Table B.5: FE results for CHS T-joint under tensile load

Temperature	CHS						EN 1993-1-2	
	CTT1	CTT2	CTT3	CTT4	CTT5	CTT6	$k_{y,\theta}$	$k_{E,\theta}$
20 °C	1.00	1.00	1.00	1.00	1.00	1.00	1.00	1.00
200 °C	0.98	0.95	0.98	0.97	0.99	0.97	1.00	0.90
300 °C	0.95	0.91	0.95	0.92	0.96	0.93	1.00	0.80
400 °C	0.92	0.89	0.94	0.89	0.90	0.90	1.00	0.70
500 °C	0.72	0.71	0.74	0.71	0.72	0.72	0.78	0.60
600 °C	0.43	0.42	0.44	0.42	0.43	0.42	0.47	0.31
700 °C	0.21	0.21	0.21	0.20	0.20	0.20	0.23	0.13
800 °C	0.10	0.10	0.11	0.10	0.10	0.11	0.11	0.09

Appendix B.4 : Case 4: K-joints and N-joints with equal but opposite loads in the brace members

Table B.6: FE results for K-joints

Temperature	K-joints					EN 1993-1-2	
	CK1	CK2	CK3	CK4	SK1	$k_{y,\theta}$	$k_{E,\theta}$
20 °C	1.00	1.00	1.00	1.00	1.00	1.00	1.00
200 °C	0.99	0.99	0.99	0.98	1.00	1.00	0.90
300 °C	0.97	0.98	0.96	0.96	0.94	1.00	0.80
400 °C	0.96	0.96	0.94	0.95	0.93	1.00	0.70
500 °C	0.76	0.76	0.74	0.74	0.77	0.78	0.60
600 °C	0.46	0.45	0.43	0.44	0.44	0.47	0.31
700 °C	0.22	0.22	0.21	0.20	0.20	0.23	0.13
800 °C	0.11	0.11	0.11	0.11	0.11	0.11	0.09

Table B.7: FE results for N-joints

Temperature	CHS N-joints			EN 1993-1-2	
	CN1	CN2	CN3	$k_{y,\theta}$	$k_{E,\theta}$
20 °C	1.00	1.00	1.00	1.00	1.00
200 °C	0.99	0.99	0.99	1.00	0.90
300 °C	0.96	0.99	0.99	1.00	0.80
400 °C	0.93	0.95	0.94	1.00	0.70
500 °C	0.74	0.75	0.76	0.78	0.60
600 °C	0.43	0.44	0.43	0.47	0.31
700 °C	0.21	0.21	0.20	0.23	0.13
800 °C	0.11	0.11	0.11	0.11	0.09

Appendix B.5 : Case 5: Y-joints

Table B.8: FE results for Y-joints under compression

Temperature	Under compression					
	CYC1	CYC2	CYC3	CYC4	CYC5	CYC6
20 °C	1.00	1.00	1.00	1.00	1.00	1.00
200 °C	0.96	0.96	0.95	0.97	0.95	0.95
300 °C	0.88	0.89	0.89	0.89	0.88	0.88
400 °C	0.76	0.80	0.81	0.80	0.80	0.80
500 °C	0.62	0.65	0.65	0.65	0.65	0.65
600 °C	0.33	0.37	0.37	0.37	0.36	0.37
700 °C	0.13	0.16	0.17	0.16	0.16	0.16
800 °C	0.09	0.09	0.09	0.09	0.09	0.09

Table B.9: FE results for Y-joints under tension

Temperature	Under Tension			EN 1993-1-2	
	CYT1	CYT2	CYT3	$k_{y,\theta}$	$k_{E,\theta}$
20 °C	1.00	1.00	1.00	1.00	1.00
200 °C	0.97	0.98	0.99	1.00	0.90
300 °C	0.93	0.95	0.98	1.00	0.80
400 °C	0.91	0.94	0.98	1.00	0.70
500 °C	0.71	0.74	0.76	0.78	0.60
600 °C	0.42	0.44	0.46	0.47	0.31
700 °C	0.21	0.21	0.23	0.23	0.13
800 °C	0.10	0.10	0.11	0.11	0.09

Appendix B.6 : Effects of Pre-stress in Chord Member

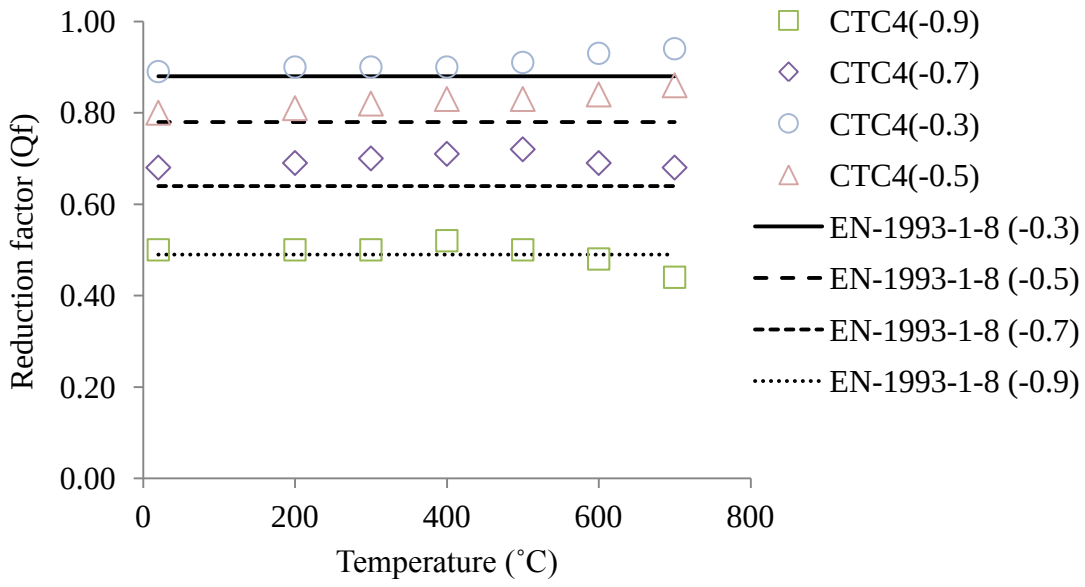

a) Effects of compressive pre-load in chord member on T-joint strength

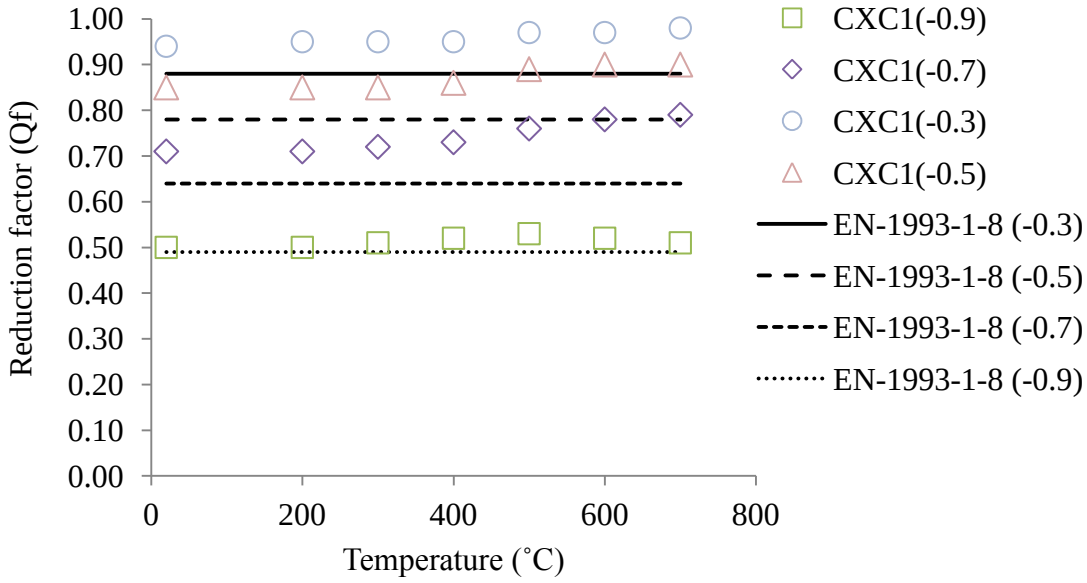

b) Effects of compressive pre-load in chord member on X-joint strength

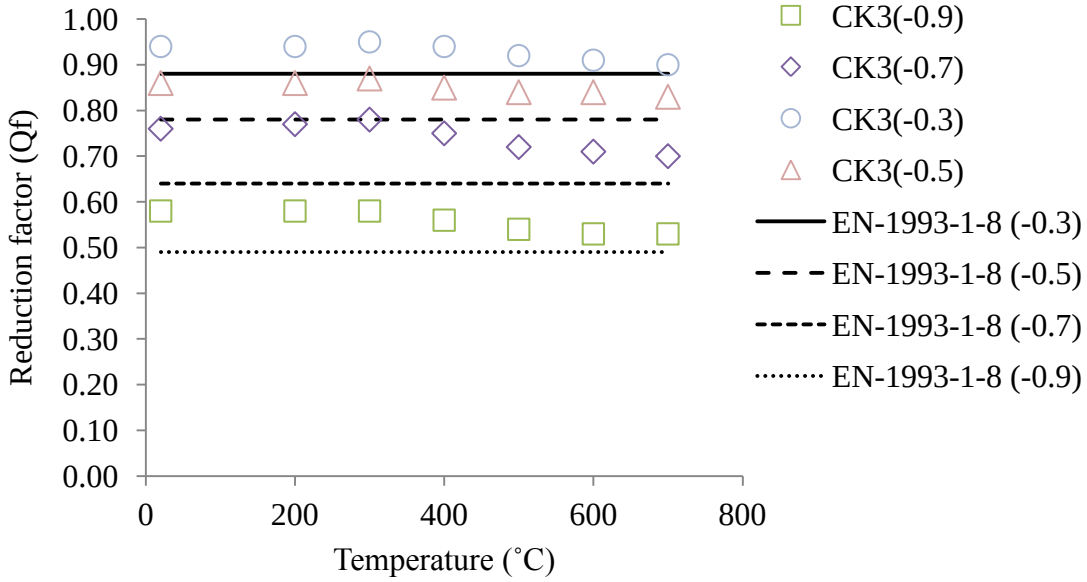

c) Effects of compressive pre-load in chord member on K-joint strength

Figure B.1 Comparison of joint reduction factors for CHS T-, X- and K-joints with compressive pre-stress in the chord member between numerical simulation and EN-1993-1-8

APPENDIX C : DIMENSIONS OF THE UNIFORMLY HEATED TRUSSES

Table C.1: Dimensions of the truss members

Truss	Member Type	Dimensions (mm)
WT1	Bottom and top chords	Φ 323.9x8
&	Outer bracings (Member 4 and 5)	Φ 193.7x4
WT3	Inner bracings (Member 6, 7 and 8)	Φ 114.3x5
	Bottom and top chords	Φ 244.5x8
WT2	Outer bracings (Member 4 and 5)	Φ 139.7x8
	Inner bracings (Member 6, 7 and 8)	Φ 114.3x5
	Bottom and top chords	Φ 323.9x8
WT4	Outer bracings (Member 4 and 5)	Φ 168.3x6
	Inner bracings (Member 6, 7 and 8)	Φ 114.3x5
	Bottom and top chords	Φ 219.1x12
WT5	Outer bracings (Member 4, 5, 6 and 7)	Φ 168.3x5
	Inner bracings (Member 8 and 9)	Φ 48.3x3.2
	Bottom and top chords	Φ 219.1x12
WT6	Outer bracings (Member 4, 5, 6 and 7)	Φ 168.3x5
	Inner bracings (Member 8 and 9)	Φ 60.3x3
	Bottom and top chords	Φ 219.1x12
WT7	Outer bracings (Member 4, 5, 6 and 7)	Φ 168.3x5
	Inner bracings (Member 8 and 9)	Φ 88.9x3
	Bottom and top chords	Φ 406.4x16
WT8	Outer bracings (Member 4, 5, 6, 7, 8 and 9)	Φ 168.3x10
	Inner bracings (Member 10 and 11)	Φ 114.3x3.6
	Bottom and top chords	Φ 406.4x12
WT9	Outer bracings (Member 4, 5, 6 and 7)	Φ 168.3x10
	Inner bracings (Member 8 and 9)	Φ 114.3x3.6
	Bottom and top chords	Φ 406.4x12
WT10	Outer bracings (Member 3 and 4)	Φ 168.3x10
	Inner bracings (Member 5 and 6)	Φ 114.3x3.6

PT1	Bottom and top chords	Φ 193.7x10
	Compression brace members (Member 4, 6 and 8)	Φ 114.3x5
	Tension brace members (Member 5, 7 and 9)	Φ 168.3x6.3
	Middle brace member (Member 10)	Φ 76.1x2.5
PT2	Bottom and top chords	Φ 457x12
	Brace members	Φ 219.1x10
PT3	Bottom and top chords	Φ 406.4x16
	Member 7 and 9	Φ 244.5x12
	Member 6, 8, 10, 11, 12, 13 and 14	Φ 168.3x10
	Member 15 and 16	Φ 114.3x3
HT1	Bottom and top chords	Φ 193.7x10
	Outer bracings (Member 5, 6 and 7)	Φ 168.3x6.3
	Inner bracings (Member 4, 8 and 9)	Φ 76.1x5

APPENDIX D DIMENSIONS OF THE LOCALLYLY HEATED TRUSSES

Table D.1: Dimensions of the locally truss members

Truss	Member Type	Dimensions (mm)
WT1, WT2 & WT3	Bottom and top chords	Φ 219.1x12
	Outer bracings	Φ 168.3x5
	Inner bracings (Member 1, 2, 3 and 5)	Φ 60.3x3
WT4	Bottom and top chords	Φ 168.3x10
	Outer bracings	Φ 168.3x5
	Inner bracings (Member 1, 2, 3 and 5)	Φ 60.3x3
WT5	Bottom and top chords	Φ 193.7x12
	Outer bracings	Φ 168.3x5
	Inner bracings (Member 1, 2, 3 and 5)	Φ 60.3x3
WT6	Bottom and top chords	Φ 168.3x10
	Outer bracings	Φ 168.3x5
	Inner bracings (Member 1, 2, 3 and 5)	Φ 42.4x4
WT7	Bottom and top chords	Φ 244.5x12
	Outer bracings	Φ 168.3x5
	Inner bracings (Member 1, 2, 3 and 5)	Φ 60.3x3
WT8	Bottom and top chords	Φ 244.5x12
	Outer bracings	Φ 168.3x5
	Inner bracings (Member 1, 2, 3 and 5)	Φ 42.4x4
WT9	Bottom and top chords	Φ 219.1x12
	Outer bracings	Φ 168.3x5
	Inner bracings (Member 1, 2, 3 and 5)	Φ 42.4x4
WT10	Bottom and top chords	Φ 168.3x10
	Outer bracings	Φ 168.3x5
	Inner bracings (Member 1, 2, 3 and 5)	Φ 76.1x3
WT11	Bottom and top chords	Φ 168.3x10
	Outer bracings	Φ 168.3x5
	Inner bracings (Member 1, 2, 3 and 5)	Φ 76.1x3

PT1	Bottom and top chords	Φ 193.7x10
	Compression brace members (Member 4, 6 and 8)	Φ 114.3x5
	Tension brace members (Member 5, 7 and 9)	Φ 168.3x6.3
	Middle brace member (Member 10)	Φ 76.1x2.5
PT2	Bottom and top chords	Φ 193.7x10
	Compression brace members (Member 4, 6 and 8)	Φ 76.1x4
	Tension brace members (Member 5, 7 and 9)	Φ 76.1x6.3
	Middle brace member (Member 10)	Φ 42.4x4
PT3	Bottom and top chords	Φ 193.7x10
	Brace members	Φ 76.1x2.5
HT1	Bottom and top chords	Φ 193.7x10
	Outer bracings (Member 5, 6 and 7)	Φ 168.3x6.3
	Inner bracings (Member 4, 8 and 9)	Φ 76.1x5

REFERENCES

ABAQUS/Standard. (2010) *In:* Ed (ed.) *K. a. S. Hibbitt,*. Version 6.10-1 ed. USA: K. a. S. Hibbit.

Ali, F. A., Shepherd, P., Randall, M., Simms, I. W., O'Connor, D. J. & Burgess, I. (1998) The effect of axial restraint on the fire resistance of steel columns. *Journal of Constructional Steel Research,* 46**,** 305-306.

Boresi, A. P. & Schmidt, R., J. (2003) *Advanced mechanics of materials* (6th Ed. ed.): John Wiley and Sons.

BSI. (2003) BS 5950: Part8: Code of Practice for the Fire Protection of Structural Steelwork. UK.

BSI. (2009) BS 476: Part 10: Guide to the principles, selection, role and application of fire testing and their outputs. UK.

Burns, R., Hanley, D., Choi, S., Burgess, I. & Butterworth, N. (2009) Development of a light-weight composite lattice joist for fire resistance. *In:* Nordic steel Conference. 188-195.

CEN. (2002) Actions on structures. *Part: EN 1991-1-2: General actions – Actions on structures exposed to fire.* British Standard.

CEN. (2005a) Design of Steel Structures. *In:* Part: (ed.) *EN 1993-1-2-Structural Fire Design.* London: British Standard Institute.

CEN. (2005b) Design of Steel Structures. *In:* Part: (ed.) *EN 1993-1-8-Design of Joints.* London: British Standard Institute.

CEN. (2005c) Design of Steel Structures. *In:* Part: (ed.) *EN 1993-1-1-General Rules and Rules for Building.* London: British Standard Institute.

Chang, J., Buchanan, A. H. & Moss, P. J. (2005) Effect of insulation on the fire behaviour of steel floor trusses. *Fire and materials,* 29(4)**,** 181-194.

Chen, C. & Zhang, W. (2012) Structural behaviors of steel roof truss exposed to pool fire. *Journal of Central South University,* 19(7)**,** 2054-2060.

Choi, S.-K. (2004) *The Structural Behaviour of Composite Truss Systems in Fire.* PhD, University of Sheffield.

Choi, S., Burgess, I. & Plank, R. (2003) The behaviour of lightweight composite floor trusses in fire. *In:* ASCE Specialty Conference: Designing Structures for Fire, Baltimore,(Oct 2003) pp. 24-32.

Choo, Y., Qian, X., Liew, J. & Wardenier, J. (2003a) Static strength of thick-walled CHS X-joints—Part I. New approach in strength definition. *Journal of Constructional Steel Research,* 59(10)**,** 1201-1228.

Choo, Y., Qian, X., Liew, J. & Wardenier, J. (2003b) Static strength of thick-walled CHS X-joints—Part II. Effect of chord stresses. *Journal of Constructional Steel Research,* 59(10)**,** 1229-1250.

Cofer, W. F. & Jubran, J. S. (1992) Analysis of welded tubular connections using continuum damage mechanics. *Journal of Structural Engineering,* 118(3)**,** 828-845.

Dexter, E. & Lee, M. (1999a) Static strength of axially loaded tubular K-joints. I: behavior. *Journal of Structural Engineering,* 125(2)**,** 194-201.

Dexter, E. & Lee, M. (1999b) Static strength of axially loaded tubular K-joints. II: Ultimate capacity. *Journal of Structural Engineering,* 125(2)**,** 202-210.

Du, Y. & Li, G. Q. (2012) A new temperature–time curve for fire-resistance analysis of structures. *Fire Safety Journal,* 54**,** 113-120.

Edwards, M. (2004) Fire Performance of SHS Lattice Girders. *Tubular Structures V,* 5**,** 95-103.

Flint, G., Usmani, A., Lamont, S., Torero, J. & Lane, B. (2006) Effect of fire on composite long span truss floor systems. *Journal of Constructional Steel Research,* 62(4)**,** 303-315.

Franssen, J.-M. (2000) Failure temperature of a system comprising a restrained column submitted to fire. *Fire Safety Journal,* 34(2)**,** 191-207.

Franssen, J. (2011) User's manual for SAFIR 2011 a computer program for analysis of structures subjected to fire. *University of Liege, Liege*.

Gann, R. (2005) NIST NCSTAR 1: Final report of the National Construction Safety Team on the collapse of the World Trade Center Twin Towers. *National Institute of Standards and Technology (NIST). Gaithersburg, MD.*

Gibstein, M. B. (1976) The static strength of T-joints subjected to in-plane bending moments. *In:* Det Norske Veritas Report No. 76-137, Oslo, Norway.

Hasemi, Y. & Tokunaga, T. (1984) Flame geometry effects on the buoyant plumes from turbulent diffusion flames. *Fire Science and Technology,* 4(1)**,** 15-26.

Kotsovinos, P. (2013) *Analysis of the structural response of tall buildings under multi foor and travelling fires.* PhD, The University of Edinburgh.

Kurobane, Y., ASCE, M., Makino, Y. & Ochi, K. (1984) Ultimate resistance of unstiffened tubular joints. *Journal of Structural Engineering,* 110**,** 385-400.

Kurobane, Y., Ogawa, K., Ochi, K. & Makino, Y. (1986) Local buckling of braces in tubular K-joints. *Thin-Walled Structures,* 4(1)**,** pp. 23-40.

Lin, S.-M., Du, Y. & Fu, J.-X. (2014) Design strategies of fire safety for steel roof trusses exposed to localised fire. *In:* 8th International Conference on Structures in Fire, Shanghai, China. 163-170.

Liu, D. & Wardenier, J. (2006) Effect of chords on the strength of RHS uniplanar gap K-joints. *In:* &Willibald, P., ed. Tubular Structures XI, Canada. 539-544.

Liu, D., Wardenier, J. & Van der Vegte, G. J. (2002) Survey of chord load functions for hollow section joints. *CIDECT Report 5BK-4/02*.

Liu, M. L., Zhao, J. C. & Jin, M. (2010) An experimental study of the mechanical behavior of steel planar tubular trusses in a fire. *Journal of Constructional Steel Research,* 66(4)**,** 504-511.

Lu, L. H., De Winkel, G. D., Yu, Y. & Wardenier, J. (1994) Deformation limit for the ultimate strength of hollow section joints. *In:* Proceedings of the Sixth International Symposium on Tubular Structures, Melbourne,Australia. 341-347.

Makino, Y., Kurobane, Y. K. O., Van der Vegte, G. J. & Wilmshurst, S. T. (1996) Introduction to unstiffened CHS tubular joint database. *In:* Tubular Structure VII, Rotterdam, Netherlands. 157-164.

Marshall, P. W. & Toprac, A. A. (1974) Basis for tubular joint design. *Welding Journal,* 53(5)**,** 192-201.

McAllister, T. & Corley, G. (2002) *World Trade Center Building performance study: Data collection, preliminary observations, and recommendations*: Federal Emergency Management Agency, Federal Insurance and Mitigation Administration.

Meng, J., Jincheng, Z., Minglu, L. & Jing, C. (2010) Parametric analysis of mechanical behaviour of steel planar tubular truss under fire. *Journal of Constructional Steel Research,* 67(2011)**,** 75-83.

Najjar, S. & Burgess, I. (1996) A nonlinear analysis for three-dimensional steel frames in fire conditions. *Engineering Structures,* 18(1)**,** 77-89.

Nguyen, M. P., Fung, T. C. & Tan, K. H. (2010) An experimental study of structural behaviours of CHS T-joints subjected to brace axial compression in fire condition. *In:* Tubular Structures XIII – Young (ed). CRC Press/Balkema, 725-732.

Nguyen, M. P., Tan, K. H. & Fung, T. C. (2012) Performance of CHS T-joints in a standard fire test. *In:* Tubular Structures XIV, London. 599-606.

Packer, J. A. (2003) Whiter tubular structures research? *In:* Jaurrieta, M. A., Alonso, A. & Chica, J. A., eds. Tubular Structures X, Madrid, Spain. 3-11.

Qian, X. (2005) *Static strength of thick-walled CHS joints and global frame behaviour*. PhD Thesis, Dept of Civil Engrg, National University of Singapore.

Qian, X., Choo, Y., Van der Vegte, G. & Wardenier, J. (2008) Evaluation of the new IIW CHS strength formulae for thickwalled joints. *In:* Proceedings of the 12th International Symposium on Tubular Structures, Shanghai. Taylor & Francis, London. 271-280.

Qian, X., Wardenier, J. & Choo, Y. (2007) A uniform approach for the design of 100% CHS overlap joints. *Proc. 5th International Conference on Advances in Steel Structures***,** 172-182.

Tan, K., Fung, T. & Nguyen, M. (2012) Structural Behavior of CHS T-Joints Subjected to Brace Axial Compression in Fire Conditions. *Journal of Structural Engineering,* 139(1)**,** 73-84.

Togo, T. (1967) *Experimental study on mechanical behaviour of tubular joints.* PhD Dissertation, Osaka University.

Usmani, A., Chung, Y. & Torero, J. L. (2003) How did the WTC towers collapse: a new theory. *Fire Safety Journal,* 38(6)**,** 501-533.

Van der Vegte, G., Liu, D., Makino, Y. & Wardenier, J. (2003) New chord load functions for circular hollow sections joints. *Delft University of Technology, Delft, Cidect report 5BK-04/03*.

Van der Vegte, G. & Makino, Y. (2005) Ultimate strength formulation for axially loaded CHS uniplanar T-joints. *In:* The Fifteenth International Offshore and Polar Engineering Conference. International Society of Offshore and Polar Engineers, 305-312.

Van der Vegte, G. & Makino, Y. (2006) Ultimate strength formulation for axially loaded CHS uniplanar T-joints. *International Journal of Offshore and Polar Engineering,* 16(4)**,** 305-312.

Van der Vegte, G., Makino, Y., Choo, Y. & Wardenier, J. (2001a) The influence of chord stress on the ultimate strength of axially loaded uniplanar X-joints. *In:* Ninth International Symposium on Tubular Structures. 165-174.

Van der Vegte, G., Makino, Y., Liu, D. & Wardenier, J. (2000) New chord load function for CHS joints. *Delft University of Technology, Delft, CIDECT Report 5BK-6/00*.

Van der Vegte, G., Makino, Y. & Wardenier, J. (2002) The effect of chord pre-load on the static strength of uniplanar tubular K-joints. *In:* proceedings of Twelfth International Offshore and Polar Engineering Conference. 1-10.

Van Der Vegte, G., Wardenier, J. & Makino, Y. (2007a) Effect of chord load on ultimate strength of CHS X-joints. *International Journal of Offshore and Polar Engineering,* 17(4)**,** 301-308.

Van der Vegte, G., Wardenier, J., Qian, XD & Choo. (2008a) Re-analysis of the moment capacity of CHS joints. *In:* Proc. 12th International Symposium on Tubular Structures. 579-588.

Van der Vegte, G., Wardenier, J., Zhao, X. & Packer, J. (2008b) Evaluation of new CHS strength formulae to design strengths. *In:* Proceedings of the 12th international symposium on tubular structures, Shanghai, China. Taylor & Francis, Group. 313-22.

Van der Vegte, G. J. (1995) *The static strength of uniplanar and multiplanar tubular T- and X- joints.* Doctoral Dissertation, Delft University of Technology.

Van der Vegte, G. J., Makino, Y. & Wardenier, J. (2001c) New chord load function for CHS joints. *CIDECT Report 5BK-5/01*.

Van der Vegte, G. J., Makino, Y. & Wardenier, J. (2007b) New ultimate strength formulation for axially loaded CHS K-joints. *In:* Proceedings 5th International Conference on Advances in Steel Structures, Singapore.

Wang, P., Wang, Y. C. & Li, G. Q. (2010) A new design method for calculating critical temperatures of restrained steel column in fire. *Fire Safety Journal,* 45(6)**,** 349-360.

Wang, Y. C. (2004) Postbuckling behavior of axially restrained and axially loaded steel columns under fire conditions. *Journal of Structural Engineering,* 130(3)**,** 371-380.

Wang, Y. C. & Moore, D. B. (1994a) The effect of frame continuity on the critical temperature of steel columns. *In:* Third Kenrensky Conference on Flobal Trends in Structural Engineering, Singapore. 681-686.

Wang, Y. C. & Moore, D. B. (1994b) Effect of thermal restraint on column behaviour in a frame. *In:* 4th International Symposium on Fire Safety Science, Ottawa, IAFSS, Kashiwagi T, editor. 1055-1066.

Wardenier, J. (1982) *Hollow section joints.* TU Delft, Delft University of Technology.

Wardenier, J. (2007) A uniform effective width approach for the design of CHS overlap joints. *In:* Proc. 5th International Conference on Advances in Steel Structures. 155-165.

Wardenier, J., Kurobane, Y., Packer, J. A., van der Vegte, G. J. & Zhao, X. L. (2010a) *Design guide for circular hollow section (CHS) joints under predominantly static loading*. CIDECT, Geneva, Switzerland.

Wardenier, J., Packer, J. A., Zhao, X. L. & van der Vegte, G. J. (2010b) *Hollow Sections in Structural Applications*. Bouwen met Staal, The Netherlands.

Wardenier, J., van der Vegte, G. & Liu, D. (2007) Chord stress function for rectangular hollow section X and T joints. *In:* Proceedings of the 17th international offshore and polar engineering conference. 3363-70.

Yu, H. X., Sun, X. Q. & Wong, K. (2014) Resistance of steel space frames subjected to localized traveling fire. *In:* 8th International Conference on Structures in fire, Shanghai, China. 1121-1128.